EXPERIMENTAL DETERMINATION OF GAS PROPERTIES AT HIGH TEMPERATURES AND/OR PRESSURES

E. H. Carnevale, C. Carey, T. Marshall and S. Uva

Panametrics, Inc.

Waltham, Massachusetts

June 1968

ARNOLD ENGINEERING DEVELOPMENT CENTER
AIR FORCE SYSTEMS COMMAND
ARNOLD AIR FORCE STATION, TENNESSEE

NOTICES

When U. S. Government drawings specifications, or other data are used for any purpose other than a definitely related Government procurement operation, the Government thereby incurs no responsibility nor any obligation whatsoever, and the fact that the Government may have formulated, furnished, or in any way supplied the said drawings, specifications, or other data, is not to be regarded by implication or otherwise, or in any manner licensing the holder or any other person or corporation, or conveying any rights or permission to manufacture, use, or sell any patented invention that may in any way be related thereto.

Qualified users may obtain copies of this report from the Defense Documentation Center.

References to named commercial products in this report are not to be considered in any sense as an endorsement of the product by the United States Air Force or the Government.

EXPERIMENTAL DETERMINATION OF GAS PROPERTIES AT HIGH TEMPERATURES AND/OR PRESSURES

E. H. Carnevale, C. Carey, T. Marshall and S. Uva

Panametrics, Inc.
Waltham, Massachusetts

AF - AEDC
Arnold AFS Tenn

FOREWORD

The research presented herein was sponsored by the Arnold Engineering Development Center (AEDC), Air Force Systems Command (AFSC), under Program Element 6240533F, Project 8951, Task 895102.

The results of research were obtained by Panametrics, Inc., Waltham, Massachusetts, under Contract AF 40(600)-1191. The work was performed between August 1966 and October 1967, and the manuscript was submitted for publication on May 17, 1968.

The reproducibles used in the reproduction of this report were supplied by the authors.

The authors wish to acknowledge David Winslow for running the shock tube measurements and Joseph Caruso for aid in reduction and review of data.

This technical report has been reviewed and is approved.

Terry L. Hershey	Edward R. Feicht
Captain, USAF	Colonel, USAF
Research Division	Director of Plans
Directorate of Plans and Technology	and Technology

ABSTRACT

The available viscosity and thermal conductivity data in helium, argon, hydrogen, nitrogen, are reviewed. Deviation charts vs temperature are drawn up for each of the gases of interest in the temperature range 200-2500°K. High temperature thermal conductivity measurements in air, argon and nitrogen are also reviewed at temperatures between 2000 and 12,000°K. The methods of measuring thermal conductivity and viscosity are discussed with emphasis on the extension of available techniques to higher temperatures and/or pressures. Major emphasis is placed on constricted arc, heat transfer, schlieren, and ultrasonic techniques. Finally, measurements of helium thermal conductivity in the temperature range ~400-3000°K by the ultrasonic technique in the shock tube are presented.

CONTENTS

APPENDIXES

II. ILLUSTRATIONS

NOMENCLATURE

η_e, λ_e	Experimental viscosity and thermal conductivity
η_r, λ_r	Reference viscosity from some readily available tabulation. Reference values are tabulated on deviation charts
$\Delta_\eta, \Delta_\lambda$	Percent deviation between theory and experiment (Eq. 1)
η_o, λ_o	Low density (~1 amagat) viscosity and thermal conductivity
η^+, λ^+	Excess viscosity and thermal conductivity over the low density values
ρ	Density
f	Eucken factor defined by Eq. (5)
D_{int}	The diffusion coefficient for internal energy. In some cases internal energy may be passed from molecule to molecule faster than the molecules themselves diffuse
τ_c	Mean time between collisions, taken as $\tau_c = \frac{1}{4} \frac{\pi \eta}{p}$
τ_i	Relaxation time for the ith internal mode defined by Eq. (48)
Z_i	Collision number for the ith mode $Z_i = \frac{\tau_i}{\tau_c}$
R	Perfect gas constant usually used in dimensionless equations
p	Pressure
T	Temperature
D_{ij}	Diffusion coefficient of the ith species due to a concentration gradient in the jth species. For $i \neq j$ D_{ij} is the binary diffusion coefficient for i = j, the self-diffusion coefficient

X_i	Mole fraction of the i species
r	Capillary radius at any point along its length
L	Capillary length
Ra	Rayleigh number
Gr	Grassoff number (see p 20)
Pr	Prandtl number $\frac{\eta C_p}{\lambda}$
Q	Heat flux
Q_r	Radiative heat flux
S(x)	Total radiative intensity from a cord of an arc $\frac{\text{erg}}{\text{sec cm}^3 \, d\Omega}$
Ω	Solid angle subtended by the receiving volume at the center of the radiating volume element
I_ν	Radiative intensity
B_ν	Planck function $\frac{h_\nu^3}{c^2} \left(e^{\frac{h_\nu}{k_T}} - 1 \right)$
α_ν	Spectral absorption coefficient for light
ν	Light frequency
τ_ν	Optical path
ΔT_w	End wall temperature jump behind reflected shock boundary layer
η	Similarity parameter which replaces distance in the compressible case (Eq. 34)

h	Enthalpy
h_e	Enthalpy in reflected shock region
h_w	Enthalpy at the wall in an end wall reflected shock boundary layer
C	Contrast in a photographic negative
C_p	Specific heat (cps) at constant pressure
C_v	Specific heat at constant volume
C_i	Contribution of the ith interval mode to the specific heat
γ	Specific heat ratio $\frac{C_p}{C_v}$
ω	Sound frequency
α_T	Thermal diffusion ratio
x_i	Mole fraction of the ith species
m_i	Atomic mass of the ith species
c	Sound speed at frequency ω
c_o	Sound speed at $\omega = 0$
z	Compressibility factor $z = \frac{p}{\rho R T}$
K	Wave number of a phonon in the fluctuation spectrum
K_o, K_s	Wave number of incident and scattered light, respectively
$\Delta\rho\ (\vec{r}, t)$	The instantaneous fluctuation in density at the point $\vec{r}$ and the time t

$\frac{\Omega}{2\pi}$	Frequency shift of scattered light
k	Boltzmann' s constant
$\delta(r)$	The delta function
a	Effective collision frequency
$\Delta\omega_B, \Delta\omega_R$	Half width of Brillouin line and Rayleigh lines, respectively
y	Parameter describing the ratio of phonon wavelength to mean free path of the gas molecules

SECTION I
INTRODUCTION

The objective of this work is the experimental determination of gas properties at high temperatures and/or pressures, with emphasis on transport properties. The immediate goals of the present work are to extend existing tabulations for immediate engineering needs and to provide long range support for theoretical work. The temperature range is 300°K to $20,000^{\circ}$K, and the pressure range is 1 to 10^4 atmospheres. The principal transport properties of interest are viscosity, thermal conductivity and diffusion. In addition, consideration of other properties such as electrical conductivity, optical depth and certain thermodynamic properties are of interest.

The theory of energy transport in dilute gases is well understood at sufficiently low temperatures that chemical reactions may be neglected, and at sufficiently low pressures that only binary collisions must be considered (Refs. 1, 2, 3). Two types of practical information are provided by kinetic theory. First, given the interaction potential for the chemical species in the gas of interest (Ref. 4), kinetic theory provides formulas for the calculation of the transport properties. Such calculations have been carried out by Amdur and Mason (Ref. 5) for inert gases and mixtures between 1000°K and $15,000^{\circ}$K. Subsequent transport property measurements in arcs (Refs. 6, 7) and shock tubes (Refs. 8, 9) have shown general agreement with the calculations of Amdur and Mason. A second type of practical information provided by kinetic theory is the relationship between the various measurable gas properties. A good example is the derivation of diffusion coefficients of a mixture from the viscosity (Ref. 10) or thermal conductivity (Ref. 11) of the mixture and the pure gases. Again, for the inert gases the mixing rules from kinetic theory are in agreement with experiment within a few percent.

The transport of energy in polyatomic gases must include energy transported by internal modes such as molecular rotation. Recent calculations of transport properties of polyatomic gases above 2000°K proceed in two steps. First, using the kinetic theory appropriate for monatomic gases and cross sections (from molecular beam experiments, for example) the transport due to the translational motion of the molecules is calculated. The effects of internal modes are then added based on semiempirical relations (for instance, by creating a Eucken factor for internal energies).

Recently the formal kinetic theory has been extended to polyatomic gases through the efforts of Wang Chang, Uhlenbeck and DeBoer (Ref. 12). The resulting expressions are too complicated to serve as a recipe for the practical calculation of transport coefficients. However, further development due to Mason, Monchick and their associates (Refs. 13-16) has provided a firm kinetic theory basis for separating the translational and internal modes of transport. The most important feature of the kinetic theory of polyatomic gases is the dependence of energy transport on diffusion coefficients and relaxation times. Although theory and experiment are not in complete accord at the present time (Ref. 17), this information is basic for the calculation of the transport properties of polyatomic gas mixtures such as air.

At sufficiently high temperatures all gases become mixtures due to chemical reactions such as dissociation and ionization. The presence of chemical reactions in the gas leads to an increase in thermal conductivity (Ref. 18) which is described as a reaction conductivity. The reaction conductivity results from dissociated or ionized species diffusing to low temperature regions and recombining. The heat of recombination is released in the low temperature region resulting in energy transport. This effect may be very large. For instance, in air at 7000°K the thermal conductivity including reaction conductivity is a factor of ~10 greater than frozen thermal conductivity (Ref. 19) (translational plus internal).

Pressure affects the transport properties of chemically reacting gases both by shifting the chemical equilibrium and by causing multiple collision effects. Shifting the chemical reaction changes the transport properties by changing the composition of the mixture. In addition, the reaction conductivity is affected by pressure. For instance, at 7000°K the thermal conductivity in air decreases by a factor of 2 (Ref. 19) when pressure is increased to 30 atm. This is due to the reaction conductivity. The effect of multiple collisions on the transport properties at the same temperature and pressure on the other hand is negligible.

Ionization introduces additional problems in the determination of transport properties both in theory and experiment. Electrons are very efficient at exciting internal modes. There is also charge exchange between ions and neutrals (Ref. 20). Because the coulomb force is long range it is necessary to consider multiple collisions even at low densities. A Chapman-Enskog procedure has been developed to handle ionized gases. However, higher Chapman-Enskog approximations may be necessary to calculate satisfactory transport properties (Refs. 3, 21).

Two additional transport properties become important in ionized gases, radiative flux and electrical conductivity. For instance, the cascade arc techniques of Burhorn (Ref. 22) and Maecker and Wienecke (Ref. 23) require both of these properties as inputs. Other techniques for measuring transport properties at temperatures where ionization is important are affected at least by radiative transport. The electrical conductivity in some cases is the only experimental check possible on transport property calculations.

Finally, the effect of pressure (density) on transport properties as well as the thermodynamics of ionized gases is open to serious question. The problem arises because it is difficult to define what is meant by a free electron, since for sufficiently high densities the electron always has a potential energy equivalent to its thermal energy. In addition, radiative transport becomes very important at the higher densities.

The temperature-pressure range of available transport data is limited by the experimental methods. The classical methods such as capillary flow or thin wire, require friction or heat transfer on a solid surface. These methods are limited by the destruction temperature of solids. Depending on the pressure, the classical methods are limited by the strength of these solids at elevated temperature. Viscosity at temperatures less than 2000°K is the best known transport property. There are uncertainties in the order of 5 to 10% in thermal conductivity in the same temperature range. The reasons for the uncertainty in thermal conductivity are due to difficulties in handling convection, radiation and gas wall energy exchange (accommodation) (Refs. 24, 25). The radiation problem is aggravated by high pressures. Diffusion coefficients have the largest uncertainties, 10% at room temperature. Diffusion coefficients at temperatures above room temperature have become available only recently with the advent of the point source technique (Refs. 26, 27). More recently, ultrasonic techniques have extended diffusion coefficients to 5000°K (Ref. 28). Very few measurements of diffusion coefficients at high pressures are available.

As mentioned above, the kinetic theory of gases with internal modes involves diffusion coefficients, relaxation times and bulk viscosity. When calculating transport properties from molecular potentials or extrapolating rare gas properties to high densities, it is convenient to separate the internal modes from the translational modes of transport. This can be done if one knows the appropriate diffusion coefficients and relaxation times. There are several experiments

which are capable of measuring either translational thermal conductivity or relaxation times. Some of these experiments are free jet expansion (Ref. 29), thermal transpiration (Ref. 30), and ultrasonic absorption (Ref. 31). While in the first approximation the effects of internal modes are not a function of density, some high density measurements of these properties would be interesting.

During the past year three experiments were chosen to answer some immediate needs in the area of transport properties for engineering purposes. A heat transfer experiment was investigated for measuring the effects of pressure on thermal conductivity. A schlieren experiment was set up. This experiment will provide the thermal conductivity of gases at high temperature ($2000^{\circ}K < T < 11,000^{\circ}K$), and moderate pressures ($p \sim 300$ atm). Finally, ultrasonic absorption measurements were made in helium at temperatures up to $3000^{\circ}K$ and pressures of 2 atm.

SECTION II
DATA REVIEW

2.1 DEVIATION CHARTS

A review of available transport data for He, Ar, H_2, N_2 and Air was undertaken to determine what additional measurements would best contribute to present knowledge and to assess the accuracy of extrapolation procedures for present needs. In addition, a limited comparison was made between theory and experiment for mixtures of these gases. The viscosity and thermal conductivity of each of the gases under investigation are presented in the form of deviation charts. The temperature deviation charts are constructed by taking a reference viscosity from available compilations and plotting

$$\Delta_\eta = \frac{\eta_e - \eta_r}{\eta_r} \tag{1}$$

vs temperature, where η_e is the measured viscosity and η_r is the reference viscosity. The excess viscosity, η^+, charts are plots of

$$\eta^+ = \eta_e - \eta_o \tag{2}$$

vs pressure where η_o is the low pressure limit (measured in the same experiment where possible). The η_o's are included in the temperature deviation chart for comparison with other low pressure measurements. The pressure was used instead of the more meaningful variable density (Ref. 32) because in applications pressure is given more often than density. The notation for the other transport coefficients is analogous.

The deviation chart presentation is chosen because it allows rapid determination of the accuracy of theory relative to experiment. The consistency of measurements from different sources may be determined by inspection. In general, the internal consistency of measurements is much better than the agreement between theory and experiment. Finally, transport properties for use in engineering applications may be obtained by adding the deviations to the reference values. For instance, for viscosity

$$\eta = \eta_r (1 + \Delta_\eta) . \quad (3)$$

The deviation charts may be continuously updated as new measurements become available.

2.2 HELIUM

The viscosity of helium has been measured at pressures up to 820 atm (Ref. 33) and temperatures up to 2340°K (Ref. 34) by the capillary flow technique. Additional measurements have been made using ultrasonic absorption (Ref. 6) at temperatures up to ~4000°K in the experimental part of the present effort. A deviation chart of the normalized viscosity of helium vs temperature is shown in Figure 1 from several recent investigations. The reference viscosity was taken from the work of Lick and Emmons (Ref. 35). The low temperature ($T < 3000°K$) viscosities from the various sources agree to within 2 to 7%. The ultrasonic measurements have a small uncertainty, ~2%, because Prandtl numbers based on the work of Lick and Emmons had to be used to reduce the sound absorption to viscosity.

The average of the measured viscosities is about 2% higher than the theoretical calculations of Lick and Emmons. At the high temperature the viscosities of Amdur and Mason (Ref. 5) deviate from the values of Lick and Emmons by about 12%. Recently revised scattering results published by Amdur and Jordan (Ref. 4) should give viscosities which are even closer to the values of Lick and Emmons. Some calculations by Devoto and Li (Ref. 3) have been carried out above 4000°K but the resulting viscosities are systematically 3% higher than the values of Lick and Emmons based on the same high energy potentials (Ref. 36). The interaction potential of Mason and Rice (Ref. 37) at low temperature, $T < 2000°K$, is probably the best description of the viscosity of helium. At temperatures between 2000°K and 10,000°K the tabulation of Lick and Emmons should be used. For ionized helium the calculations of Devoto and Li appear to be the most reliable.

The thermal conductivity of helium (at 1 atm) vs temperature deviation chart is shown in Figure 2. The thermal conductivity has been measured at temperatures up to 2400°K (Ref. 38) using the thin wire technique. Measurements up to this temperature have also been made by Blais and Mann (Ref. 39) with an adaptation of a thermal diffusion column. These measurements are most likely too high by about 20% at the highest temperature (Refs. 37, 40) (~2000°K). Measurements at

temperatures up to about 600°K and pressures up to 500 atmospheres were recently made (Ref. 41). The reference thermal conductivities are again taken from Lick and Emmons.

The experimental measurements of thermal conductivity before 1962 have been reviewed by Ho and Leidenfrost (Ref. 42). The experimental data is consistent within 5% at temperatures up to 2400°K. The overall behavior of the thermal conductivity is similar to the viscosity with the exception that the deviations amongst data from various sources are about 5% greater.

Some high temperature measurements of the temperature dependence of thermal conductivity (Ref. 43) using the heat transfer to the end wall of a shock tube are shown in Figure 2. These measurements deviate from Amdur and Mason's (Ref. 5) thermal conductivity data by up to 30%. However, the thermal conductivity from the end wall experiment agrees more closely with thermal conductivity calculated from the recent theoretical He-He cross sections of Phillipson (Refs. 3, 36) at temperatures above 4000°K. This is of questionable significance since the shock tube data reported does not contain significant information about thermal conductivity above 4000°K. In fact, the significance of the end wall data is weighted toward the lower temperatures. However, the low temperature data are in general agreement with the potential functions of Mason and Rice. They were able to correlate all the existing data (up to 1954) for viscosity, thermal conductivity and second virial coefficients for He to within 2%.

The viscosity and thermal conductivity of helium show only a slight pressure dependence. For this reason definitive experimental measurements of this effect have only recently become available.

The deviation chart for viscosity vs pressure for several investigators is shown in Figure 3. The viscosity increases only 5% with a 300 atm pressure increase at 100°C. The Chapman-Enskog (Ref. 2) theory gives results which agree rather well with available data (Ref. 32). Values of A_λ, B_λ and D_λ which fit the equation

$$\eta = \eta_o + A_\lambda \rho + B_\lambda \rho^2 \ln \rho + D_\lambda \rho^2 + \qquad (4)$$

have been investigated by Sengers.

Similar results for the thermal conductivity of helium are shown in Figure 4. The thermal conductivity at high pressures has been reviewed by Ho and Leidenfrost. They found that the expression of Snider and Curtiss (Ref. 44) agreed with these data much better than the Enskog theory.

2.3 ARGON

The viscosity of argon at atmospheric pressure has been reviewed by several authors (Refs. 45, 46, 47). Argon measured viscosities up to 1800°K are consistent to within 1%. However, several efforts have failed to find a simple potential function which reproduces the viscosity within the experimental uncertainties over the temperature range 700°K to 1800°K. Extrapolation of experimental viscosities of argon to 4000°K using a potential function based on low temperature data leads to errors of the order of 50%. High temperature measurements of argon viscosity have been made using the ultrasonic technique at temperatures up to 7000°K. At the highest temperature, the measured thermal conductivity from the cascade arc experiment of Knopp and Cambel (Ref. 7) was used to obtain viscosity. A deviation chart for argon viscosity is shown in Figure 5. The measured viscosity above 1000°K agrees with the Amdur and Mason (Ref. 5) calculations up to temperatures where ionization occurs, ~6000°K.

The thermal conductivity of argon has been measured over a much larger temperature range than any other gas. The data from most investigations below 3000°K is consistent to within 3% as may be seen by inspecting the deviation chart in Figure 6. The scatter in the data from each investigation for $T < 2000°K$ shows that thermal conductivity data is not as self-consistent as the viscosity measurements.

The thermal conductivity of argon in the temperature range from $3000°K < T < 12,000°K$ is shown in Figure 7. The thermal conductivity has been measured by the cascade arc technique (Refs. 7, 48, 49, 50) and an ultrasonic technique (Refs. 6, 8, 9). The measurements are compared to the calculations of Devoto (Ref. 21) and Yos (Ref. 19). The Maecker type measurements contain the translation thermal conductivity and the reaction thermal conductivity (equilibrium conductivity). The average thermal conductivity falls about 10% above theory with a possible uncertainty of about $\pm$ 30% due to the lack of accurate electrical conductivity and radiative properties for argon. The ultrasonic data measures the translational (frozen) thermal conductivities of argon. The reference thermal conductivity for the cascade arc measurements is the equilibrium

value and for the ultrasonic method is the translational value. The largest contribution to the sound absorption in argon between 7000 and 12,000°K is the thermal conductivity. Therefore, the viscosity from Devoto's theory was used with the sound absorption to obtain the thermal conductivity data points. The ultrasonic measurements indicate that Devoto's viscosity as well as thermal conductivity are accurate.

The viscosity of argon at elevated densities has been measured at pressures up to about 2000 atm. The excess viscosity chart for argon vs pressure is shown in Figure 8. The pressure effect in argon is much larger than helium, about a 15% increase with a pressure increase of 100 atm at 25°C. The thermal conductivity of argon increases somewhat faster than viscosity, 30% in 100 atm. An excess thermal conductivity plot is drawn up in Figure 9. The transport properties of high pressure argon have been compared to a modified Chapman-Enskog theory (Ref. 33) and are within 12% of each other over the temperature range from 250°K to 375°K and from 100 to 700 atm.

2.4 POLYATOMIC GASES

The review of the polyatomic gas data requires some new concepts largely to account for the transport of energy by internal modes. Similar considerations must be applied to monatomic gases at high temperatures to describe energy transport due to exchange between translation and electronic states. The viscosity depends on the internal mode only to the extent that the cross sections depend on the internal state of the particle. Thus, for the calculation of viscosity the gas is a mixture of different particles each corresponding to a degree of excitation. The thermal conductivity on the other hand may be expressed as a sum of a translational (analogous to viscosity) and an internal thermal conductivity. The internal thermal conductivity describes an excited molecule diffusing into a cooler region of the gas and giving up its internal energy to the neighboring cooler molecules at a rate depending on the relaxation time for the exchange process (Ref. 17).

The problem of internal modes (Ref. 13) was first approached by considering deviations of the Eucken factor (units chosen to make f dimensionless)

$$f = \frac{\lambda}{\eta C_v} \tag{5}$$

from the theoretical value for monatomic gases. The Eucken factor for monatomic gases as a function of temperature (Ref. 26) is shown in Figure 10. An inverse power law interaction potential gives a Eucken factor which varies from 2.522 (n = 5) to 2.50 (n = ∞ for a hard sphere). The addition of an attractive potential to the hard sphere interaction causes the Eucken factor to vary with temperature. Examination of Figure 10 shows monatomic gases have Eucken factors which fall within 8% of the simplest theory. In addition, there are experimental indications that the Eucken factor systematically increases with temperature and atomic number for the monatomic gases (Ref. 25). This should be expected if f depends only on the interaction potential. The Eucken factor for polyatomic gases on the other hand deviates typically by 50% from the classical value of f. The f for polyatomic gases depends in a very complicated way on temperature and molecular properties (Refs. 13, 51). In general, the Eucken factor for polyatomic gases is expressed as the sum of an internal and a translational part so that

$$\frac{\lambda}{\eta} = C_{v_{tr}} f_{tr} + C_{v_{int}} f_{int} \quad . \tag{6}$$

The value of the translational Eucken factor, f_{tr}, may be obtained from viscosity or diffusion data. The value of the internal Eucken factor on the other hand must be evaluated from theory unless both λ and η are known.

As mentioned in the Introduction, the exact kinetic theory for polyatomic gases has been developed in recent years. The resulting relations will be used below to analyze experimental transport data in hydrogen and nitrogen. The expressions obtained directly from the Boltzmann equation for polyatomic gases (Refs. 13, 15) are used below. For a gas with a single internal degree of freedom the internal thermal conductivity is

$$\frac{\lambda_{int}}{\eta} = \frac{\rho D_{int}}{\eta} \left(C_{int} + F \right) \tag{7}$$

where

$$F = \frac{2}{\pi} \frac{C_{int}}{Z} \left(\frac{5}{2} - \frac{\rho D_{int}}{\eta} \right) \left[1 + \frac{2}{\pi} Z \left(\frac{5}{3} \frac{C_{int}}{R} + \frac{\rho D_{int}}{\eta} \right) \right]^{-1} \tag{8}$$

and D_{int} is the diffusion coefficient for the internal mode, C_{int} is the specific heat for that mode, and Z is the average number of collisions necessary to exchange internal and translational energy. In most cases the denominator of F may be neglected. The translational thermal conductivity is

$$\frac{\lambda_{tr}}{\eta} = \frac{5}{2}\left(C_{v_{tr}} - F\right) . \tag{9}$$

The Eucken factor may be found from (7) and (9) if the collision number, viscosity and internal diffusion coefficient are known.

In practice rotation and electronic excitation are the only important degrees of freedom for the calculation of thermal conductivity from (7) and (9). Since accurate experimental data is available only up to about 2000°K only rotation need be considered. The internal diffusion coefficient for rotation may be taken to be the self-diffusion coefficient.

For most gases the quantity $\frac{\rho D_{11}}{\eta}$ is ~1.13. The rotational collision numbers may be calculated using an expression due to Parker (Ref. 52) with constants adjusted to reproduce experimental Z_{rot} at room temperature. Theoretical Eucken factors based on the above assumptions agree with the experiment for most gases within the experimental error (Refs. 13, 51).

These concepts may now be applied in the analysis of the experimental data for H_2 and N_2.

2.5 HYDROGEN

The transport properties of hydrogen are not as well known as the other common gases. The deviation chart for the viscosity of H_2 vs temperature at one atmosphere is shown in Figure 11. During the past few years the viscosity of hydrogen has been measured up to 2400°K. The early results are consistent within 2%. The most recent measurements (Ref. 34) are systematically 6% higher than earlier work of Trautz et al. (Refs. 53, 54) and the tabulation of Hilsenrath (Ref. 55). At temperatures above 1300°K the viscosities of Guevara and Wageman are systematically higher than the viscosities based on the potential function of Mason and Rice by about 10%. Heat transfer measurements

on the end wall of the shock tube are suited to resolve the above mentioned discrepancy.

A very limited number of viscosity measurements for hydrogen are available at high pressures, the most recent being the Russian (Ref. 56) measurements relative to nitrogen at temperatures up to 1000°K and pressures up to about 500 atm. Sengers (Ref. 32) has compared the viscosity of hydrogen up to 800 amagats to the Enskog theory.

The thermal conductivity of hydrogen has been studied extensively at temperatures up to 2400°K at one atmosphere. Thermal conductivity measurements have been attempted up to 3000°K by a new technique (Ref. 57). However, further experiments have to be done to assess the errors in this system.

The deviation chart for thermal conductivity of hydrogen vs temperature (Figure 12) shows a large amount of scatter, 6%, in the measurements from different investigators at temperatures up to 1000°K. Higher temperature data shows even less consistency. The data of Blais and Mann are too high by about 20% at the highest temperatures. This same discrepancy was pointed out in the helium measurements of Blais and Mann above.

The translation thermal conductivity is somewhat difficult to calculate for hydrogen. The Eucken factor for hydrogen (Figure 13) does not behave as expected at high temperatures. Saxena (Ref. 40) and Mason (Ref. 37) conjectured that the difficulties were due to errors in the thermal conductivity measurements. The most recent measurements seem to bear this out. Fortunately, the internal thermal conductivity of hydrogen is a much smaller effect than it is in other diatomic gases.

2.6 NITROGEN

The transport properties of N_2 are known better than any other gas with the possible exception of Ar. The viscosity has been measured (Ref. 58) up to 1400°K with a majority of the points within 1%. Near room temperature several investigators have obtained the same results to within a tenth of one percent. The deviation chart for these measurements is shown in Figure 14. Some measurements of viscosity by Wienecke in an electric arc are available. However, these values are very different from theoretical results. Other measurements must be done to confirm the work of Maecker and Wienecke (Ref. 23).

The viscosity of nitrogen at high pressure has been investigated up to 820 atmospheres at temperatures up to 500°K (Ref. 33). The pressure effect is quite large, the viscosity almost doubling in 10^3 atmospheres. The deviation chart for the available high density nitrogen viscosity was compared to the modified Chapman-Enskog (Ref. 32) relation and found to be within 4%. The available excess viscosity data are shown in Figure 15.

The thermal conductivity of nitrogen has been measured up to 1400°K at atmospheric pressure. The earliest work tabulated by Hilsenrath et al. showed a self-consistency within 1% up to 600°K. At higher temperatures more recent data showed scatter of 10%. Bargaftik and Zimina (Ref. 58) reviewed the available thermal conductivity data at high temperatures, applying corrections for temperature jump (Ref. 25) to the measurements of several authors, and they found the available data consistent to within 2%. These corrections reduced the scatter in the Eucken factor vs temperature curves for N_2 and brought the theory of Mason et al. into much closer agreement with experiment. A deviation chart for thermal conductivity is shown in Figure 16.

The Eucken factor vs temperature plot is given in Figure 17. The rotation numbers up to 1500°K for this graph were taken from jet expansion experiments of Miller and Andres (Ref. 29) and ultrasonic measurements (Ref. 31). The temperature variation of the Eucken factor of nitrogen is an excellent test of the polyatomic gas theory because the necessary numbers are available.

The thermal conductivity of nitrogen has been measured in the constricted arc at one atmosphere and temperatures above 5000°K by several investigators (Refs. 23, 50, 59, 60). A deviation chart of experimental high temperature thermal conductivity values vs temperature is shown in Figure 18. The recent calculations of Yos (Ref. 19) are used as the reference values. The original data of Maecker (Ref. 24) are in good agreement with theory between 5000 and 6000°K. However, from 7000 to 15,000°K the measured values are high and depend on arc current. The recent work at Avco (Ref. 61) showed that a reasonable radiative correction brought the Maecker data in reasonable agreement with theory, and eliminated the current dependence. The same correction applied to the thermal conductivity measurements at Avco also eliminates the current dependence. However, the Avco data are about 50% above the Maecker data and the calculations of Yos.

The theoretical uncertainties in these measurements are largely due to uncertainties in the calculated radiation and electrical properties

of gases which are necessary to reduce the data. Again it should be noted that near 7000°K and again near 15,000°K the reaction thermal conductivity dominates over the translational thermal conductivity. Only at about 10,000°K do these experiments have any information on the translational thermal conductivity. The errors associated with the cascade arc technique are further discussed below in the methods section.

2.7 AIR

The viscosity of air has been the subject of a recent review by Hing Yi Lo et al. (Ref. 62). The experimental results for viscosity vs temperature are very consistent, 2% up to temperatures of 1000°K and 1% up to 2000°K. This is shown in the deviation chart in Figure 19. The reference viscosity for the chart is taken from the correlation formula given in Ref. 62. The pressure data correlates especially well at high pressures, while the scatter at lower pressures is mainly due to lack of significance in the excess viscosity. An excess viscosity chart is drawn up for viscosity vs pressure in Figure 20. The correlation formula from Ref. 62 was used for the low density viscosities.

The mixing rules for the thermal conductivity of a polyatomic gas mixture such as air are not fully understood. Part of the difficulty is that insufficient information on collision numbers and diffusion coefficients (especially the latter) exists to test the relative merits of various theories. Another problem is the complexity of the exact theory. The available experimental data for mixtures involving polyatomic gases have been compared to theory by several authors (Refs. 16, 63). The expression due to Hirschfelder (Ref. 64), seems to agree with experiment better than the recent attempts to treat polyatomic mixtures more exactly (within 10% in the worst case). Hirschfelder's expression is

$$\lambda_{mix} = \lambda^{o}_{mix} + \sum_{i=1}^{n} \frac{\lambda_i - \lambda^{o}_i}{1 + \sum_{j=1}^{n} \frac{D_{ii} X_j}{D_{ij} X_i}} \qquad (10)$$

where λ^{o}_{mix} is the thermal conductivity of the mixture with frozen internal modes (translational thermal conductivity). λ_i and λ^{o}_i are the total and translational thermal conductivity, respectively, of the pure gases. D_{ii} and D_{ij} are the self-diffusion and binary diffusion coefficients, respectively. The X_i are the mole fractions. The collision

numbers enter into λ_{mix} mainly through λ_i.

The most appropriate way to calculate the thermal conductivity of a mixture is to obtain the thermal conductivity of the pure gases exactly from Eq. (9), and to use these values in Eq. (10). The inverse problem arises when the total thermal conductivity is given and the translational thermal conductivity must be found. For instance, if we wish to apply a density correction, the internal thermal conductivities of the pure components λ_i, λ^o_i may be calculated at one atmosphere, and the internal thermal conductivity of the mixture calculated from

$$\lambda_{mix,\,int} = \sum \frac{\lambda_i - \lambda^o_i}{1 + \sum_j \frac{D_{ii} X_j}{D_{ij} X_i}} \quad . \tag{11}$$

It could be noted that because of the very unsatisfactory state of the mixing rules at high pressures, internal thermal conductivities should be calculated from low density data.

The thermal conductivity of air is not as well known as the viscosity. The early measurements tabulated by Hilsenrath up to about 600°K show about 5% scatter. Tsederberg (Ref. 25) reports some data which he tabulates after some modification up to 1300°K. In the same reference thermal conductivity measurements by other Russian workers are quoted up to 400 atm. However, Tsederberg noted that their low pressure values for nitrogen differed by 6-9% from other reliable values. A deviation chart for the thermal conductivity of air is shown in Figure 21.

Eucken factors have been calculated from the data in Figures 19 and 21 and are somewhat lower than direct measurements of Eckert et al. (Ref. 65). A deviation chart for the pressure effect for the thermal conductivity of air is shown in Figure 22. The experimental data are compared to a calculated thermal conductivity. The internal thermal conductivity was calculated from Eq. (11) and the data for pure oxygen and nitrogen. The translational thermal conductivity was then found by subtracting the internal contribution calculated above from the measured thermal conductivity at one atmosphere. The modified Chapman-Enskog theory was then used to extrapolate the translational thermal conductivity to high pressures. The internal component was added again to the extrapolated translational thermal conductivity to

obtain the total thermal conductivity at high pressures. The calculated and experimental values are within 16%.

An experimental determination (Ref. 66) of thermal conductivity of air between 1000°K and 6500°K has recently been made using a schlieren interferometer technique on the end wall boundary layer of the shock tube. The measurements were made at a constant density of one-tenth room temperature atmospheric density. The pressure range of the data varies from one-third atmosphere at 1000°K to about 3 atmospheres at 6000°K. A deviation chart for these measurements is shown in Figure 23. The reference thermal conductivities were taken from Hansen (Ref. 67). Also shown are the recent calculations of Yos (Ref. 19). The quoted uncertainties in the measurement are 50%. However, this is greater than the maximum error, the average of which is probably a good representation of the thermal conductivity of air. At temperatures below 2000°K the measured values agree with the recent calculations of Yos. At higher temperatures the experimental data varies by up to a factor of two from the two theoretical values, depending on the temperature. The uncertainties at this time in the thermal conductivity of air above 2000°K are as large as $\pm$ 75%, especially near temperatures where dissociation and ionization are about 50% complete. Since dissociation and ionization depend markedly on pressure between 1 and 10 atm, this uncertainty exists over the entire temperature range of 2000°K-20,000°K. Until the pressure effects of chemical reactions on the thermal conductivity of air are better known, consideration of higher order collisions will not improve the situation. Fortunately, at the higher temperatures, T > 3000°K, and at a fixed pressure, the density is reduced by factors of 10 to 100 over the density at room temperature. At the higher temperatures, pressures of 10^3 to 10^4 atm are needed to cause up to 30% increase in thermal conductivity due to triple collisions.

SECTION III
METHODS

3.1 CLASSICAL TECHNIQUES

The problem of measuring transport properties reduces to creating flows which are amendable to analysis. This means flows with high degrees of symmetry and small variations in velocity, temperature, pressure or species concentration. At low temperatures, $T < 3500^{\circ}K$, it is feasible to confine the gas to very small regions by solid boundaries. At high temperatures, $T > 3500^{\circ}K$, it is no longer possible to contain the gases with any known material. The hot gases must be sensed through boundary layers using light and sound waves. Indirect information on transport properties of a high temperature gas may be obtained by measuring the heat flux through the boundary layer. However, even this technique requires accurate knowledge of the temperature and pressure of the high temperature gas. These thermodynamic quantities must then be sensed through a thermal boundary layer. The biggest problem is to obtain a uniform, stable high temperature gas source. This problem becomes more severe as the pressure is increased. Development of high temperature gas sources has proved to be the most expensive and time consuming task in obtaining transport properties above $3500^{\circ}K$.

The classical techniques for measuring viscosity and thermal conductivity are discussed and appropriate references given by Sengers (Ref. 68). The present discussion will be limited to methods which are most suitable for extension to the extremes of temperature and pressure ($p \lesssim 10^4$ atm, $T \lesssim 3500^{\circ}K$). The main reason for further work below $3500^{\circ}K$ is to support theoretical developments in dense gas transport properties. A secondary purpose is to obtain adequate potential functions for extrapolation of gas properties to higher temperatures. Past experience has shown that both types of activities require extremely accurate (0.1%) measurements to be of any use.

The capillary flow method is the simplest technique for the measurement of viscosity. The basic technique consists of forcing a steady state flow rate, Q, through a capillary and measuring the resulting pressure drop, p. The essentials of a high pressure-high temperature capillary viscometer (in cutaway view) are shown in Figure 24. The capillary is a hole drilled in the wall of the interior cylindrical heater (Guevara and Wageman Ref. 34). A second guard heater with a much thinner wall

is used to maintain the uniform temperature of the inner heater. The ends are attached to water-cooled copper flanges which are maintained at room temperatures. The heaters must be sufficiently long to bring the test gas up to the wall temperature before it enters the capillary. For high pressures the cell must be surrounded by a cooled high pressure support.

The advantage of drilling the capillary in the wall of the inner heater is that uniform temperatures are easily obtained. In addition, for high pressure applications the geometry in Figure 24 has high strength. The disadvantage is that the short length of the capillary requires large corrections to the simple Poiseuille law. The wall thickness of the inner heater is limited by the power necessary to maintain it at a high temperature. A quarter inch wall thickness on a 6" long cylinder requires in the order of tens of kilowatts. Some new techniques have been developed for manufacturing small bore refractory metals (Mo, W) tubes by spraying the refractory metal on a form and etching the form away. However, the short capillary with appropriate corrections is the most promising technique for obtaining accurate viscosity measurements at temperatures from 1500°C to 3000°C and pressures up to 10^3 atm.

The capillary flow technique requires a method for measuring the pressure drop across the capillary and a pump to maintain a constant flow rate and average pressure. The pressure drop of about 7 cm Hg must be measured by a device which is capable of withstanding the high mean pressures. The pump usually has a working fluid other than the gas which has a low compressibility thermal expansion and vapor pressure. Mercury has become the standard choice. Some investigators have used bellows to act directly on the test gas as a pump.

High pressure capillary viscometers have recently been fully discussed by Giddings, Kao and Kobayashi (Ref. 69). The generalized relation between viscosity and the experimental parameters is

$$\eta = \left[\frac{\pi \bar{a}^4}{8 (L + n \bar{a})} \frac{\Delta p}{Q} \frac{1}{\xi} \frac{\rho_{av}}{\rho_1} \right] - \frac{m \rho_1 Q_c}{8 \pi (L + n \bar{a})} . \qquad (12)$$

The first term in brackets is essentially the simple Poiseuille law with some modifications. The radius of the capillary is replaced with an average radius over the length of the tube

$$\bar{a} = \left[\frac{1}{L} \int_0^L \frac{d\ell}{r^2} \right]^{-1/2} . \qquad (13)$$

Since η depends on $\bar{a}^4$ most investigators go to great pains to determine the radius accurately. The length of the capillary is increased by a constant multiple of the average radius (n $\bar{a}$) to account for the forces necessary to change the velocity distribution of the incoming fluid to the parabolic distribution characteristic of steady state Poiseuille flow. The correction for the compressibility of the gas is expressed as the ratio of the average density ρ_{av} defined to the density at the entrance of the capillary ρ_1. The average density is given by

$$\rho_{av} = \frac{p_1 + p_2}{Z_{av} RT} \qquad (14)$$

where

$$Z_{av} = \frac{\rho_1^2 - \rho_2^2}{a \int_{\rho_2}^{\rho_1} \left(\frac{p}{2}\right) d\rho} . \qquad (15)$$

This correction is important near phase changes. A correction factor for the uniformity of the capillary ξ is included which must be determined by calibration with a known gas.

The second term in Eq. (12) (the Hagenbach factor) corrects for the acceleration the fluid experiences going from reservoir flow into the capillary flow. Further corrections for thermal expansion and compressibility of the capillary walls are not shown. Also an additive correction for slip roughly equal to the ratio of mean free path to capillary diameter is important at pressures of one atmosphere and less.

Thermal conductivity has proved to be a much more difficult measurement to make at the extremes of temperature and pressure than viscosity. Even after the very difficult problems of obtaining a uniform region of test gas and correcting for end effects and edge effects have been accomplished, serious problems remain (Ref. 25). The problems are convection, temperature jump, radiation and temperature measurement.

Convection occurs when dense fluids are generated above lighter fluids. Gravitational forces cause the dense fluid to fall and the lighter gas to rise. The lighter fluid carries its heat with it adding to the total heat flux. The magnitude of the convective effects depends on a dimensionless quantity, the Rayleigh number (Refs. 69, 70),

$$Ra = Gr \cdot Pr = \frac{\rho^2 \beta \Delta T g \ell^3}{\eta^2} \cdot \frac{\eta C_p}{\lambda} \tag{16}$$

where g is the acceleration of gravity, Gr the Grassoff number, and Pr the Prandtl number (these are indicated by the product). The new quantities in Eq. (16) are the acceleration of gravity g, the thermal expansion coefficient β, the temperature difference ΔT and the thickness of the gas layer ℓ. The heat transfer due to convection is negligible for Rayleigh numbers less than 500. For ordinary gases, at atmospheric densities and with typical temperature differences, this criterion demands gas paths of 1-0.1 mm in a thermal conductivity apparatus.

The technique which is least sensitive to convection is a horizontal parallel plate apparatus with the high temperature plate on top. This technique has been used for measurements near the critical density where convection is a very large effect (Ref. 71). However, it is difficult to achieve a simple temperature field between parallel plates. The other extreme is the technique of Blais and Mann illustrated in Figure 25. The convection is driven by maintaining room temperature on the outer cylinder (a wire held at $\sim 10^3$ °K). The only regions with significant temperature drops in the z direction are near the ends of the tube. Therefore, near the middle of the diffusion column (A B in Figure 25) the heat flux due to convection,

$$Q_c = v \rho C_v \frac{\partial T}{\partial z} \tag{17}$$

is zero and the heat conduction equation reduces to the radial term only. The well-known solution to the radial heat equation with large temperature ranges ($\lambda \neq$ constant) is

$$Q = \frac{2\pi L}{\ln \frac{r_o}{r_1}} \int_{T_o}^{T_1} \lambda\,(T)\, dT, \tag{18}$$

where the symbols are provided in Figure 25. The power dissipated, Q, in the length of wire, L, is measured over an entire range of central wire temperatures, T_1. The resulting curve of Q vs T_1 may be differentiated to give, according to Eq. (18), the thermal conductivity,

$$\lambda\,(T_1)\quad \frac{\ln \dfrac{r_o}{r_1}}{2\pi L}\quad \frac{dQ}{dT_1} \qquad (19)$$

The most interesting aspect of this experiment is that while Q is significantly sensitive to convection, $\frac{dQ}{dT}$ is not. This technique has been suggested as a method to extend thermal conductivity measurements to temperatures from 2000°C to the destruction temperature of tungsten. The earliest measurements in helium (Ref. 39) shows serious discrepancies with other measurements and theory. However, Saxena seems to have successfully applied this technique (Refs. 72, 73, 74), and is currently extending it.

A more conventional technique for eliminating convection is to minimize spacing between the cold and the hot elements, the temperature difference, ΔT, and operate at low densities. Even the technique of Blais and Mann is restricted to low densities because at high Rayleigh numbers convection is unstable and turbulence develops. However, low pressures lead to a phenomenon called temperature jump. Energy transfer upon collision with a wall is different from the energy transfer of a similar collision with a gas molecule. Therefore, there is a region up to 30 mean free paths long where the temperature gradient is affected by the efficiency of energy transfer with the wall. As a result the hot wall temperature is hotter than expected by extrapolating the gradient in the gas to the wall. Similarly, the cold wall is colder than one would expect.

The measured temperature difference between the walls of the thermal conductivity cell must be corrected to obtain the temperature drop in the gas. The corrections for the temperature jump in different types of thermal conductivity cells have been discussed by several authors (Refs. 58, 39). The basic technique is to measure the thermal conductivity (or its equivalent) at different pressures and to extrapolate to infinite pressure. One has to be careful to avoid the curvature which tends to develop at the higher pressures in polyatomic gases. These corrections are most important in the thin wire variation of the concentric cylinder method. Some authors (Refs. 58, 75) have shown the

temperature jump to account for 2-7% errors in reported thermal conductivity measurements.

The major problem at higher temperatures ($1000^{\circ}K < T < 3000^{\circ}K$) in conventional thermal conductivity techniques is radiation. The radiative transfer may be minimized by making the surface area of the thermal conductivity cell and the temperature difference, ΔT, as small as possible. Mainly for this reason the accurate measurements of thermal conductivity at higher temperatures have been made with the thin wire technique. The diagram in Figure 25 shows the essential features of the thin wire apparatus. The temperature difference between the central wire and the outer wall is of the order of $10^{\circ}K$ in typical systems. Equation (18) relates the thermal conductivity to the measured heat flux (electrical power dissipated in the length L) and temperature difference. Because the temperature difference is small, λ is essentially constant. The integral in (18) reduces to the product of the average thermal conductivity and the temperature difference.

More recently a variable path parallel plate thermal conductivity cell has been developed (Ref. 76) and used to determine the thermal conductivity of helium. This type of apparatus has the advantage in that extrapolation of the effective thermal conductivity to zero plate separation may be used to eliminate the effects of radiation. In addition, as mentioned above, this configuration minimizes convection. Therefore, the variable path parallel plate system holds promise for measurements at higher temperatures and densities.

Finally, a problem which arises in any thermal conductivity cell is the accurate measurement of temperature. The difference between two measured temperatures is needed to determine the thermal conductivity. When temperature differences of the order of $10^{\circ}K$ are involved the temperatures must be accurate to $0.1^{\circ}K$ to provide 1% accuracy. Thermocouples have been used but these are limited to temperatures below $2000^{\circ}C$. The resistance of the central wire provided accurate measurement of temperatures for most of the measurements with the thin wire technique. The transit time of an ultrasonic wave has been used to measure temperatures up to $2800^{\circ}K$ in a rhenium wire (Ref. 77). The ultrasonic technique in solids along with an ultrasonic helium gas thermometer for calibration (Ref. 78) will do much to improve the conventional techniques of thermal conductivity determination.

3.2 CASCADE (MAECKER) ARC

The flow in a low velocity arc discharge in a circular channel (constricted arc, Figure 26) which is long in comparison to its radius, is strongly dependent on the thermal conductivity of the gas. The measurement of the flow in constricted arcs has been used to measure the thermal conductivity of nitrogen (Refs. 23, 50, 59, 60, 61) and argon (Refs. 7, 48, 49). Some investigators have used previously reported measurements of arc characteristics to deduce the thermal conductivity of nitrogen (Ref. 79) and hydrogen (Refs. 50, 61). Measurements to date have been restricted to pressures of one atmosphere and temperatures between 5000°K to about 15,000°K in the arc.

In the original technique of Burhorn (Ref. 22) and Maecker (Ref. 23), the gas temperature was measured spectroscopically and estimates of radiation losses and electrical conductivity were made. The estimates were checked by calculating the integrated radiation loss and electrical conductivity and comparing them with measured values. Recent work has been concerned with a better determination of electrical conductivity and radiative transport. The major problem involved in extending the arc experiment to higher pressures rests in determining the contribution of radiation to the energy balance.

Since the constricted arc is usually operated with very low flow velocities, the only important transport process in this case is the transfer of heat between the electrically heated gas in the center of the arc and the water cooled walls by thermal conduction. The arc is usually cylindrically symmetrical for large enough length over diameter ratio (L/D ~15). When the constricted arc is made up of alternate copper and insulator discs as shown in Figure 26, the thickness of the insulating material must be about 1/20 of the thickness of the copper discs to preserve cylindrical symmetry. The energy balance for the constricted arc is then (Ref. 50)

$$\frac{1}{r}\frac{d}{dr}\left[r\lambda\frac{dT}{dr}\right] + \sigma E^2 - Q_r = 0 \qquad (20)$$

where r is the radial distance from the center of the arc, T is the temperature, σ the electrical conductivity, E the field strength and Q_r the radiative energy flux. Assuming that σ and Q_r are known, and that the electric field intensity and temperature as a function of r have been measured, the thermal conductivity may be calculated by integrating

Eq. (20) between the wall and the center of the arc, giving

$$\lambda = \lambda_w + \frac{\int_{T_w}^{T_o} \left[\sigma E^2 - Q_r\right] r \, dr}{r \frac{dT}{dr}} \tag{21}$$

The temperature gradient is measured spectroscopically along a line perpendicular to the axis of the arc. Most authors have used intensity measurement of line radiation assuming the transition probability is known and checked the temperature by measuring the continuum intensity. The temperature measurement relies on the gas being optically thin at the wavelength used for the temperature determination. The population of electronic states and the ionization must also be in equilibrium with the translational temperature of the heavy particles. The rate at which the electronic states are populated by electron-heavy particle collisions must be much larger than the rate at which depopulation by spontaneous radiation occurs in order to reconcile the optically thin criterion with the equilibrium population of electronic states. The first problem is to obtain the intensity of the radiation as a function of r from the integrated intensity measurements. Solution of this problem depends on the cylindrical symmetry of the arc and is discussed below in the section on radiation.

The spectroscope sees the radiation from the volume element along a cord of the arc as shown in Figure 26. The optics are held stationary and the arc is moved perpendicular to the arc axis and another measurement of radiative intensity is made. The intensity from such volume elements as a function of distance from the center of the arc S(x) is thus obtained. The desired quantity is the radiative intensity from a volume element around a point at a radius r from the center of the arc, I(r). An integral relation between the two quantities may be derived by considering the volume element along the cord to be made up of cubic elements at different radii. From the geometry of Figure 26 we have

$$S(x) = \int I(r) \, dy \, . \tag{22}$$

Relating the distance along the cord y to x and r an integral equation

relating S(x) to I(r) is obtained

$$S(x) = \int_x^R \frac{I(r)\, dr}{\left(r^2 - x^2\right)^{1/2}} \quad . \tag{23}$$

Since S(x) and x(r) are known functions, I(r) may be determined analytically using Abel's transformation when radial symmetry is assumed. The inversion process is discussed at length by several authors (Refs. 50, 80) and leads typically to about a 2% error in the temperature profile. The most difficult experimental problem is maintaining the absolute calibration of the intensity measurement. This can be done by, for instance, comparison with a standard source such as a calibrated carbon filament.

The second problem is to relate the intensity radiated by a volume element to its temperature. The type of radiation (line, molecular band, continuum) used for the temperature measurement depends largely on the temperature and species present. The radiative intensity from line radiation is better known than other forms of radiation. Radiative intensity versus temperature may also be constructed for other types of radiation such as continuum and molecular radiation. However, theory may be relied on only for the temperature dependence of other types of radiation, and the absolute value should be checked by measuring atomic or ionic lines in the same frequency range.

The absolute intensity per unit volume and solid angle of an atomic line is given by (Ref. 80)

$$I = \frac{C}{4\pi} A_{nm} h\nu_{nm} N_a \frac{g_n}{Q(T)} e^{-E_n/RT} \frac{\text{erg}}{\text{sec cm}^3\, d\Omega} \tag{24}$$

where C is the speed of light, ℓ the length of the source (volume element), h the Planck constant, N_a the number density of atoms, Q the partition function of the atomic specie, g_n the statistical weight of the upper state of the transition, E_n the energy of the upper level, ν_{nm} the wave number of the line, and A_{nm} the transition probability.

The number of atoms and the partition function are known rather well (~2%) for an equilibrium gas from the usual thermodynamic

calculations. The transition probabilities have large uncertainties. However, large uncertainties in the transition probabilities (~20%) lead to small uncertainties in the gas temperature (Ref. 50). Equation (24) may be used to obtain a table of intensity per unit volume versus temperature.

The radiative loss term in Eq. (20) is usually determined by integrating the measured radiation from the arc, the assumption again being that the gas is optically thin. Early arc measurements indicated that over much of the temperature range (N_2, 4000-7000°K; Ar, 6000-10,000°K) the radiation is not large and the optically thin assumption is adequate. However, recently the group at Avco showed that applying appropriate radiation corrections to Maecker's data removed the anomalous current dependence of the nitrogen thermal conductivity. In addition, the experimental thermal conductivities from Maecker's experiment are in surprisingly good agreement with recent transport property calculations. The large scatter in the Maecker arc runs occurs near the dissociation peak (~7000°K). Both the Maecker and Avco data also show a marked current dependence (~ a factor of three between 250 amp runs and 17 amp runs) above 8000°K as a free-free and free-bound continuum becomes important. Another approach was taken by Asinovskii and Kirillin (Ref. 49) where the thermal conductivity of argon was determined in arcs of different diameters. As the arc diameter was reduced the thermal conductivity fell closer to the theoretical value. The thermal conductivity versus arc radius from this experiment is shown in Figure 27 along with the theoretical value (see argon data review, Figure 7). Also shown in Figure 27 are the argon data of Avco and that of Emmons and Knopp. The high current data of the first two investigators lies much higher than the low current data of Emmons and Knopp, indicating the importance of radiative transport.

High arc currents mean high centerline temperatures. The vacuum ultraviolet becomes more important at the high temperatures because the continuum cutoff is higher and the higher energy levels radiate more. The radiative transport term Q in Eq. (20) then includes absorption. Since the temperature is known as a function of position, the radiative intensity may be calculated at each position in the arc using the equation of transfer

$$I_\nu(r) = \int_r^{r'} a_\nu B_\nu e^{-\tau_\nu} dr' \qquad (25)$$

where r' is the radial distance from the element of fluid under

consideration to the source of the radiation, a_ν is the absorption coefficient, B_ν is the Planck function and τ_ν is the optical path between the point at which I(r) is being calculated and the source point r',

$$\tau_\nu = \int_r^{r'} a_\nu \, dr . \tag{26}$$

The absorbed radiation in the volume element is the previously calculated intensity (Eq. 25) times the spectral absorption coefficient integrated over all solid angles and all frequencies. The net flux of energy Q which must be inserted into the energy equation (20) is the difference between the absorbed energy and the radiated energy

$$Q(r) = \int_0^\infty \left\{ a_\nu \int_0^{4\pi} I_\nu \, d\Omega - 4 a_\nu B_\nu \right\} d\nu . \tag{27}$$

When the usual optically thin approximation is applicable a_ν is small and recalling that

$$I_\nu = a_\nu B_\nu , \tag{28}$$

Q(r) in Eq. (20) reduces to the usual form,

$$Q(r) = 4\pi \int_0^a I_\nu \, d\nu \tag{29}$$

since the first term is second order in a_ν.

The major problem is to obtain values of spectral absorption coefficient a_ν and optical path τ_ν at the far ultraviolet wavelengths. Theoretical calculations are available from many sources. Experimentally, however, plasma radiation has not been measured below 2000Å. The major reason is that the vacuum ultraviolet is absorbed in the cool outer layer of the arc. Indications are that continuum ultraviolet should be significant down to about 800Å (Refs. 81, 82, 83, 84, 85, 86) in the gases and temperatures of current interest. Calculations of

radiative losses in acoustic waves indicate that ultrasonic absorption may provide information on the vacuum ultraviolet (Refs. 9, 87, 88, 89). The acoustic technique has the advantage of reaching into the hot gas thus avoiding the boundary layer problems of other techniques.

Finally, the electrical heating term σE^2 in Eq. (20) has to be evaluated. The electrical field strength may be measured by two techniques. First, the length of the arc is increased by moving the electrodes a known distance, keeping the total arc current constant. The slope of the resulting voltage drop versus arc length is the electrical intensity. Accurate measurements require that the voltage drop in the region of cathode and anode be a reasonably small faction of the voltage drop in the central portions of the arc. A second method is used in arcs made up of copper plates alternated with plates of insulating material. The voltage of successive plates near the center of the arc are plotted versus position and the slope provides the field intensity. Typical errors reported for field intensity measurements are 6%.

The electrical conductivity may in principal be determined from the known temperature distribution, field intensity, and the measured total current. The electrical conductivity as a function of temperature (Ref. 49) may be obtained by inverting the integral equation

$$\frac{1}{2\pi E} = \int_0^R \sigma r \, dr \tag{30}$$

where R is the radius of the arc and σ and r are known functions of T. In practice nonequilibrium and contact potentials in the cooler regions of the arc may lead to errors and calculated values are preferable. The most recent calculation and probably the most reliable are given by Devoto (Ref. 21) for argon. Argon electrical conductivities have been reviewed by others. For nitrogen only theoretical electrical conductivities are available. Electrical conductivity is of interest in its own right as a transport property.

The constricted arc experiment has produced some of the best thermal conductivity measurements obtained to date at extremely high temperatures. Radiative transport in the far ultraviolet is important at about 50% dissociation and once ionization becomes significant. Knowledge of the absorption coefficient is particularly necessary at

temperatures above 1300°K and for work at higher pressures. In the high temperature (13, 000°K < T for argon) and pressure regions (1 atm < p) the radiative term should be evaluated using the optically thick equation of transfer. Theoretical electrical conductivities seem adequate (within ~6%) for argon. However, independent electrical conductivity measurements should be obtained in nitrogen and other gases before the constricted arc is used to measure thermal conductivity. The effect of pressure on electrical conductivity must also be investigated before the constricted arc is extended to higher pressures.

3.3 HEAT TRANSFER

The heat transfer to the end wall after the reflection of a normal shock in the shock tube has been suggested as a means of obtaining thermal conductivity at high temperatures (Refs. 90, 91). The reflection of the incident shock in the first approximation creates a uniform sample of high temperature gas extending about a foot between the reflected shock front and the end wall. In the vicinity of the end wall a thermal boundary layer is set up. Since the boundary layer is thin the pressure is constant throughout and equal to the free stream pressure. The gas temperature and density in the end wall boundary layer varies between the free stream temperature of the reflected shock region and the wall temperature. The end wall geometry is shown in Figure 28. The isotherms (which are also the isopycnals) are shown as lines parallel to the end wall and the reflected shock front. The close spacing of the isotherms near the wall indicates a steepening of the temperature gradient near the wall. Because of the large mass of the shock tube the end wall experiences only a slight temperature rise as it cools the boundary layer gases.

The experimental measurement of heat flux to the end wall of the shock tube is very simple. The heat transfer gauges are 1 cm thick Pyrex or quartz blanks with a thin film platinum thermometer deposited on the surface as shown in Figure 28. The surface temperature of the Pyrex blank is an integral function of the heat flux versus time to the surface of the blank. Therefore, the thin film thermometer response is an integral function of the heat flux versus time. In the usual mode of operation the thin film thermometer is made sufficiently thin so that it measures the Pyrex surface temperature without appreciably perturbing the temperature versus time history in the Pyrex slab.

The ideal end wall response is a step increase in temperature (voltage)upon reflection of the shock. Boundary layer theory shows that the heat flux to the end wall of a shock tube should decrease with the

square root of time as the boundary layer grows (Refs. 92, 93). Heat transfer theory (Ref. 94) indicates that the response of an infinite slat of material subjected to such a heat flux is a step rise in surface temperature. The temperature rise is given by

$$\Delta T_w = \left(\frac{\pi}{\overline{\rho c_p \lambda}}\right)^{1/2} \dot{Q} \sqrt{t} \quad . \tag{31}$$

This in turn is related to the enthalpy gradient at the wall by Eq. (32). The quantities $\overline{\rho c_p \lambda}$ are the properties of the glass blank. In the first approximation the thermal properties of the Pyrex are constant since the temperature rise at the wall is usually of the order of 10°K. A correction for the temperature dependence of $\overline{\rho c_p \lambda}$ has been worked out by Hartunian and Varwig (Ref. 95).

The heat flux from the end wall boundary layer of the shock tube is susceptible to simple analysis. The flow in the boundary layer is described (after a small transient effect) by the one dimensional Navier-Stokes conservation equations of mass, energy momentum, and by the equation of state. The equations of motion are further simplified because the pressure is constant in the boundary layer and viscous dissipation may be neglected. However, convection terms must be retained because of thermal expansion. The early attempts (Refs. 96, 97) to measure thermal conductivity of polyatomic gases on the end wall of the shock tube were in error since they neglected convection and dissociation relaxation.

One of the most frequently misunderstood concepts is the dependence of the flow at the wall on the conditions throughout the boundary layer. The heat flux to the wall may be written in the following way:

$$\dot{Q} = -\lambda_w \frac{\partial T}{\partial x} = -\frac{\lambda_w}{C_p} \frac{\partial h\,(x, t)}{\partial x} \tag{32}$$

where $\dot{Q}$ is the heat flux and λ_w is the thermal conductivity at the wall temperature. The temperature gradient at the wall depends on the solution to the boundary layer equations subject to the free stream and wall boundary conditions. The temperature gradient at the wall therefore reflects the behavior of thermal conductivity throughout the boundary

layer.

The energy equation (8) for the end wall boundary layer may be written as

$$\frac{d}{d\eta}\left(\frac{\rho\lambda}{C_p}\frac{dh}{d\eta}\right) + \eta\frac{dh}{d\eta} = 0 \tag{33}$$

where the distance from the end wall y has been replaced by

$$\eta = \frac{1}{\sqrt{2t}}\int \rho\, dy \tag{34}$$

as the independent variable to reduce the energy equation to the incompressible form. ρ is the density, C_p the specific heat in the boundary layer and λ the thermal conductivity. The enthalpy

$$h = \int_{T_w}^{T_e} C_p\, dt \tag{35}$$

replaces temperature as the dependent variable. The quantity $\frac{\rho\lambda}{C_p}$ is enthalpy dependent coefficient of Eq. (33).

Once $\frac{\rho\lambda}{C_p}$ is a known function of h Eq. (33) is a second order differential equation which has a unique solution

$$h = h(\eta) = h(x,t) \tag{36}$$

if two boundary conditions are specified. The boundary conditions are that the enthalpy at the wall is zero and the enthalpy at the free stream (in the reflected shock region) is known at reflected shock pressures and temperatures.

For any gas where $\frac{\rho\lambda}{C_p}$ is known as a function of the enthalpy and pressure (which are equivalent to temperature and pressure), Eq. (33)

has a unique solution, h (x, t), which may be differentiated to calculate the heat flux to the wall according to Eq. (32). This process may be turned around to obtain the temperature dependence of $\frac{\rho\lambda}{C_p}$ from the measurements of heat flux and reflected shock conditions in the shock tube. Because the heat flux depends on the functional relationship between thermal conditivity and temperature rather than on the value of the thermal conductivity at one temperature, we say that the heat flux is a functional of thermal conductivity.

An integral relation to replace the differential equation (33) which was derived by Jepson (Ref. 92) is discussed in Appendix I. This relation provides the heat flux in terms of the transport properties and the enthalpy range of the boundary layer. The expression is

$$Q^2 = \frac{(1.13)^2}{2t} \int_{h_w}^{h_e} \int_{h_w}^{h'} \frac{\rho\lambda}{C_p} \, dh \, dh' . \tag{37}$$

Equation (37) has been investigated as a technique for determining the temperature dependence of $\frac{\rho\lambda}{C_p}$. It was found that extremely accurate (Ref. 98) heat transfer measurements over a wide range of temperatures were necessary to differentiate between various possible functional dependencies for $\frac{\rho\lambda}{C_p}$ which would give similar values for Q.

However, both theoretically and experimentally, the end wall experiment is suited to determine the density dependence of thermal conductivity. The theory takes advantage of the fact that the excess thermal conductivity is a function of density alone. In Sengers' notation (Ref. 68)

$$\lambda = \lambda_o + A_\lambda \rho + B_\lambda \rho^2 \ln \rho \tag{38}$$

where λ_o is the low pressure thermal conductivity, ρ is the density and A_λ, B_λ are the virial coefficients of the thermal conductivity. Since the virial coefficients are essentially independent of temperature, the heat flux then becomes

$$Q^2 = Q_o^2 + A_\lambda \left[\frac{(1.13)^2}{2t} \int_{h_w}^{h_e} \int_{h_w}^{h_e} \rho \, dh \, dh \right] + B_\lambda \left[\frac{(1.13)^2}{2t} \int_{h_w}^{h} \int_{h_w}^{h} \rho^2 \ln \rho \, dh \, dh \right] + \cdots \quad (39)$$

The first term is the heat flux which may be calculated from the presumably known values of the low pressure thermal conductivity, λ_o, density, ρ, and specific heat, C_p. The other integral is a known thermodynamic quantity except for multiplicative constants indicated by Equations (37) and (38).

Writing the above equation explicitly in terms of the derived quantities A_λ and B_λ from Eq. (38)

$$Q^2 = Q_o^2 + Q_1^2 A_\lambda + Q_2^2 B_\lambda \quad (40)$$

where Q_1 and Q_2 are integrals over functions of density. Measurements of Q at at least two temperatures will allow A_λ and B_λ to be calculated. A_λ and B_λ may not correspond to the theoretical virial coefficients due to the fact that it is difficult to separate the effect of higher order terms in the density expansion. However, the density dependence of $\lambda - \lambda_o$ may be established to about 1%.

For the pressure dependence of thermal conductivity we are interested in free stream temperatures of less than 2000°K. Ionization and dissociation relaxation do not occur at these temperatures. The effects of shock attenuation (Ref. 8) may be avoided by making measurements a few μsecs after the reflection of the incident shock. The thermodynamic state is determined by wave speed measurements close to the end wall. This should be corroborated with a pressure measurement using a fast response pressure gauge.

The calibration of the heat transfer gauge must be carefully monitored for accurate results. The end wall thin film gauges tend to pit and

wear (Ref. 8). A measurement of gauge resistance after each shock is necessary at the high Mach number and presumably at high pressures. Determination of the thermal coefficient of resistivity should be carried out for each gauge. The gauge characteristics have to be calibrated after every four or five shocks. The easiest method of calibration is firing low Mach number shocks in a standard gas such as argon or nitrogen. At the extremes of pressure, $p \sim 10^4$ psi, the gauge may be destroyed during the measurement.

The heat transfer technique provides a simple method to obtain information concerning thermal conductivity at high temperature and pressure. The measured quantity, heat transfer to the wall, depends on the thermal conductivity throughout the boundary layer. Therefore, extremely accurate heat transfer measurements (~0. 1%) are necessary. In addition, care must be taken to avoid relaxation effects such as ionization and dissociation. At low densities the heat transfer method measures the temperature dependence of thermal conductivity. However, the technique is very insensitive to the thermal conductivity at the higher temperatures in the boundary layer.

The heat transfer technique is best suited to measure variations in thermal conductivity which are systematic with temperature. For instance, the heat transfer technique can choose the best parameters for a given potential function. Another area where heat transfer measurements may contribute is in establishing the mixing rules for the thermal conductivity at high temperatures and pressures. Finally, as discussed above, the heat transfer technique is particularly suitable for the determination of the density dependence of thermal conductivity.

3.4 SCHLIEREN TECHNIQUE

Optical techniques may be used to measure density and density gradients in the end wall boundary layer in the shock tube (Ref. 8). This information together with the energy equation for the end wall boundary layer may be used to obtain thermal conductivity. Measurements have been carried out by Smeets (Ref. 99) in air up to 6000°K. During the past year the schlieren system shown in Figure 29 was set up on an end wall of the shock tube for thermal conductivity measurements.

A schematic of the system is shown in Figure 30. A line source of light is made by mounting a mercury flash tube A behind a source slit S_1, located at the focus of the collimating lens B. Parallel light

then passes through the reflected shock region. The arrow (Figure 30) pointing away from the end wall denotes the object which is imaged at the film plane. The boundary payer extends from the foot of the arrow to the head where the free stream begins.

Rays which travel through the head of the arrow remain parallel because the index of refraction is constant in the free stream and corresponds to ρ_e. Rays which pass closer to the end wall travel slower than rays passing through the free stream because the density near the wall is greater than the free stream density. Therefore the wave front D passing through the region close to the end wall is bent toward the wall.

The parallel light from the free stream region is focused by the mirror C at the focal point of C. A knife edge S_2 is put into the field so as to block the undeviated light. The free stream region then appears black on the photographic plate. On the other hand the light traveling through the boundary layer is bent so that it is no longer parallel to the undisturbed light. Consequently, the rays from the image closer to the wall are focused at a point above the knife edge S_2. The boundary layer region therefore appears light on the photograph. This is illustrated in the schlieren photograph of the boundary layer taken (Figure 31) 400 μsec behind a reflected shock in argon. A densitometer trace of the contrast on the negative of the photograph ideally will provide the density gradient in the boundary layer. Putting the density gradient in the linearized energy equation (Ref. 8) for the end wall boundary layer equations allows the thermal conductivity to be determined

$$\lambda = - \frac{C}{\sqrt{2t}} \frac{dC}{dy} C_p \tag{41}$$

where C is the measured contrast on the schlieren photograph.

Quantitative measurements with the usual schlieren system has proved extremely difficult because of effects due to diffraction, light reflection from the end wall, and uneven illumination. These difficulties are largely eliminated by using schlieren interferometry (Refs. 100, 101, 102). The fringes are produced by replacing the end slit S_1 with a wire of small diameter D subject to the condition

$$D \leq 1.2 \lambda / \pi d \tag{42}$$

where f is the focal length of the mirror, λ is the wavelength of the source, and d is the thickness of the boundary layer. The schlieren interferometer described above responds to density, not density gradients, and two differentiations are necessary to determine thermal conductivity from the end wall boundary layer equation.

An interferometric method in which the fringe shift is proportional to the density gradient has been used by Smeets to determine the thermal conductivity of air from measurements of the end wall boundary layer. The experimental arrangement is similar to that pictures in Figure 30. The essential new features are the addition of polarizers and Wollaston prisms between S_1 and the collimating lens B as well as between the focal point (S_2) of the schlieren lens C, and the camera lens G. The Wollaston prisms are placed in symmetrical positions in the source and image parts of the optical system. Further details which improve the performance of the optics are given in the original paper (Ref. 103). Smeets reduced his interferometer measurements by calculating the expected fringe shift from a linearized approximation to Eq. (33). The thermal conductivity at the free stream was determined by making the expected fringe shift agree with the measured fringe shift. Data reduction for this type of experiment is discussed further in Appendix I.

Optical measurements on the end wall of the shock tube are one of the few ways of obtaining high temperature thermal conductivities. In addition, the pressure in the reflected region of the shock tube may be varied easily. However, measurements must be made at long times ($T > 400$ μsec) and low pressures so that the boundary layer is suffiently thick to be resolved optically. Long times are also necessary to allow relaxation due to dissociation and ionization to occur and the boundary layer to return to equilibrium. The pressure and temperature in the reflected region can vary up to 20% in times of the order of 100 μsec due to attenuation and boundary layer interaction. Therefore the pressure and temperature should be measured simultaneously with the optical measurements.

3.5 ULTRASONIC TECHNIQUE

The ultrasonic technique has recently been developed for the determination of transport properties of high temperature gases. The absorption of ultrasonic waves in a gas is well understood and depends on many factors. In monatomic gases at low temperatures the sound absorption depends on thermal conductivity and viscosity and is given by

$$\alpha_c = \frac{1}{2} \frac{\omega^2}{pc\gamma} \left[\frac{4}{3} \eta + \frac{\gamma - 1}{C_p} \lambda \right] \tag{43}$$

where ω is the angular frequency of the sound wave and the other quantities are previously defined. Since viscosity is much easier to measure than thermal conductivity, measured values of viscosity and sound absorption will provide a useful technique for the measurement of thermal conductivity. This technique has been applied in helium and argon up to temperatures of about 11,000°K.

Sound absorption in mixtures of monatomic gases (Refs. 9, 104) depends on the diffusion coefficients as well as thermal conductivity and viscosity of the mixture. The absorption is then given by

$$\alpha = \alpha_c + \alpha_D \tag{44}$$

where

$$\alpha_D = \frac{1}{2} \frac{\omega^2}{pc} x_1 x_2 \rho D_{12} \left[\frac{m_2 - m_1}{\bar{m}} + \frac{(\gamma - 1)}{\gamma} \alpha_T \right]^2 . \tag{45}$$

These new quantities are the thermal diffusion coefficient α_T, the mole fractions x_1, x_2, and the atomic masses m_1 and m_2 ($m_1 > m_2$). The size of the α_D compared to α_c depends largely on the size of the term in brackets and the mole fractions. When the α_D is sufficiently large the ultrasonic technique is probably the best technique for measuring diffusion coefficients. Ultrasonic measurement of diffusion coefficients have been made by several authors (Refs. 105, 106, 28), the highest temperature being 5000°K in the reflected region of the shock tube.

Polyatomic gases and inert gases at high temperatures are more complicated because of relaxation processes such as vibration, rotation, electronic excitation and chemical reactions (Ref. 9). At sufficiently low temperatures ($T < 2000$°K for O_2, $T < 5000$°K for N_2) there are no chemical degrees of freedom. Vibration and rotation are the most common internal degrees of freedom. The absorption due to a single internal degree of freedom is given by (Ref. 107)

$$\alpha = \frac{\omega}{2} \frac{c}{c_o^2} \frac{C_p}{C_v} \left[\frac{C_v - C_i}{C_p - C_i} - 1 \right] \frac{\omega \tau'}{1 + \omega^2 \tau'^2} \tag{46}$$

where C_p and C_v are the total or equilibrium of specific heats and C_i is the specific heat of the internal degree of freedom. The relaxation time τ' is related to the true relaxation time of the internal mode τ by the relation

$$\tau' = \frac{C_p - C_i}{C_p} \tau \tag{47}$$

and the true relaxation time is defined by the equation of change (Ref. 15)

$$\frac{dE_i}{dt} + \frac{1}{\tau} \left(E_i - E_{o_i} \right) = 0 . \tag{48}$$

The internal modes also cause a velocity dispersion. The ratio of the low frequency limit sound speed (c_o) to the sound speed at the operating frequency is

$$\left(\frac{c}{c_o} \right)^2 = \left\{ \frac{C_p}{C_v} \frac{C_v - C_i}{C_p - C_i} \frac{\omega^2 \tau'^2}{1 + \omega^2 \tau'^2} \right\}^{-1} \tag{49}$$

where the low frequency sound speed is

$$c_o^2 = \frac{C_p}{C_v} \left(\frac{\partial p}{\partial \rho} \right)_T . \tag{50}$$

The physical content of these equations is that the energy in the internal modes do not follow the energy in the translational modes for all frequencies. The sound wave consists of periodic fluctuations of

the kinetic energy of the gas particles. In the process the internal mode absorbs energy from translation in the high temperature regions and releases energy to translation in the low temperature regions. The rate of the energy exchange between an internal mode with translation is smaller than the rate of translation-translation exchange. The exchange process may be described by the time required for the internal modes to come isothermally (Ref. 107) to equilibrium with translation after a step in translational temperature. This is identical to the relaxation time defined by Eq. (48).

When the period of the wave is much greater than the relaxation time for energy exchange, that is, at low frequencies $\omega\tau << 1$, the sound speed and absorption contain contributions from the internal modes. As the frequency of the sound wave is increased the energy in the internal modes begins to fall off because it becomes more difficult for them to adjust to the changes in translational temperature. Finally, at frequencies so high ($\omega\tau >> 1$) that the period of the sound wave is much shorter than the relaxation time the internal mode exchanges very little energy with the sound wave. The sound wave then propagates as though the slow internal mode were not there and the internal mode is said to be frozen out.

The sound absorption in a gas with internal modes is made up of the classical contributions given by Equations (43) and (45) with the absorption due to relaxation as given by (46) added on. Although relaxation times are of interest in themselves the primary interest is in transport properties. Therefore, the absorption due to internal modes must be subtracted from the total absorption. There are several methods for handling these problems. The simplest technique is simply to operate at sufficiently high frequencies that the internal mode is frozen out. This may be done for vibration, dissociation and ionization with ultrasonic waves in the megahertz region up to 10,000°K. Alternatively the pressure may be varied.

The second approach is to use auxiliary experiments to define the relaxation times and calculate the absorption due to internal modes using Eq. (46). Rotation and electronic excitation must be handled in this fashion. For internal modes which have relaxation times longer than roughly 10^{-8} sec, ultrasonic absorption vs frequency will provide the necessary information. There are many other techniques such as thermal transpiration (Ref. 30), electron beam fluorescence (Ref. 29), as well as various shock tube experiments which can provide relaxation times where necessary.

The experimental problems associated with the ultrasonic technique depend upon the pressure-temperature range of the measurements. At temperatures which may be obtained in conventional furnaces (2000 to 2500°K), the transducers have to be protected by buffer rods of high temperature materials or water-cooling must be employed. Recently developed piezoelectric materials can be used at temperatures up to 1000°C (Ref. 108). At least two acoustic paths must be used to cancel out the effects of thermal boundary layers. At higher temperatures momentary contact must be employed.

The main problem at high pressures is the necessity of using high frequency sound waves since the absorption in general decreases with an increase in pressure. Generally, a change of about 10 db is necessary to obtain a good absorption measurement. Typically, 1-3 MHz give good results at one atmosphere and temperatures of the order of 10,000°K. Since absorption increases with $\frac{f^2}{p}$, increasing the frequency by a factor of $\sqrt{p}$ maintains a constant sound absorption as the pressure is increased. Therefore, extension of the ultrasonic technique to 10^4 atmosphere requires frequencies of the order of 100 MHz.

Arc heated gases have been probed ultrasonically between 5000°K and 20,000°K. The lower temperature limit is imposed because a certain amount of ionization is necessary for arc heating (Ref. 9). It is possible to probe the exhaust of arc heated gases sufficiently down stream to obtain gas temperatures below 5000°K. However, arc exhausts tend to be very turbulent leading to scattering of the ultrasonic wave and acoustic noise from pressure fluctuations. High pressure arcs have high radiation losses which make the power supply and cooling problem more difficult. In addition, at high pressures radiation becomes a significant transport mechanism.

The most promising gas source in the intermediate temperature range 1000°K to 10,000°K is the reflected region of the shock tube. Several gases have been probed in the shock tube and agreement with ultrasonic measurements in other gas sources is within the experimental scatter. It is especially easy to vary pressure in the shock tube at high temperatures. The major drawbacks are the impulse the ultrasonic transducers receive from the shock front, and the presence of acoustic noise from boundary layer interaction (Ref. 109) and discontinuities in the shock tube. At present ultrasonic measurements in the shock tube are restricted to test gases with at least 50% inert gas because of the noise associated with boundary layer interaction and separation in polyatomic gases.

3.6 ULTRASONIC MEASUREMENTS OF THERMODYNAMIC PROPERTIES

The ultrasonic velocity may be used to obtain the equation of state of moderately dense gases. The velocity of sound measured as a function of temperature and pressure is sufficient to determine the compressibility if independent values of C_p and C_v are known (Ref. 110). The sound speed is given by

$$c^2 = \gamma \left(\frac{\partial p}{\partial \rho}\right)_T \tag{51}$$

Substituting the usual equation of state

$$p = z \rho R T \tag{52}$$

into (51) and integrating, we obtain

$$z\,(p_1\ T_1 = \frac{p_1}{R T_1 \int_0^{p_1} \left(\frac{\gamma}{c^2}\right) dp} . \tag{53}$$

The experimental values of γ (from C_p and C_v) and c^2 as a function of pressure may be numerically integrated to obtain z from Eq. (53).

When experimental determinations of γ are not available from other sources a theoretical value of γ may be used as a first guess. The estimated $\gamma(p)$ is then used to obtain a first approximation to z(T) using Eq. (53). The resulting z(T) then may be used to obtain improved values of γ from the thermodynamic formulas (Ref. 111) for C_p and C_v ;

$$C_v - C_v^{\,o} = -T \int_0^P \left[2\rho R \frac{\partial z}{\partial T} + \rho R T \frac{\partial^2 z}{\partial T^2}\right] d\left(\frac{1}{p}\right) \tag{54}$$

and

$$C_p - C_p^{\,o} = C_v - C_v^{\,o} - R + \frac{T \left[\rho R T \frac{\partial z}{\partial T} + 2 pR\right]^2}{\rho^2 z R T} \tag{55}$$

where C_p^o and C_v^o are the ideal gas specific heats. This process may be repeated until the best approximations to γ and z are obtained.

Sound speed has been used for thermodynamic property measurements by many investigators (Ref. 55). Using the technique available at Panametrics the thermodynamic properties of gases may be measured up to about 2000°K at pressures up to about 10^3 atm.

A typical experimental apparatus which has been used up to about 100 atm is shown in Figure 32. Some room temperature measurements taken in this apparatus are shown in Figure 33. The difference between the increasing and decreasing pressure data points is due to systematic deviation in temperature due to compression and expansion. The temperature difference is about 0.8°K. The sound speed measurements are compared to recent measurements by other investigators in Figure 34. The sound speed measured by El-Hakeem (Ref. 112) is lower than the Panametrics measurements by an amount which is roughly what one would expect based on the temperature difference of the measurements and the rule of thumb $c \sim \sqrt{\gamma RT}$.

3.7 LASER ACOUSTICS

When electromagnetic radiation passes through a medium some of the radiation is scattered as a result of fluctuations in local index of refraction or more properly dielectric constant. The fluctuations (Ref. 113) in dielectric constant, ϵ, are responsible for the scattering of radiation. These fluctuations are caused, in turn, by the fluctuations in density, temperature, and orientation of the molecules. In gases near one atmosphere the fluctuations in the number density, ρ, completely predominate, and the cross section, σ, per unit solid angle and unit volume for polarized light can be shown to be (Refs. 114, 115)

$$\sigma\ (\vec{K}, \Omega) = \left[(\sin\ \phi/4\pi)\ \left(\frac{\partial \epsilon}{\partial \rho}\right)_T\right]^2 K_o^4$$

$$\times \int d^3r\ dt\ \Delta\rho\ (\vec{r}, t)\ \Delta\rho\ (0, 0) \qquad (56)$$

$$\times \exp i\ (\vec{K} \cdot \vec{r} - \Omega t)\ ,$$

where $\Omega/2\pi$ is the frequency shift of the scattered radiation, ϕ is the angle between the electric field of the incident radiation and the wave vector $\vec{K}_s$ of the scattered radiation, $\vec{K}_o$ is the wave vector of the incident radiation in the medium, and $\Delta\rho$ is the fluctuation of the number density about its average ρ_o. The wave vector of the fluctuation being observed, $\vec{K}$, is the vector difference between $\vec{K}_s$ and $\vec{K}_o$, and its magnitude is given by $K = 2K_o \sin(\theta/2)$, since $K_s \approx K_o$. The correlation function for the fluctuations in density is related to the classical limit of Van Hove's density-density correlation function (Ref. 116), G(r, t), by

$$< \Delta\rho\ (\vec{r},\ t)\ \Delta\rho\ (0,\ 0) > \ = \ \rho_o\ (G(r,\ z) - \rho_o). \tag{57}$$

Van Leeuwen and Yip (Ref. 117) have shown that for a dilute gas

$$< \Delta\rho\ (\vec{r},\ t)\ \Delta\rho\ (0,\ 0) > \ = \ \rho_o \int d^3p\ f\ (\vec{r}, \vec{p}, t) \tag{58}$$

where $f\ (\vec{r}, \vec{p}, t)$ is the particle distribution function satisfying the linearized Boltzmann equation subject to the initial condition

$$f\ (\vec{r}, \vec{p}, o) \ = \ (2\pi\ mk\,T)^{-3/2}\ \exp\ (-p^2/2\ mk\,T)\ \delta\ (r). \tag{59}$$

Here m is the mass of the molecule, k is the Boltzmann constant, and p is the particle momentum. It follows that $\sigma\ (K, \Omega)$ is proportional to the double Fourier transform of the space and time distribution function for the gas molecules. In the laser scattering experiment the scattered intensity vs wavelength is interferometrically determined, where the trace that is recorded is the convolution of $\sigma\ (K, \Omega)$ with the instrument profile of the interferometer.

The form of the spectrum of the scattered light is determined by a parameter (Ref. 118) y, which is a measure of the ratio of the wavelength of the fluctuation observed by the collision mean free path

$$y \ = \ (2\pi/K)\ /\ (2\pi/a)\ (2\,k\,T/m)^{1/2}, \tag{60}$$

where α is an effective collision frequency. When $y > 10$ the hydrodynamic description is very good. The spectrum consists of three distinct, nonoverlapping lines: an unshifted component due to nonpropagating fluctuations (the Rayleigh component) and a symmetrically shifted doublet due to the scattering from thermally excited sound waves (Brillouin scattering). The frequency of ω of the Doppler shifted Brillouin components is related to the sound velocity by

$$c = \omega/K . \tag{61}$$

As a result of acoustic attenuation the Brillouin lines are broadened and assume a Lorentzian shape with half intensity widths

$$\Delta\omega_B = 2TK^2 . \tag{62}$$

T is proportional to the sound attenuation coefficient and is given as

$$T = \frac{1}{2}\left(\frac{\frac{4}{3}\eta + \eta'}{\rho} + \frac{\lambda}{\rho C_p} - \frac{\lambda}{\rho C_v}\right). \tag{63}$$

Since the time decay of thermal fluctuations at constant pressure is determined by the thermal diffusivity $\lambda/\rho C_p$, the Rayleigh line is also broadened and assumes a Lorentzian shape with half intensity width $\Delta\omega_R$ given by

$$\Delta\omega_R = \frac{2\lambda}{\rho C_p} K^2 . \tag{64}$$

Theoretical considerations from the thermodynamics of fluctuations (Ref. 113) relate the area under the Rayleigh component to the total area under the Brillouin lines to the specific heats ratio, C_p/C_v. However, since the central line and the Brillouin lines all have Lorentzian shape, the area ratio becomes just the ratio of intensities, $I_R/2I_B$.

$$\frac{I_R}{2I_B} = \frac{C_p - C_v}{C_v} \tag{65}$$

the Landau-Placzek ratio (Ref. 119) for intensities. Figure 35 illustrates the configuration of the scattered intensity spectrum.

In the region $2 < y < 10$, the three lines begin to overlap since their widths increase faster with K than does their splitting; yet, the spectrum can still be described rather accurately by the hydrodynamic equations. However, when $y < 2$ the hydrodynamic equations no longer adequately describe the spectrum. A kinetic theory must now be used to take into account the effects of the distribution in molecular velocities.

It will prove to be instructive to examine a model laser gas scattering system such as the one illustrated in Figure 36. As will be shown, the wavelength of incident light must be strongly monochromatic. The required high spectral purity can be obtained from a single mode stabilized laser. Light from the laser scattered in the scattering cell is collimated by a conical lens, however, since the scattering amplitude is small the unscattered light is occluded by an aperture in the diagonal mirror. The unscattered light is detected and fed back to a servo control system for the single mode laser. The scattered light is reflected by the diagonal mirror into a sweeping interferometer, phototube detector and pulse amplifier-discriminator.

In order to gain some notion as to the refinements necessary for the experimental apparatus consider the test gas to be argon at NTP and assume for purposes of simplicity that $y = 10$. Argon at NTP has a mean free path of 10^{-5} cm so that for $y = 10$ the fluctuation wavelength becomes 10^{-4} cm. Now $K = \frac{4\pi}{\lambda_o} \sin \frac{\theta}{2}$, giving

$$\sin \frac{\theta}{2} = .3165 \tag{66}$$

for the He-Ne laser line at 6330Å and

$$\theta = 36.9^{o} \tag{67}$$

as the scattering angle. $\Omega = 2.976 \times 10^{15}$ radians/sec corresponding to $\lambda_o = 6330$Å. From $\omega = Kc$ for the Brillouin line shift

$$\omega = 2.03 \times 10^{9} \text{ radians/sec} . \tag{68}$$

The ratio of center frequency to the frequency shift

$$\frac{\omega}{\Omega} \simeq 1.5 \times 10^{6} . \tag{69}$$

In order to unambiguously detect frequency shift of these magnitudes optical instruments with resolving powers of at least $10 \frac{\omega}{\Omega}$ are required, say, of the order of 2×10^{7}. This high degree of optical resolution is obtained, for example, in Fabry-Perot interferometers.

Backscattering relaxes somewhat the resolving power requirement since for backscatter $K = \omega K_{o}$. Here $y = 3$, however, so that analysis of scattering intensity may well require recourse to kinetic theory calculations. $\omega = 2 K_{o} c$ gives

$$\omega = 6.41 \times 10^{9} \tag{70}$$

which relaxes the resolving power requirement by a factor of 3.

The laser acoustic method requires sensitive optical and electronic measurements. Since optics must be kept free from vibration, elaborate precautions may be required. The scattered light intensity is very low and thus long time counting is required to extract the scattered signal from the background. As the gas density is increased the amount of scattered light increases. From this point of view the experiment becomes easier to perform as the gas density is raised (see Equations 56 and 57).

As pointed out by several investigators, the laser acoustic technique may be used to measure sound speed, ultrasonic absorption and thermal diffusivity. This means that both viscosity and thermal conductivity are completely determined. With the usual ultrasonic technique only the sum of these properties is determined. In addition, if the gas temperature is known, the sound speed provides a check on the thermodynamic properties of the gas (i.e., the compressibility). Internal modes which are not coupled to translation (slow modes such as vibration) are easily frozen out because with visible light and at the smallest practical scattering angles the ultrasonic frequency is of the order of 100 MHz. Since laser acoustic technique provides information concerning the fluctuations of density in a temperature in the gas, this

may be the most useful result to be obtained from the laser scattering experiment (Ref. 120).

3.8 ULTRASONIC ABSORPTION MEASUREMENTS IN HELIUM

The acoustic experiments were performed during the past year in the reflected region of the shock tube. The temperature range of the experiments was from 500°K to 3000°K at pressures of 1/2 to 2 atmospheres. Frequencies of 1 to 2 MHz were employed. The measurements were made both in the 2-1/2" by 1-3/4" shock tube and a boundary layer stripper which gave 1" and 1-1/2" acoustic path lengths. The basic measurement consists of measuring the amplitude across two different path lengths of test gas. Assuming the boundary layer thickness is the same on each of the side walls of the test section, a two path measurement allows the boundary layer to be canceled out.

A diagram of the ultrasonic apparatus is shown in Figure 37. A shock wave is generated in 10 to 20 mm Hg of helium using 400 to 500 psi of helium or hydrogen as the driver gas. The time of arrival of the shock front is measured by two side wall heat transfer gauges and an end wall heat transfer gauge. The first side wall heat transfer gauge provides a reference time for the other events which occur later. The signal from this gauge is fed into a three channel delay generator. One channel triggers the dual beam oscilloscope displaying the responses of the downstream heat transfer gauges. The other channels trigger the rf oscillator and the readout oscilloscope for the ultrasonics. The use of delays allows an expanded time base to be used on the oscilloscopes improving the accuracy of the time measurements. The trigger of the ultrasonic oscillator is also delayed to send the ultrasonic pulse through the most uniform part of the reflected shock region.

There are several calibrations involved in the data reduction. The time bases of the oscilloscope are calibrated using subharmonics of a local radio station (WBZ). The amplitude calibrations (voltage scale) are accomplished by transmitting pulses through a known gas, such as He or Ar, at room temperature. The gas and the pressure are chosen to reproduce the signal amplitude obtained in the high temperature gas as closely as possible. The transmitted amplitudes in the 300°K tests calibrate the activity of the ultrasonic transducers. The sound speed at 300°K is known to within 0.1%. Therefore, the transit time and the measured path length are used to calibrate out any systematic delays in the transmit-receive system.

The frequencies of the ultrasonic wave are 1 MHz and 1.89 MHz. The sound absorption increases with temperature and follows the absorption calculated from the theoretical transport data of Emmons and Lick rather closely (within 4%). Since the Emmons and Lick thermal conductivity and viscosity are based on the most recent He-He interaction potentials, these measurements confirm the high cross sections at close interaction distances.

The reduction of the ultrasonic measurements to individual transport properties may be accomplished by several methods. The optimum technique depends on the type of auxiliary information that is available. In the present case a Eucken factor was used based on the experimental data and theory. At the lower temperature, $T < 2000^{\circ}C$, the viscosity measured by other techniques could have been used to obtain thermal conductivities to clear up the large discrepancy between various measured values. However, since the contribution of thermal conductivity to the absorption is only 30% of the contribution of viscosity, the absorption data were reduced to viscosity. The viscosity vs temperature is shown in Figure 38.

The viscosity from several sources is shown in Figure 34 in addition to the ultrasonic measurements. Both of the measured values (Guevara and Wageman, authors) fall close to the theoretical values of Lick and Emmons indicated by the solid line. Earlier ultrasonic measurements up to $1300^{\circ}K$, which were obtained in a muffle tube, are systematically higher than the present shock tube measurements. The calculated viscosities of Amdur and Mason are within a few percent up to $1500^{\circ}K$. However, at $2500^{\circ}K$ the Amdur and Mason viscosities are ~16% higher than the more recent viscosity values indicated on the graph. There are indications in Figure 34 that the Lick and Emmons values are too low by about 2% over much of the temperature range indicated in Figure 24 and that the discrepancy increases at the higher temperatures.

Since helium is a monatomic gas, a potential which gives low viscosity values also predicts low thermal conductivity values. The ultrasonic technique is very sensitive to this type of error. The absorption due to thermal conduction must be subtracted from the total absorption to obtain the viscous losses. Therefore the disagreement between theory and experiment is approximately doubled. The comparison between theory and experiment is more obvious in the deviation charge for the viscosity of helium (Figure 1). The measured viscosities are 4% higher than theory at $200^{\circ}K$, within 1% at intermediate temperatures ~$500^{\circ}K$, and appear to systematically deviate at the higher temperatures.

Similar deviations are apparent (Figure 2) between the theory of Lick and Emmons and the measured values of thermal conductivity above 1000°K. Extrapolation of the deviations indicated on the charts to 6000°K would put the transport properties of Lick and Emmons about 15% lower than experiment. Further measurements using the heat transfer and ultrasonic techniques could test the validity of this small uncertainty. At any rate, the above discussion illustrates how errors can accumulate when potential functions are used to extrapolate transport properties much beyond the range of experimental verification.

REFERENCES

1. Hirschfelder, J. O., Curtiss, C. F., Bird, R., Molecular Theory of Gases and Liquids, John Wiley and Sons, New York (1954).

2. Chapman, S., Cowling, T. G., The Mathematical Theory of Non-Uniform Gases, Cambridge University Press (1960).

3. Devoto, R. S., Li, C. P., Transport Coefficients of Partially Ionized Helium, SUDAAR No. 291.

4. Amdur, I., Jordan, E., "Elastic Scattering of High Energy Beams: Repulsive Forms", (in Molecular Beams, J. Ross, Ed.) Interscience Publishers (1966).

5. Amdur, I., Mason, E. A., "Properties of Gases at Very High Temperatures", Phys. Fluids 5, 370 (1958).

6. Carnevale, E. H., Lynnworth, L. C., Larson, G. S., "Ultrasonic Determination of Transport Properties of Monatomic Gases at High Temperatures", J. Chem. Phys. 46, 3040 (1967).

7. Knopp, C. F., Cambel, A. B., "Experimental Determination of the Thermal Conductivity of Atmospheric Argon Plasma", Phys. Fluids 9, 939 (1966).

8. Carey, C., Carnevale, E. H., Marshall, T., "Experimental Determination of the Transport Properties of Gases, Part II Heat Transfer and Ultrasonic Measurements", AFML-TR-65-141 (Wright-Patterson, 1966).

9. Carnevale, E. H., Larson, G., Lynnworth, L. C., Carey, C., Panaro, M., Marshall, T., "Experimental Determination of Transport Properties of High Temperature Gases", NASA CR-789 (1967).

10. Weissman, S., "Estimation of Diffusion from Viscosity Measurements: Polar and Polyatomic Gases", J. Chem. Phys. 40, 3397 (1964).

11. Weissman, S., "Prediction of Mutual Diffusion Coefficients from Thermal Conductivity Data", Advances in Thermophysical Properties at Extreme Temperatures and Pressures, ASME (1965).

12. Wang Chang, C. S., Uhlenbeck, G. E., DeBoer, Jr. "The Heat Conductivity and Viscosity of Polyatomic Gases", in Studies in Statistical Mechanics, Volume II, DeBoer, Jr., Uhlenbeck, G. E., John Wiley and Sons, New York (1964).

13. Mason, E. A., Monchick, L., "Heat Conductivity of Polyatomic and Polar Gases," J. Chem. Phys. 36, 1622 (1962).

14. Monchick, L., Yun, K. S., Mason, E. A., "Formal Kinetic Theory of Transport Phenomena in Polyatomic Gas Mixtures", J. Chem. Phys. 39, 654 (1963).

15. Monchick, L., "Small Periodic Disturbances in Polyatomic Gases", Phys. of Fluids 7, 882 (1964).

16. Monchick, L., Pereira, A. N. G., Mason, E. A., "Heat Conductivity of Polyatomic and Polar Gases and Gas Mixtures", J. Chem. Phys. 42, 3241 (1965).

17. Saxena, S. C., Seksena, M. P., Gambhir, R. S., "The Thermal Conductivity of Non-Polar Polyatomic Gases", Brit. Jour. Appl. Phys. 15, 343 (1964).

18. Hirschfelder, J. O., "Heat Transfer in Chemically Reacting Mixtures", J. Chem. Phys. 26, 274 (1957).

19. Yos, J. M., "Transport Properties of Nitrogen, Hydrogen, Oxygen and Air to 30,000°K", AVCO RAD-TM-63-7 (1963).

20. Sherman, M. P., "Transport Properties of Partially Ionized Nitrogen I. The Collision Integrals", General Electric Space Sciences Lab. T1 R655 D43 (1965).

21. Devoto, R. S., "Transport Coefficients of Partially Ionized Argon", Phys. Fluids 10, 354 (1967).

22. Burhorn, F., "Berechnung und Messung der Warmeleit fähigkeit vo Stickstoff bis 13,000°K", Z. Phys. K 155, 42 (1959).

23. Maecker, H., Wienecke, R., "Experimental and Theoretical Studies of the Properties of N_2 and Air at High Temperatures", AGARD Conference (1962).

24. Present, R. D., Kinetic Theory of Gases, McGraw-Hill, New York (1958).

25. Tsederberg, N. V., Thermal Conductivity of Gases and Liquids (Trans.) M. I. T. Press (1965).

26. Walker, R. E., Westenberg, A. A., "Molecular Diffusion Studies in Gases at High Temperatures, I. The Point Source Technique", J. Chem. Phys. 29, 1139 (1953).

27. Westenberg, A. A., deHass, N., "Gas Thermal Conductivity Studies at High Temperature", Johns Hopkins Appl. Phys. Lab. CM-1004 (1961).

28. Carnevale, E. H., Private Communication, NASA Quarterly (1967).

29. Miller, D. R., Andres, R. P., "Rotational Relaxation of Molecular Nitrogen", J. Chem. Phys. 46, 3418 (1967).

30. Malinauskas, A. P., "Thermal Transpiration. Rotational Relaxation Numbers for Nitrogen and Carbon Dioxide", J. Chem. Phys. 44, 1196 (1963).

31. Carnevale, E. H., Carey, C., Larson, G., "Ultrasonic Determination of Rotational Collision Numbers and Vibrational Relaxation Times of Polyatomic Gases at High Temperatures", J. Chem. Phys. (to be published 1967).

32. Sengers, J. V., "Thermal Conductivity and Viscosity of Simple Fluids", J. Heat Mass. Transfer 3, 1103 (1965).

33. Reynes, E. G., Thodos, G., "Viscosity of Helium, Neon and Nitrogen in the Dense Gaseous Region", J. Chem. Eng. Data 11, 137 (1967).

34. Guevara, F. A., Wageman, W. E., "Measurement of Helium and Hydrogen Viscosities to 2340°K," Los Alamos Scientific Laboratory Report LA-3319, UC-34, Physics TID 4500 (43rd Ed.) (1965).

35. Lick, W. J., Emmons, H. W., Transport Properties of Helium From 200 to 50,000°K, Harvard University Press (1965).

36. Phillipson, P. E., "Repulsive Interaction Between Two Ground-State Helium Atoms," Phys. Rev. 125, 1981 (1962).

37. Mason, E. A., Rice, W. E., "The Inter-Molecular Potentials of Helium and Hydrogen," J. Chem. Phys. 22, 522 (1954).

38. Timrot, D. L., Umanskii, A. S., "Investigation of the Thermal Conductivity of Helium in the Temperature Range 400-2400°K," High Tem. 3, 345 (1965).

39. Blais, N. C., Mann, J. B., "Thermal Conductivity of Helium and Hydrogen at High Temperatures," J. Chem. Phys. 32, 1459 (1960).

40. Saxena, S. C., Acrawrl, J. P., "Thermal Conductivity of Polyatomic Gases and Relaxation Phenomena," J. Chem. Phys. 35, 2107 (1961).

41. Makavetskas, R. A., Popov, V. N., Tsederberg, N. V., "Experimental Study of Viscosity of Helium and Nitrogen," High Temp. 1, 169 (1963).

42. Ho, C. Y., Leidenfrost, W., "Precise Determination of the Thermal Conductivity of Helium Gas at High Pressures and Moderate Temperatures," Sixth Conf. on Thermal Conductivity, Dayton, Ohio (1966).

43. Collins, D. J., Greif, R., Bryson, A. E., "Measurements of the Thermal Conductivity of Helium in the Temperature Range 1600 to 6700°K," Int. Jour. of Heat and Mass Trans. 8, 1209 (1965).

44. Snider, R. F., Curtiss, C. F., "Kinetic Theory of Moderately Dense Gases," Phys. Fluids 1, 122 (1958).

45. Dymond, J. H., Rigby, M., Smith, E. B., "Two Parameter Intermolecular Potential Energy Functions for Simple Molecules," Phys. Fluids 9, 1222 (1966).

46. Munn, R. J., Smith, F. J., "Interaction Potential of the Inert Gases II," J. Chem. Phys. 43, 3999 (1965).

47. Hanley, H. J. M., "Comparison of the Lennard-Jones, Exp-6, and Kihara Potential Functions from Viscosity Data of Dilute Argon," J. Chem. Phys. 44, 4219 (1966).

48. Emmons, H. W., "Arc Measurement of High Temperature Gas Transport Properties," Phys. Fluids 10, 1125 (1967).

49. Asinovskii, E. I., Kirillin, A. V., "Experimental Determination of the Thermal Conductivity of an Argon Plasma," High Temp. 3, 632 (1965).

50. "Theoretical and Experimental Studies of High Temperature Gas Transport Properties," AVCO RAD-TR-65-7 (1965).

51. Mathur, S., Saxena, S. C., "Relations Between Thermal Conductivity and Diffusion Coefficients of Pure and Mixed Polyatomic Gases," Proc. Phys. Soc. 89, 752 (1966).

52. Parker, J. G., "Rotational and Vibrational Relaxation in Diatomic Gases," Phys. of Fluids 2, 449 (1959).

53. Trautz, M., Zink, R., "Die Reibung, Warmeleitung und Diffusion in Gasmischungen XII. Gasreibung bei hohören Temperaturen," Ann der Physik 7, 427 (1930).

54. Trautz, M., Binkele, H. E., "Dei Reibung, Warmeleitung and Diffusion in Gasmischungen VIII Dei Reibung des H_2, He, Ar und ihrer binären Gemische," Ann der Physik 5, 561 (1930).

55. Hilsenrath, J., Beckett, C. W., Benedict, W. S., Fano, L., Hoge, H. J., Masi, J. F., Nuttall, R. L., Touloukian, Y. S., Woolley, H. W., Tables of Thermodynamic and Transport Properties, Pergamon Press, New York (1960).

56. Tsederberg, N. V., Popov, V. W., Andre' ev, I. I., "An Experimental Study of the Viscosity of Hydrogen," Thermal Engineering (Russian) 4, 117 (1965).

57. Israel, S. L., Hawkins, T. D., Slater, R. T., Hyman, S. C., "Hydrogen Thermal Conductivity from 2000 to 4600°F," United Nuclear Corp., UN-5082 (1962).

58. Bargaftik, N. B., Zimina, N. Kh., "Thermal Conductivity of Nitrogen at High Temperatures," High Temp. 2, 782 (1964).

59. Schmitz, G., Patt, H. J., "Die Bestimmung von Material funktionen eines Stickstoff plasmas bei Atmosharendruck bis 15,000°K," Z. Physik, 171, 449 (1963).

60. Ter Horst, D. Th. J., Pflanz, H. M., "Thermal Conductivity from Power and Center Temperatures of an Arc," Z. Physik 198, 502 (1967).

61. "Evaluation of High Temperature Gas Transport Properties," NASA CR-575 (1966).

62. Hing Yi Lo, Carroll, D. L., Stiel, L. I., "Viscosity of Gaseous Air at Moderate and High Pressures," J. Chem. Eng. Data 11, 541 (1966).

63. Mathur, S., Saxena, S. C., "Relations Between Thermal Conductivity of Pure and Mixed Polyatomic Gases," Proc. Roy Soc. 89, 753 (1966).

64. Hirschfelder, J. O., "Heat Transfer in Chemically Reacting Mixtures," J. Chem. Phys. 26, 274 (1957).

65. Eckert, E. R. G., Irvine, T. F., "A New Method to Measure Prandtl Number and Thermal Conductivity of Fluids," J. Appl. Mech. 24, 25 (1957).

66. Smeets, G., "Bestimmung der Warmeleitfahigkeit, heisser Gase aus der Temperaturgrenzchicht in Strosser," Z. Natur forschg. 20a, 683 (1965).

67. Hansen, C. F., "A Review of the Thermodynamic, Transport and Chemical Reaction Rate Properties of High Temperature Air," NACA TN-4359 (1958).

68. Sengers, J. V., "Transport Properties of Compressed Gases," Fourth Tech. Meeting of Soc. Eng., Science (1966).

69. Giddings, J. G., Kao, J. T. F., Kobayashi, R., "Development of a High-Pressure Capillary-Tube Viscometer and its Application to Methane, Propane and Their Mixtures in the Gaseous and Liquid Regions," J. Chem. Phys. 45, 578 (1966).

70. Comings, E. W., Lenoir, J. M., "Thermal Conductivity of Gases at High Pressure," Chem. Eng. Prog. 47, 223 (1951).

71. Senger, J. V., Michels, A., "The Thermal Conductivity of Carbon Dioxide in the Critical Region," in progress in International Researcher Thermodynamic and Transport Properties, Academic Press, New York (1962) (ASME).

72. Zarkova, L. P., Stefanov, B. I., "Experimental Determination of Coefficient and Thermal Conductivity of a Cesium Plasma," Foreign Tech. Div., FTD-MT-65-529 (1965).

73. Saksena, M. P., Saxena, S. C., "Measurement of Thermal Conductivity of Gases Using Thermal Diffusion Columns," Phys. Fluids 9, 1595 (1966).

74. Saxena, V. K., Saksena, M. P., Saxena, S. C., "Measurement of Thermal Conductivity of Gases Using Thermal Diffusion," Indian Journal of Physics 40, 597 (1966).

75. Vargaftik, N. B., Zimina, N. Kh., "Heat Conductivity of Argon at High Temperatures," High Temp. 2, 645 (1964).

76. Matolich, J., Deem, H. W., "Thermal Conductivity for Liquids: High Temperature, Variable-Gap Technique," Sixth Therm. Cond. Symp., Dayton, Ohio (1966).

77. Lynnworth, L. C., Carnevale, E. H., "Ultrasonic Testing of Solids at Elevated Temperatures," Fifth Int. Conf. Nondestructive Testing, Montreal (1967).

78. Carnevale, E. H., Wolnik, S., Larson, G., Carey, C., Wares, G. W., "Simultaneous Ultrasonic and Line Reversal Temperature Determination in a Shock Tube," Phys. Fluids 10, 1459 (1967).

79. Uhlenbusch, J., "Theory and Calculation of Stationary and Quasi-Stationary Cylindrical Arcs," ARL-65-109 (1965).

80. Tourn, R. H., Spectroscopic Gas Temperature Measurement, Elsevier, New York, N. Y. (1966).

81. Morris, J. C., Krey, R. U., Bach, G. R., "The Continuum Radiation of Oxygen and Nitrogen For Use In Plasma Temperature Determination," J. Quant. Spect. Radiat. Trans. 6, 727 (1966).

82. Morris, J. C., Krey, R. U., Bach, G. R., "Bremsstrahlung and Recombination Radiation of Atomic and Ionic Oxygen," Phys. Rev. 159, 159 (1967).

83. Morris, J. C., Garrison, R. L., "Nitrogen Recombination Continuum In The Vacuum Ultraviolet," J. Quant. Spect. Radiat. Trans. 6, 899 (1966).

84. Wende, B., Kontinuier licher Absorptions guerschmitt von Argon in Bogenplasma, Zeit für Physik 198, 1 (1967).

85. Horn, K. P., Wang, H., Bershader, E., "Radiative Behavior of a Shock Heated Argon Plasma Flow," J. Plasma Physics (Cambridge) 1, 157 (1967).

86. Evans, D. L., Tankin, R. S., "Measurement of Emission and Absorption of Radiation by an Argon Plasma," Phys. of Fluids 16, 1137 (1967).

87. Prokofiev, V. A., "Propagation of Forced Plane Compression Waves of Small Amplitude in a Viscous Gas When Radiation is Taken into Account," ARS Supplement, p. 988 (July 1961).

88. Smith, P. W., "Effect of Heat Radiation on Sound Propagation in Gases," J. Acoust. Soc. Am. 29, 693 (1957).

89. Long, H. R., Vincenti, W. G., "Radiation-Proven Acoustic Waves in a Confined Gas," Phys. of Fluids 10, 1365 (1967).

90. Smiley, E. F., "The Measurement of the Thermal Conductivity of Gases at High Temperatures with a Shock Tube. Experimental Results in Argon at Temperatures Between 1000°K and 3000°K," Ph. D. Thesis, Catholic University of America, Washington (1957).

91. Liley, P. E., "Survey of Recent Work on the Viscosity, Thermal Conductivity and Diffusion of Gases and Gas Mixtures," in Thermodynamic and Transport Properties of Gases, Liquids and Solids, (ASME) McGraw-Hill, New York (1959).

92. Jepson, B. M., "Heat Transfer in a Completely Ionized Gas," Magneto Hydrodynamics Laboratory, Department of Mechanical Engineering, M. I. T. Rep. 61-7, AFOSR 1562 (1961).

93. Kemp, N. H., "Calculation of Heat Transfer from Similarity Boundary Layer Equations by a Simple Integral Method," AVCO Everett, R. R. 137 (1962).

94. Vidal, R. J., "Model Instrumentation Techniques for Heat Transfer and Force Measurements in a Hypersonic Shock Tunnel," Cornell Aero. Lab. Rpt. AD-917-A-1 (1956), ASTIA AD-97238.

95. Hartunian, R. A., Varwig, R. L., "On Thin Film Heat Transfer Measurements in Shock Tubes," Phys. of Fluids 5, 169 (1962).

96. Hansen, C. F., "Effects of Variable Thermal Properties in One Dimensional Heat Flow," Phys. of Fluids 8, 2288 (1965).

97. Ahtye, W. F., Tzy-Cheng Penq, "Experimental and Theoretical Study of Heat Conduction For Air Up To 5000°K," NASA TND-687 (1961).

98. Lauver, M. R., "Shock Tube Thermal Conductivity," Phys. Fluids 1, 611 (1964).

99. Smeets, G., "Determination of Hot Gas Thermal Conductivity By Shock Tube Experiments," Proc. of the 5th International Shock Tube Symposium, 28-30, April 1965, AD 484 600.

100. Temple, E. B., "Quantitative Measurement of Gas Density by Means of Light Interference in a Schlieren System," J. Opt. Soc. Am. 47, 91 (1957).

101. Gayhart, E. L., Prescott, R., "Interference Phenomenon in the Schlieren System," J. Opt. Soc. Am. 39, 546 (1949).

102. Brackenridge, J. B., Peterka, J., "Criteria for Quantitative Schlieren Interferometry," Appl. Optics 6, 731 (1967).

103. Bertel, H., "High-Speed Photography of Hypersonic Phenomena by a Schlieren Interferometric Method," Proc. of 5th International High-Speed Photography, Soc. of Motion Picture and Television Engineers, New York, New York (1962).

104. Kohler, M., "Schallabsorption in binären Gasmischungen," Zeit. Für Physik 127, 41 (1949).

105. Holmes, R., Tempest, W., "The Propagation of Sound in Monatomic Gas Mixtures," Proc. Phys. Soc. (London), 75 (1960).

106. Law, A. K., Koronaios, N., Lindsay, R. B., "Effect of Diffusion of Sound in Monatomic Gas Mixtures," Proc. Phys. Soc. (London), 75, 898 (1966).

107. Herzfeld, K. F. and Litovitz, T. A., Absorption and Dispersion of Ultrasonic Waves, Academic Press, New York (1959).

108. Fraser, D. B., Warner, A. W., Journal Appl. Physics, 37, 3853 (1966).

109. Dyner, H. B., "Density Variations Due to Reflected Shock Boundary Layer Interaction," Phys. of Fluids 9, 879 (1966).

110. Goring, G. E., "Determination of Compressibility Factors Using Sonic Velocity Measurements," I. E. and C. Fundamentals 6, 147, (1967).

111. Hirschfelder, J. O., Curtiss, C. F., Bird, R. B., Molecular Theory of Gases and Liquids, John Wiley & Sons, New York (1954).

112. El-Hakeem, A. S., "Velocity of Sound in Nitrogen and Argon at High Pressure," J. Chem. Phys. 42, 3132 (1965).

113. Greytak, T. J., "Spectrum of Light Scattered From Thermal Fluctuations in Gases," Ph. D. Thesis M. I. T. (1966).

114. Rytov, S. M., "Correlation Theory for Rayleigh Scattering Light," J. E. T. P. 6, 401 (1958).

115. Pecora, R., "Doppler Shifts in Light Scattering From Pure Liquids and Polymer Solutions," J. Chem. Phys. 40, 1604 (1964).

116. Van Hove, L., "Correlations in Space and Time on a Borne Approximation Scattering in Systems of Interacting Particles," Phys. Rev. 95, 249 (1954).

117. Van Leeuwen, J. M. and Yip, S., "Derivation of Kinetic Equations for Slow-Neutron Scattering," Phys. Rev. 139, A1138 (1965).

118. Yip, S. and Nelkin, M., "Application of a Kinetic Model to Time-Dependent Density Correlations in Fluids," Phys. Rev. 135, A1214 (1964).

119. Landau, L. and Lifshitz, E. M., Electrodynamics of Continuous Media, Addison-Wesley, Reading, Mass. (1960).

120. Mountain, R. D., "Thermal Relaxation and Brillouin Scattering in Liquids," J. Res. Natl. Bur. Std. 70A, 207 (1966).

DATA REVIEW

121. Trautz, M., Zink, R., Ann der Physik 1, 421 (1934).

122. Wobser, R., Muller, F., Kolloid-Beih 52, 165 (1941).

123. Trautz, M., Binkele, H. E., Ann der Physik 5, 561 (1930).

124. Johnston, H. L., Grilly, E. R., J. Chem. Phys. 14, 233 (1946).

125. Tsederberg, N. V., Popov, V. N., Teploenergetica 5, 61 (1958).

126. Kannuluik, W. G., Carman, E. H., Proc. Phys. Soc. (London), B65, 141 (1923).

127. Zaitsera, L. S., Soviet Phys.-Tech. Phys. 4, 444 (1959).

128. Johanin, P., Wilson, M., Jr., Vodar, B., 2nd Symposium on Thermophysical Properties, ASME, Academic Press 418-33 (1962).

129. Lenoir, J. M., Comings, E. W., Chem. Engrg. Progr. 47 (5) (1951).

130. Trautz, M., Zink, R., Ann Physik 7, 427 (1930).

131. Johnston, H. L., Grilly, R., J. Phys. Chem. 46, 948 (1942).

132. Vasilesco, V., Ann Physik 20, 137 (1945).

133. Bonilla, C. F., Wang, S. J., Weiner, H., ASME Trans. 78, 1285 (1956).

134. Timrot, D. L., Umanskii, A. S., High Temp. 4, 285 (1966).

135. Vines, R. G., J. Heat Trans., ASME 82, 48 (1966).

136. Schäfer, K. I., Reiter, F. W., Z. Electrochem. 61 (1957).

137. Zaitsera, L. S., Soviet Phys-Tech. Phys. 4, 447 (1959).

138. Rothman, A. J., AEC (1954).

139. Schottky, W. F., Z. Electrochem. 56, 889 (1952).

140. Kestin, J., Whitelaw, T. H., Physica 24, 335 (1963).

141. Flynn, G. P., Hanks, R. V., Lemaire, N. A., Ross, J., Project Squid Rpt. BRN-3-P (AD 294401) (1962).

142. Vines, G. R., Keyes, F. G., Project Squid Rpt. MIT-34-P (1963).

143. Michels, A., Sengers, J. V., Van de Klundert, L. J. M., Physica 29, 149 (1963).

144. Trautz, M., Huseini, I., Ann Physik 26, 121 (1934).

145. Trautz, M., Heberling, Ann Physik 20, 118 (1934).

146. Trautz, M., Baumgar, A. B., Ann Physik 2, 733 (1929).

147. Johnston, H. L., McCloskey, K. E., J. Phys. Chem. 44, 1038 (1942).

148. Vargaftik, N. B., Parfenov, L. D., J. Exptl. Theoret. Phys. 8, 189 (1938).

149. Gregory, H., Proc. Roy. Soc. (London), A149, 35 (1935).

150. Yen, K., Phil. Mag. 38, 582 (1938).

151. Sibbitt, W. L., Hawkins, C. A., Solberg, H. L., Trans. Am. Soc. Mech. Engrs. 65, 401 (1943).

152. Nuttall, R. L., Ginnings, D. C., J. Res. Natl. Bur. Std. 58, 271 (1957).

153. Frank, E. V., Z. Electrochem. u. angew, Physik Chem. 55, 626 (1951).

154. Bargaftik, N. B., Olegahchukon, 1. Z. U. N. T. I., No. 6, 7 (1946).

155. Johannin, P., J. CNRS 43, 328 (1958).

156. Shilling, W. G., Laxton, A. E., Phil. Mag. 10, 721 (1936).

157. Vasilesco, V., Ann Physique 20, 292 (1945).

158. Sherrat, G. G., Griffiths, W. J., Phil. Mag. 27, 68 (1939).

159. Taylor, W. I., Johnston, H. L., J. Chem. Phys. 14, 219 (1946).

160. Keston, J., Leidenfrost, W., in Thermodynamic and Transport Properties of Gases, Liquids and Solids, (ASME) McGraw-Hill, New York, New York (1959).

161. Boelter, L. M. K., Sharp, W. H., NACA TN 1912 (1949).

APPENDIXES

I. MATHEMATICAL RELATIONS FOR THE END WALL BOUNDARY LAYER
II. ILLUSTRATIONS

APPENDIX I
MATHEMATICAL RELATIONS FOR THE END WALL BOUNDARY LAYER

The nature of the end wall boundary layer may be seen by a closer examination of the energy equation,

$$\frac{\partial}{\partial \eta}\left(\frac{\rho\lambda}{C_p}\frac{\partial h}{\partial \eta}\right) + \eta\frac{\partial h}{\partial \eta} = 0 \tag{71}$$

where

$$\eta = \frac{1}{\sqrt{2t}}\int \rho\, dy. \tag{72}$$

Dividing each term by $\frac{\rho\lambda}{C_p}\frac{\partial h}{\partial \eta}$ and integrating between the wall $\eta = 0$, and some point at the outer edge of the boundary layer η_1 we get

$$\ln\left[\left(\frac{\rho\lambda}{C_p}\right)_w\left(\frac{\partial h}{\partial \eta}\right)_w\right] = \ln\left[\left(\frac{\rho\lambda}{C_p}\right)_1\left(\frac{\partial h}{\partial \eta}\right)_1\right] + \int_0^{\eta_1}\frac{C_p}{\rho\lambda}\,\eta\, d\eta. \tag{73}$$

Since $\frac{\partial \eta}{\partial \eta} \longrightarrow 0$ as $\eta \longrightarrow \infty$, the first term on the right is a large negative constant if we chose η_1 to be a point near the free stream. The second term on the right is positive and depends on all of the values of $\frac{\rho\lambda}{C_p}$ for all the temperatures in the boundary layer. $\left(\frac{\partial h}{\partial \eta}\right)$ varies almost linearly with η until the edge of the boundary layer is reached. At this point the $\frac{\partial h}{\partial \eta}$ goes to zero as e^{-x^2}. Once $\frac{\partial h}{\partial \eta}$ becomes very small the integral on the right hand of (73) simply cancels the first term without adding significant information about $\frac{\rho\lambda}{C_p}$. Therefore, the enthalpy gradient at the wall contains significant information concerning the thermal conductivity for temperature somewhat less than the free stream temperature.

Equation (73) may be used to obtain a formula for the thermal

conductivity in the outer edge of the boundary layer in terms of the density gradients. This formula is useful for obtaining thermal conductivity from optical measurements on the end wall of the shock tube. A second equation such as (73) may be obtained by integrating to a second point near the outer edge of the boundary layer. Subtracting these equations, one obtains

$$\ln \left(\frac{\rho\lambda}{C_p}\right)_1 \left(\frac{\partial h}{\partial \eta}\right)_1 - \ln \left(\frac{\rho\lambda}{C_p}\right) \left(\frac{\partial h}{\partial \eta}\right) = \int_{\eta_1}^{\eta} \frac{C_p}{\rho\lambda}\, \eta \, d\eta \,. \tag{74}$$

Sufficiently near the outer edge the density, specific heat and thermal conductivity, are essentially the free stream values. In addition, if density is known as a function of enthalpy (the pressure in the boundary layer is constant) $h = h(\rho)$ then

$$\frac{\partial h}{\partial \eta} = \frac{\sqrt{2t}}{\rho_e} \frac{\partial h}{\partial y} = \frac{\sqrt{2t}}{\rho} \left(\frac{\partial h}{\partial \rho}\right)_p \frac{\partial \rho}{\partial y} \,. \tag{75}$$

The new thermodynamic variable $\left(\frac{\partial h}{\partial \rho}\right)_p$ may also be evaluated at the free stream density. Under these conditions the integral on the right hand side of (73) becomes

$$\frac{1}{2} \frac{C_{pe}}{\rho\lambda} \left(\eta_2^2 - \eta_1^2\right) \tag{76}$$

and η_2 may be expressed

$$\eta_2 = \eta_1 + \frac{\rho_e}{\sqrt{2t}} (y_2 - y_1) \,. \tag{77}$$

Finally, Eq. (74) becomes

$$- \ln \left(\frac{\partial \rho}{\partial y}\right) = A(y_2 - y_1)^2 + B(y_2 - y_1) + C \tag{78}$$

where

$$A = \frac{1}{2} \frac{C_{pe}}{\lambda_e} \frac{\rho_e}{\partial t} \tag{79}$$

and B and C are constants which follow by substitution of (76) and (77) in (74). Thus, fitting the logarithm of the measured density gradient (from a schlieren photograph) to a quadratic function of distance such as (78), the thermal conductivity may be obtained from

$$\lambda_e = \frac{1}{2} \frac{\rho_e}{\sqrt{\partial t}} \frac{C_{pe}}{A} . \tag{80}$$

A different approach to Eq. (71) leads to a formula which may be used to calculate thermal conductivity from heat transfer measurements. The independent variable in (71) may be changed to a heat flux potential

$$\phi = \int_{h_w}^{h_e} \frac{\rho\lambda}{C_p} \, dh \quad \text{or} \quad \phi' = \frac{\rho\lambda}{C_p} \frac{dh}{d\eta} . \tag{81}$$

The energy equation becomes

$$\phi' + \eta \frac{C_p}{\rho\lambda} \phi' = 0. \tag{82}$$

Integrating (82) between zero and infinite and noting that $\phi' = 0$ at infinity, one obtains

$$\phi'_w = \int_0^{\infty} \eta \frac{C_p}{\rho\lambda} \phi' \, d\eta . \tag{83}$$

Using (81), this becomes

$$\phi'_w = \int_{h_w}^{h_e} \eta \, dh. \tag{84}$$

The variable η may be expressed as a power series in ϕ using a Taylor expansion about $\phi = 0$. The coefficients of the expansion may be obtained by calculating $\frac{d^n\eta}{d\phi^n}$ from (71). Keeping the first term in the expression gives

$$\eta = \frac{\phi}{\phi'_w} \tag{85}$$

or substituting (85) into (84), integrating the result, and substituting in (81) we obtain

$$\left(\frac{\rho\lambda}{C_p}\right)_w^2 \left(\frac{dh}{d\eta}\right)_w^2 = a^2 \int_{h_w}^{h_e} \int_{h'_w}^{h'} \frac{\rho\lambda}{C_p}\, dh\, dh' \tag{86}$$

where a^2 is a constant which corrects the integral for the errors due to neglecting higher powers of $\frac{\phi}{\phi'_w}$ in (85).

Finally, noting that

$$d\eta = \frac{\rho_e}{\sqrt{2t}}\, d\lambda \tag{87}$$

near the wall the expression for the heat flux is

$$-\frac{\dot{Q}}{\sqrt{2t}} = \frac{\lambda_w}{C_{p_w}} \left(\frac{dh}{dx}\right) = a\left[\int_{h_w}^{h_e} \int_{h_w}^{h'} \frac{\rho\lambda}{C_p}\, dh\, dh'\right]^{1/2}. \tag{88}$$

Comparing (88) with exact numerical integrations of the energy equation Kemp showed that choosing $a = 1.13$ gave the correct answer to within 1% for the cases of interest here. In practice the approximation (the value of a) (88) should be checked by numerical integration of an ideal gas similar to the gas under investigation.

The first fact to notice about (88) is that an error of 8% in the measurement of Q reflects as an error of 16% in the integral

$$I = \int_{h_w}^{h_e} \int_{h'_w}^{h'} \frac{\rho \lambda}{C_p} \, dh \, dh' \, . \tag{89}$$

Suppose the thermal conductivity of the gas is known over half the range of integration. Then only about 50% of the integral I bears significant information on thermal conductivity in the temperature range of the outer half of the boundary layer. Therefore the uncertainties in the experimental determination of I are doubled in the thermal conductivity. Similarly, large uncertainties in the thermal conductivity over a small temperature range will not be detected in the heat transfer rate to the end wall of the shock tube. However, systematic discrepancies over large temperature ranges such as the disagreement between thermal conductivity of helium from different sources (discussed in the data review section) will show up in the heat transfer measurement.

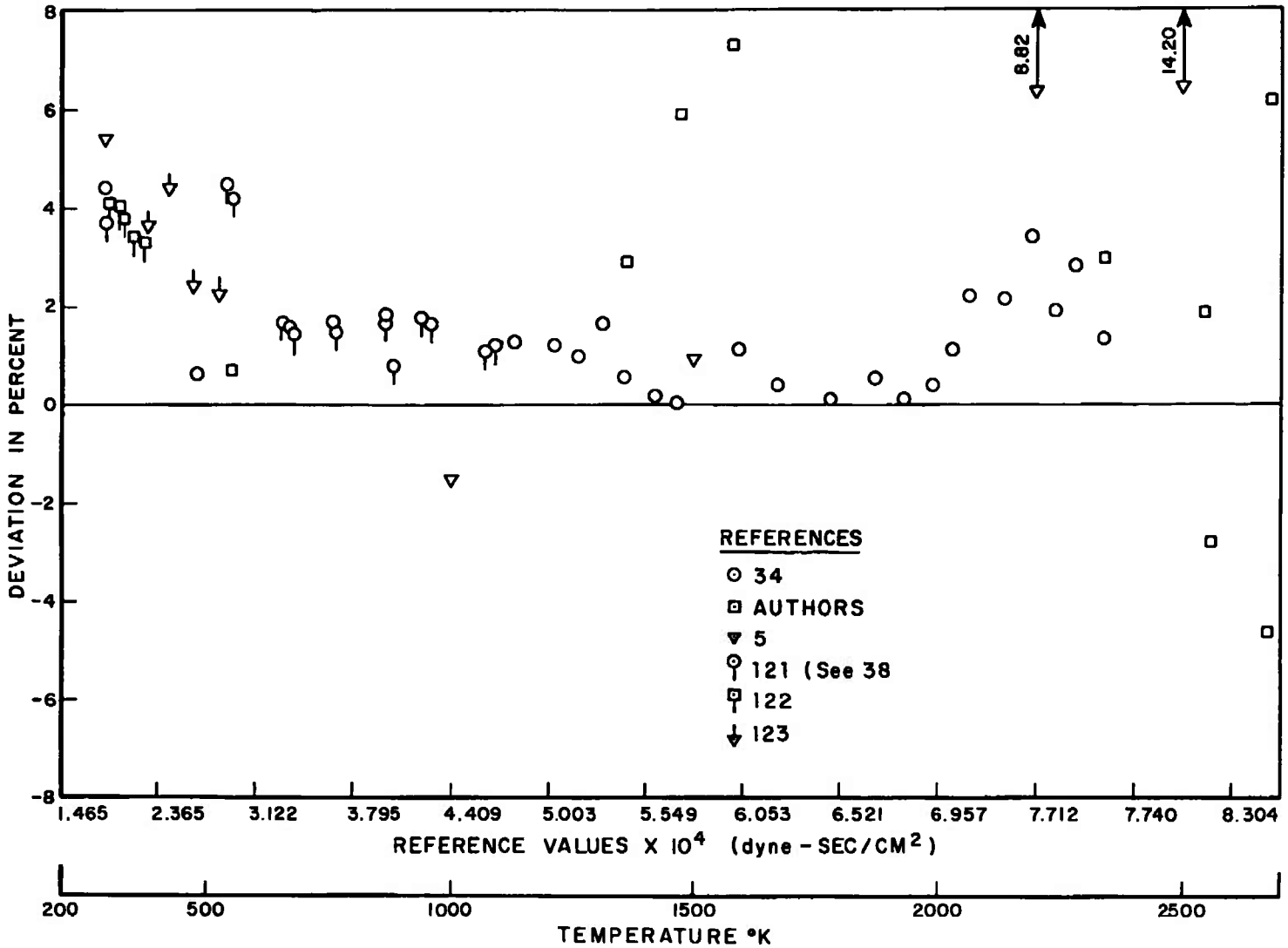

Fig. 1 Viscosity deviation chart for helium

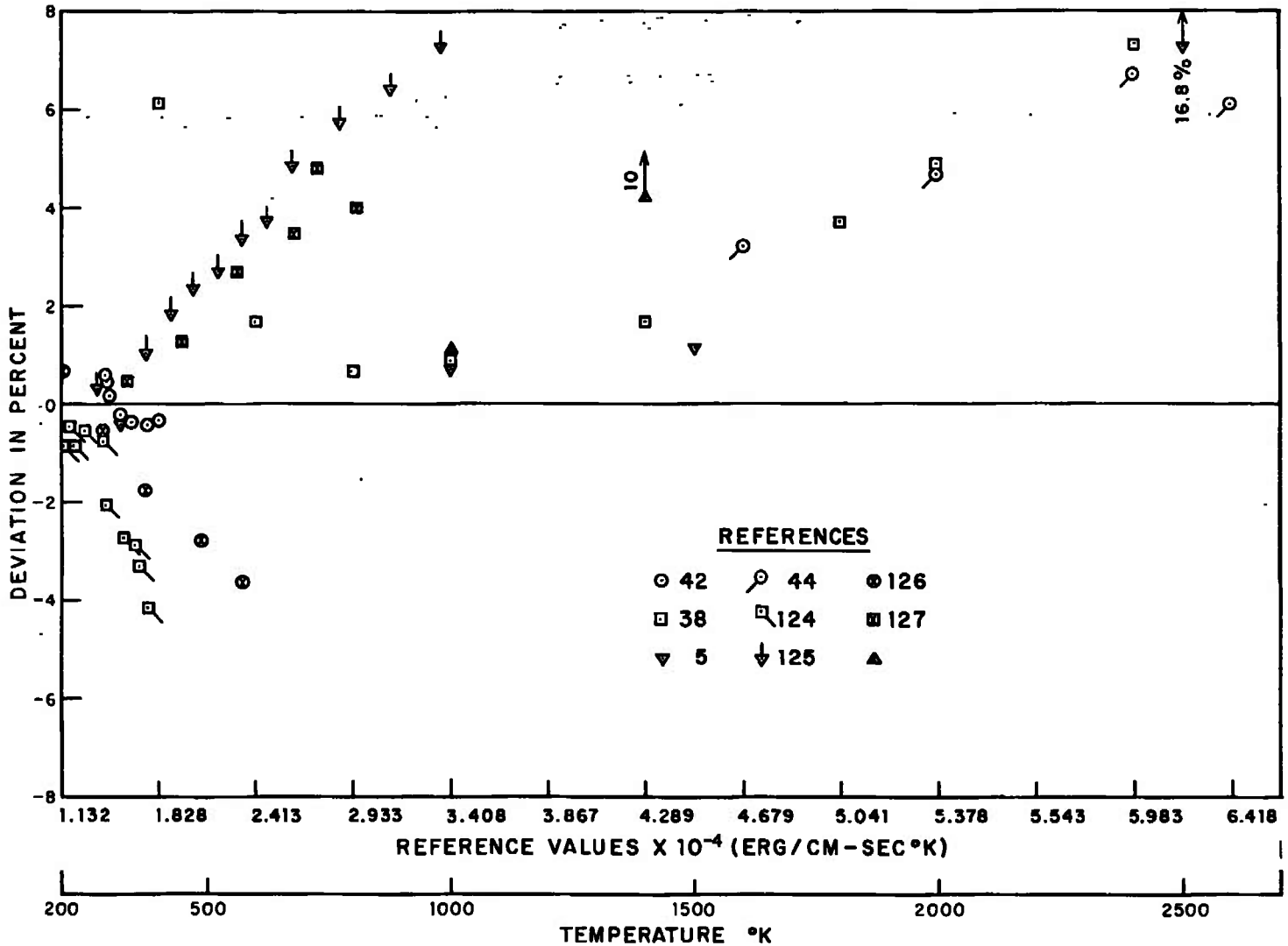

Fig. 2 Thermal conductivity deviation chart for helium

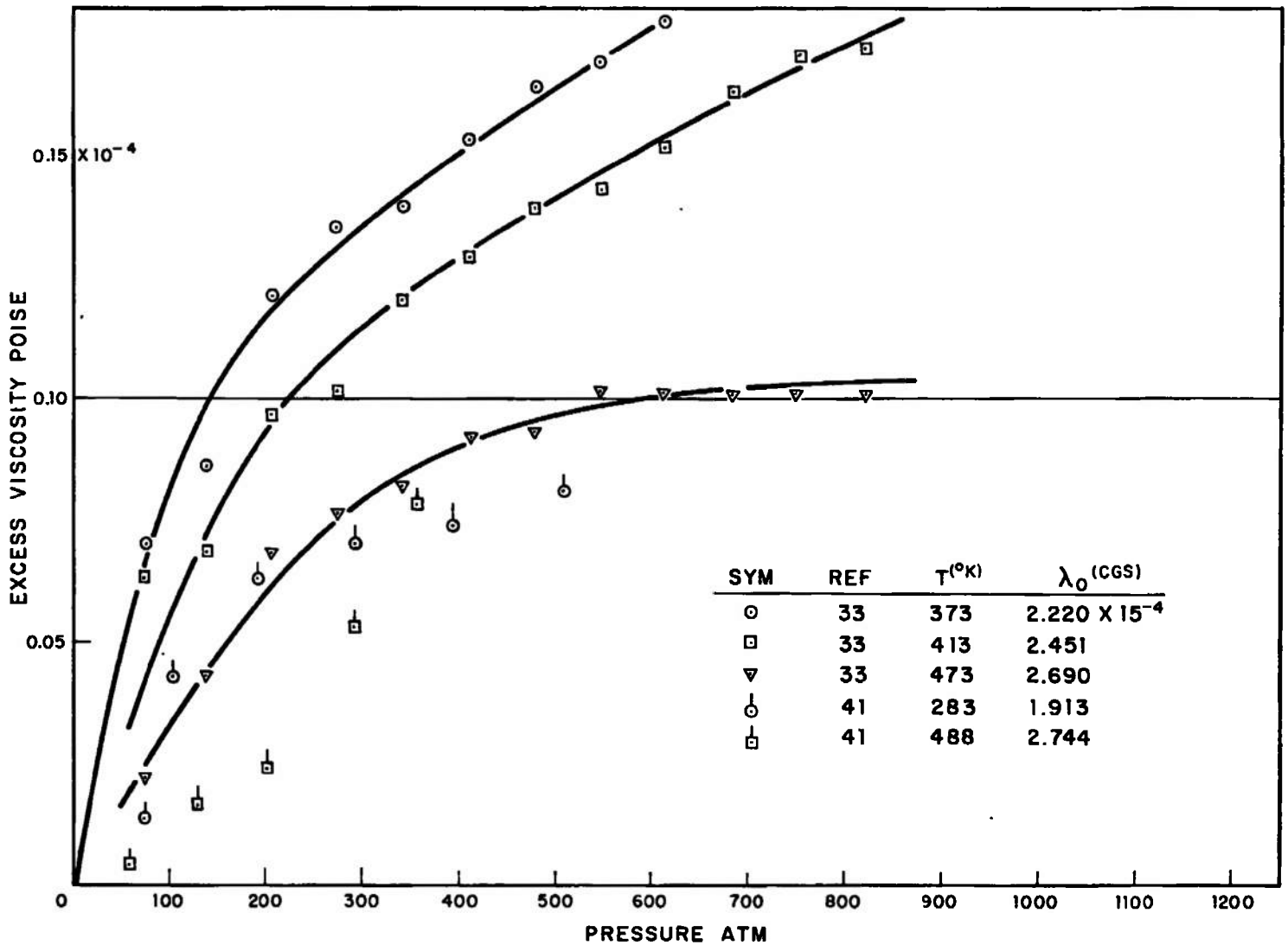

Fig. 3 Excess viscosity for helium

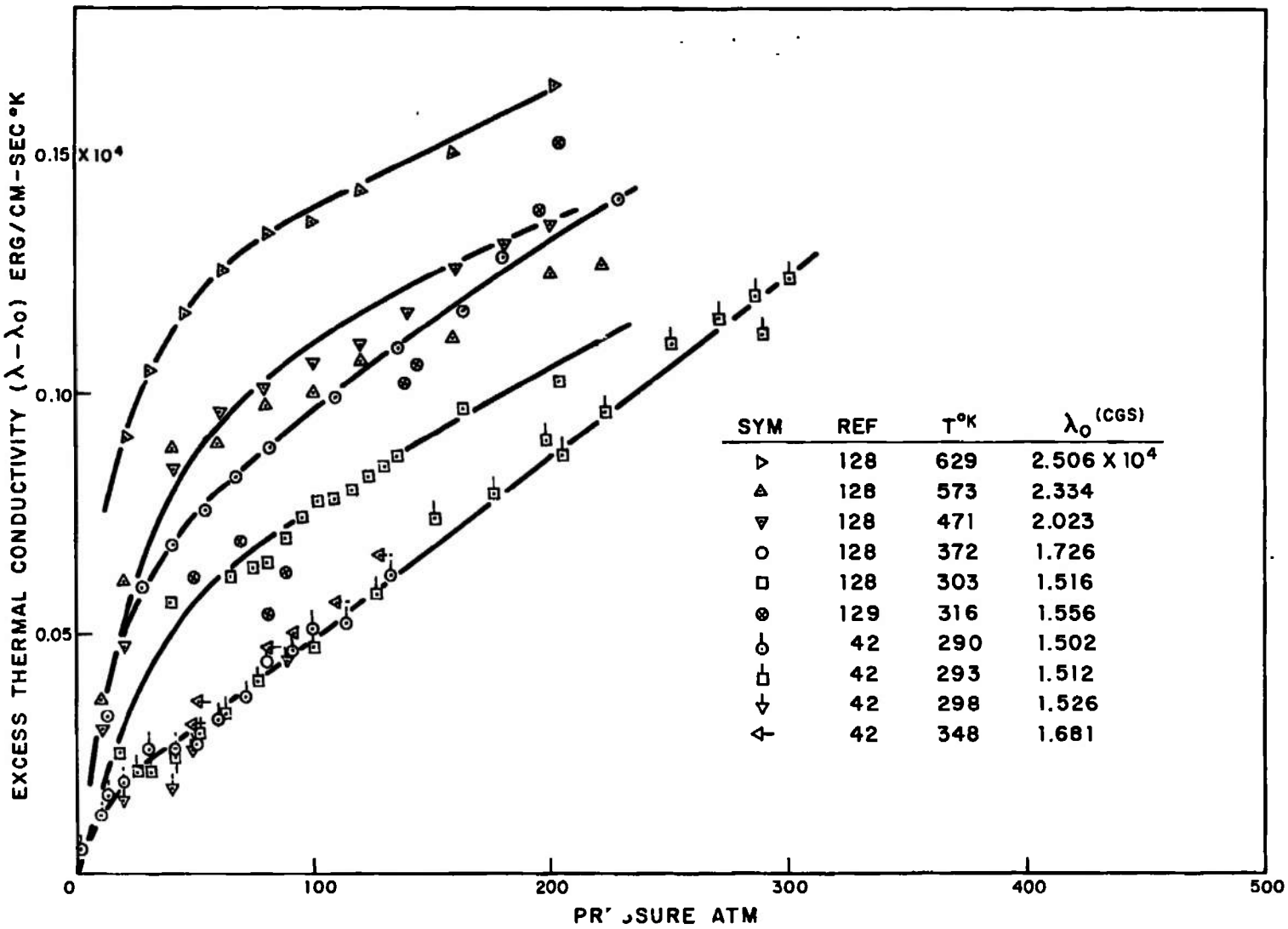

Fig. 4 Excess thermal conductivity for helium

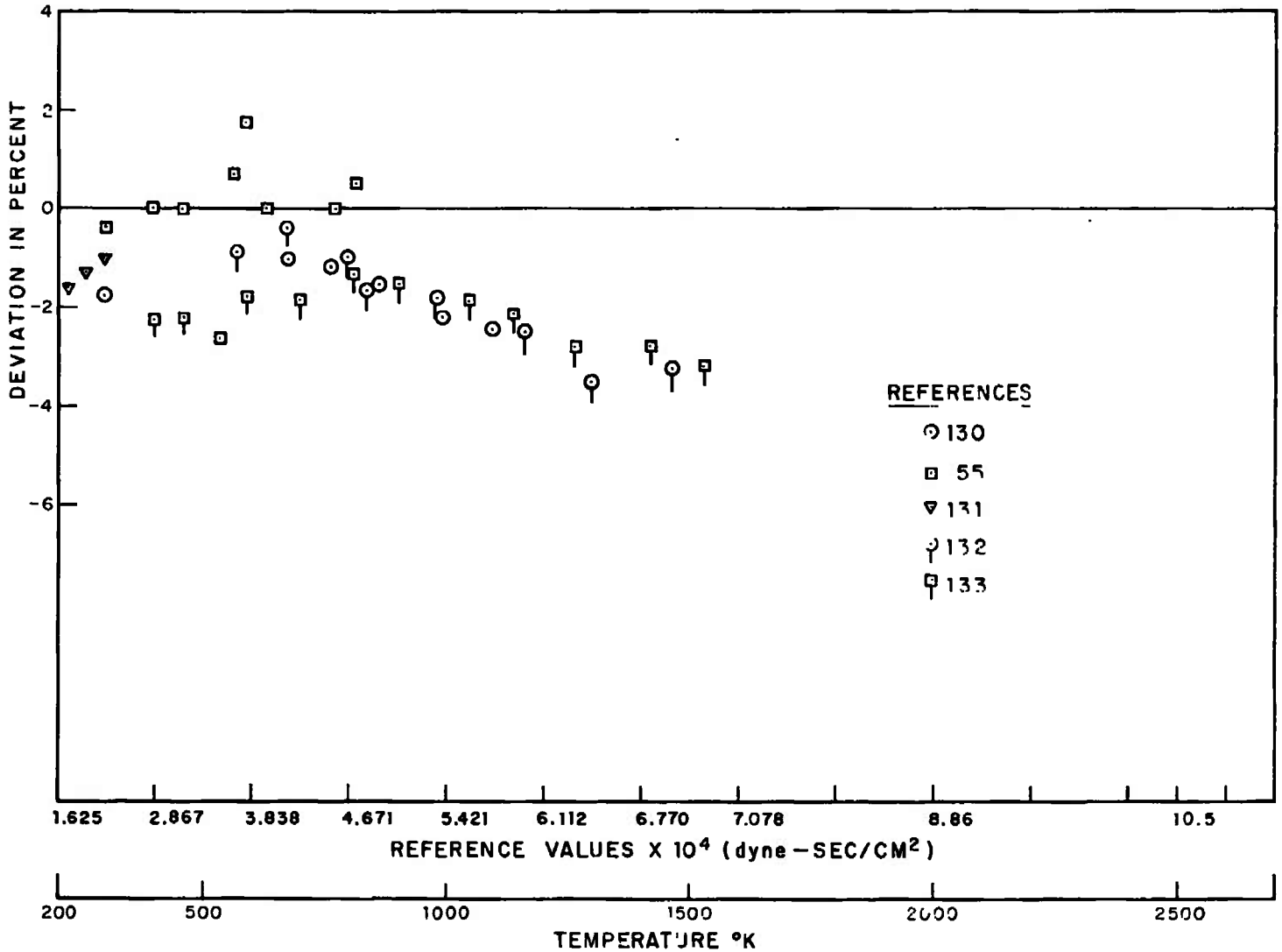

Fig. 5 Viscosity deviation chart for argon

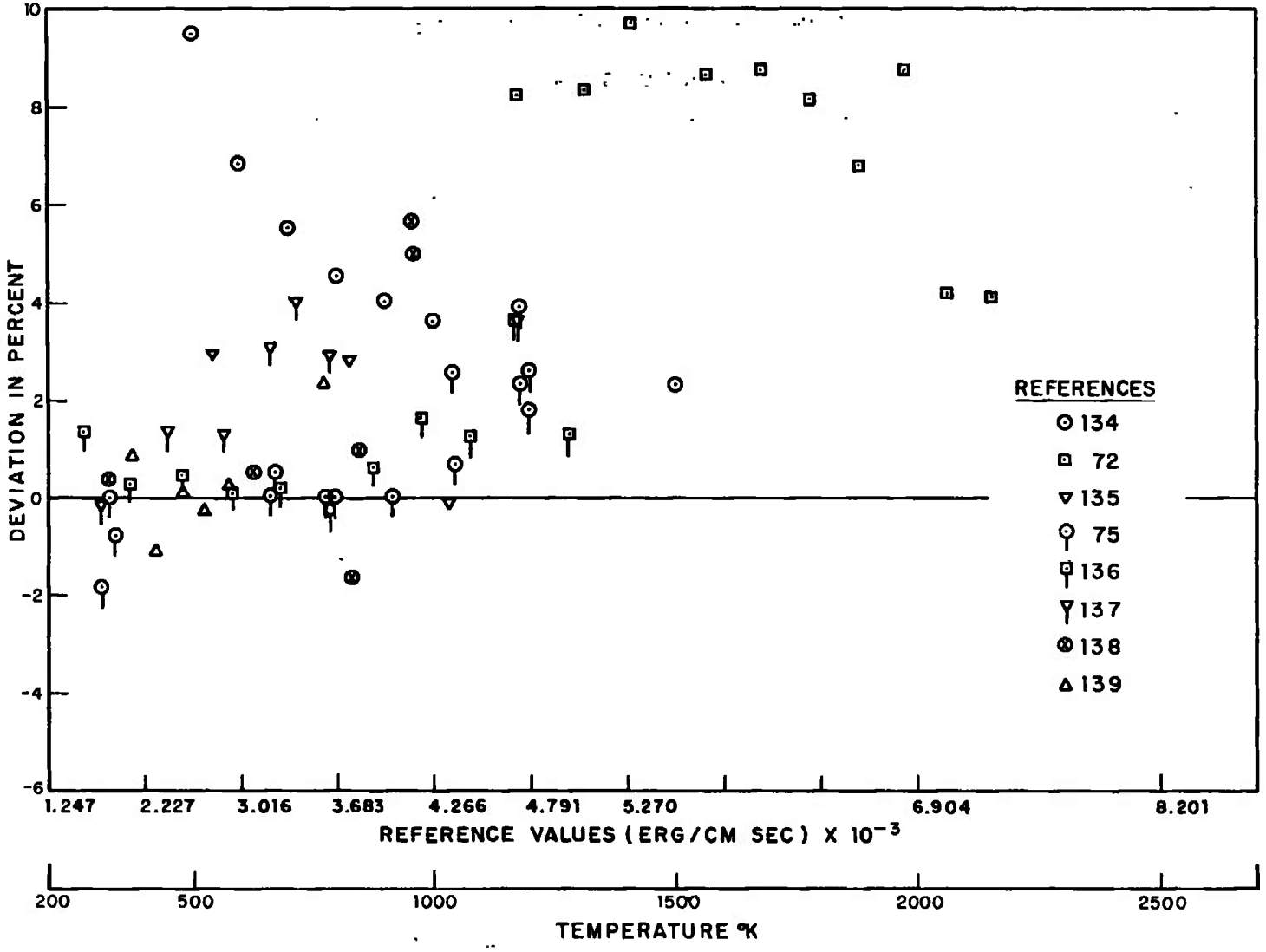

Fig. 6 Thermal conductivity deviation chart for argon

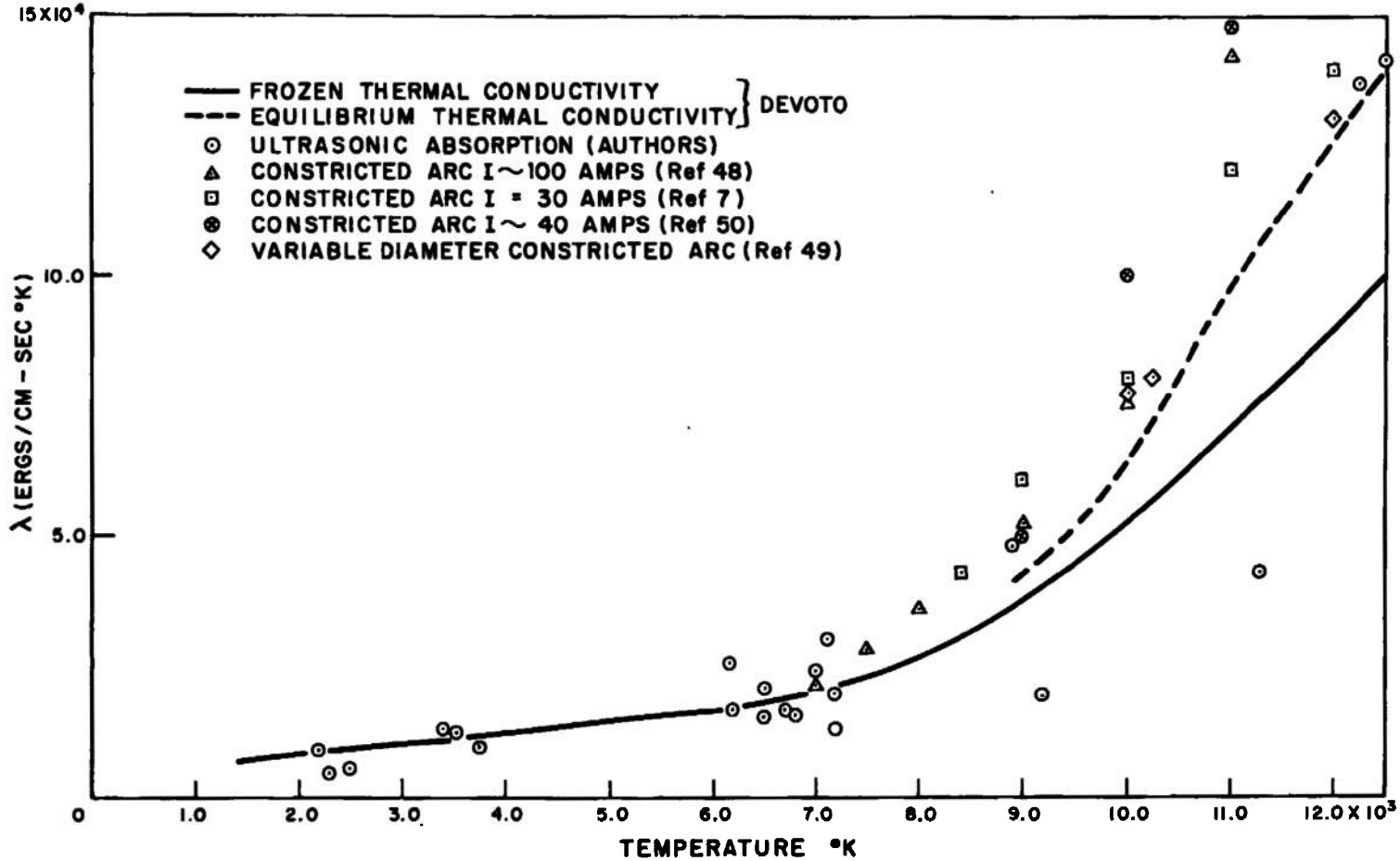

Fig. 7 Thermal conductivity for argon in the range 3000°K-12,000°K

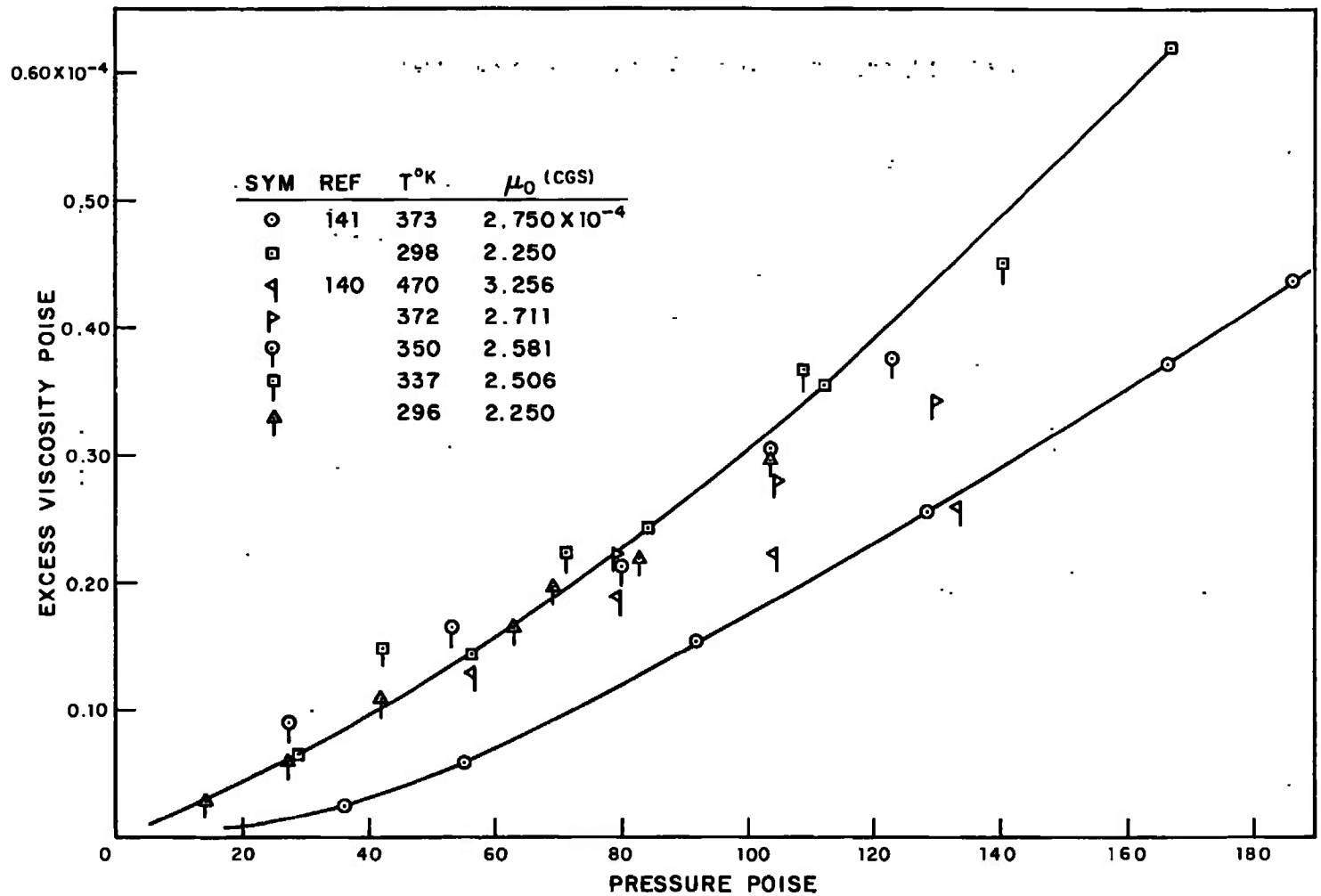

Fig. 8 Excess viscosity for argon

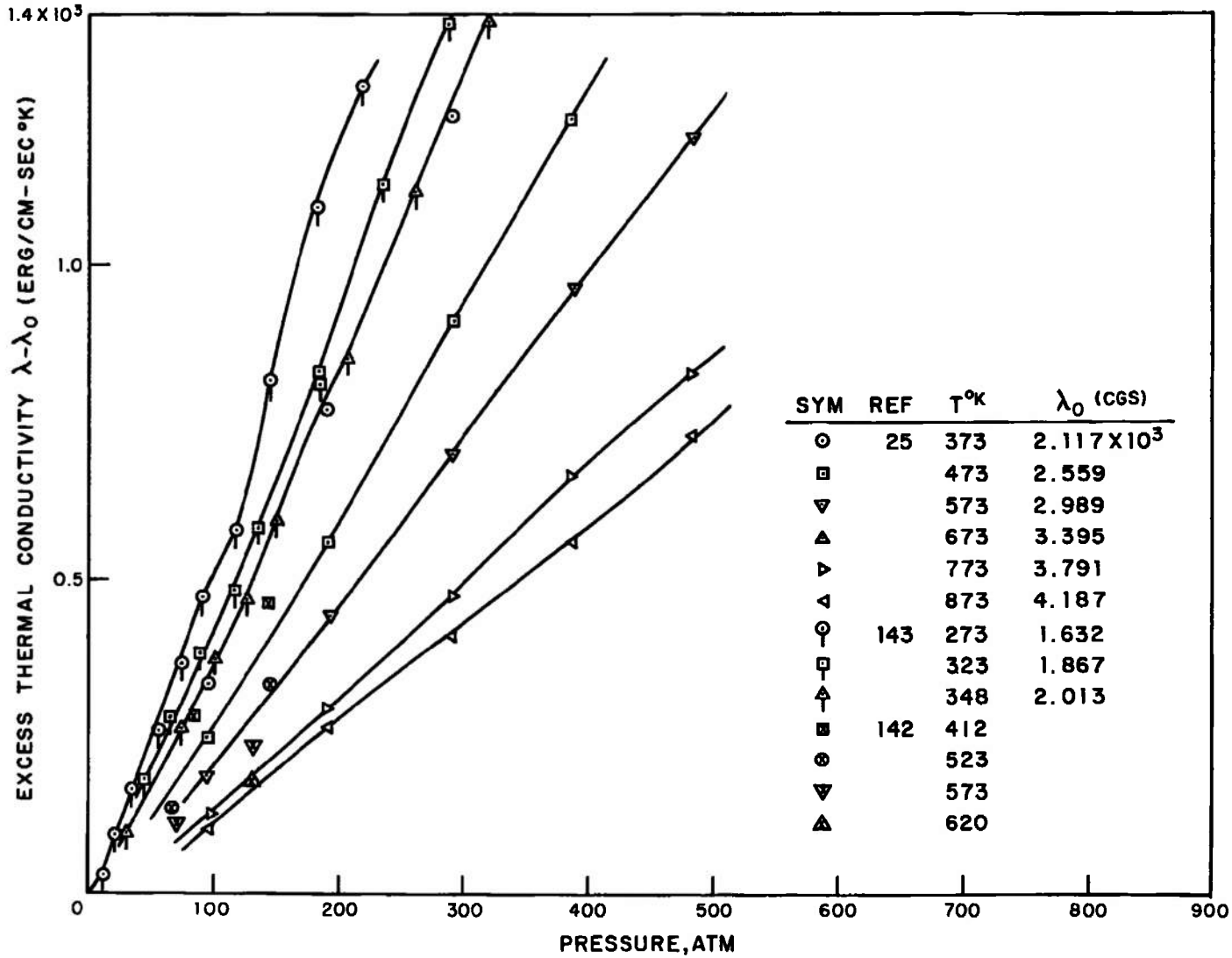

Fig. 9 Excess thermal conductivity for argon

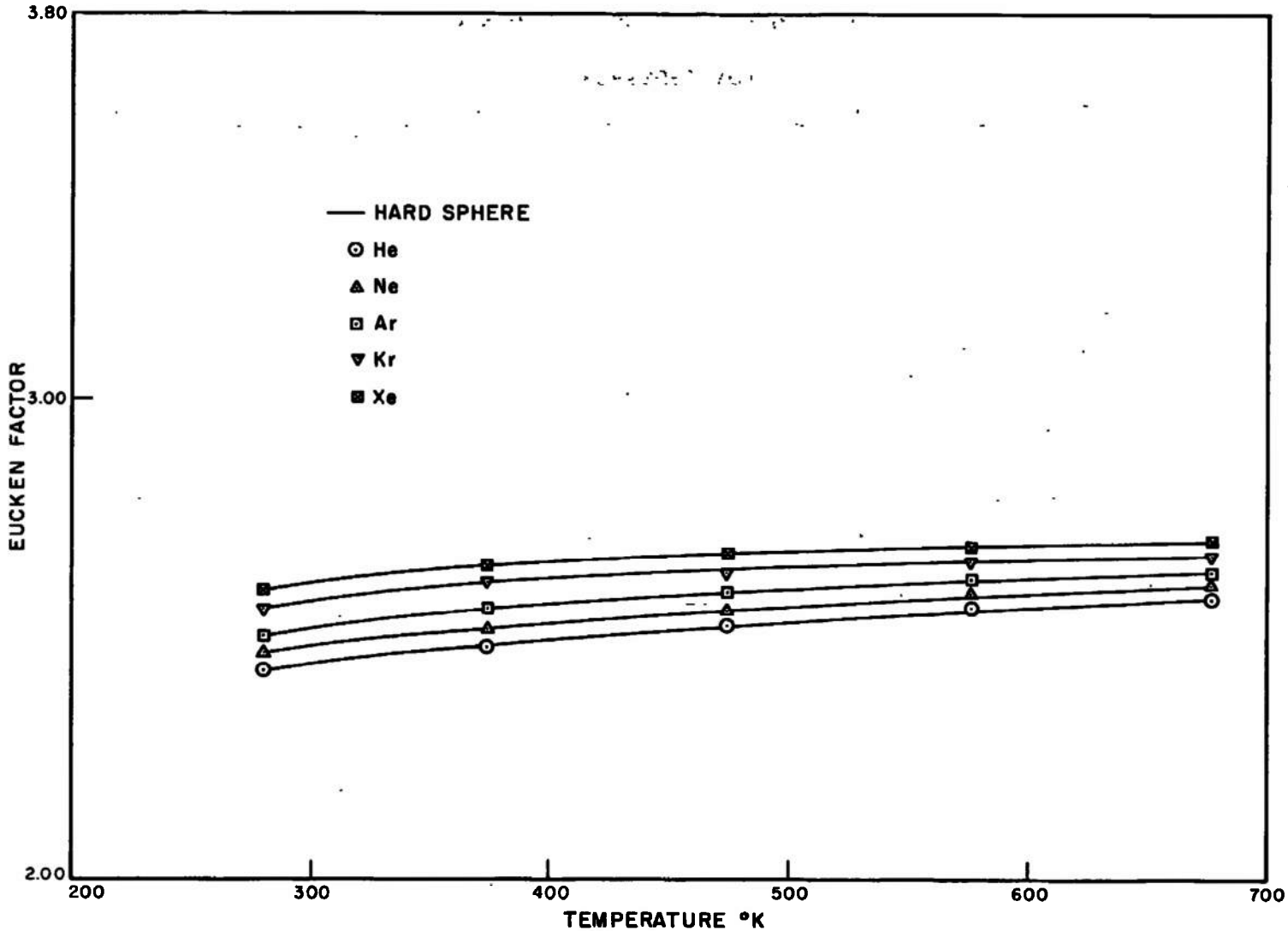

Fig. 10 Eucken factor for monatomic gases as a function of temperature

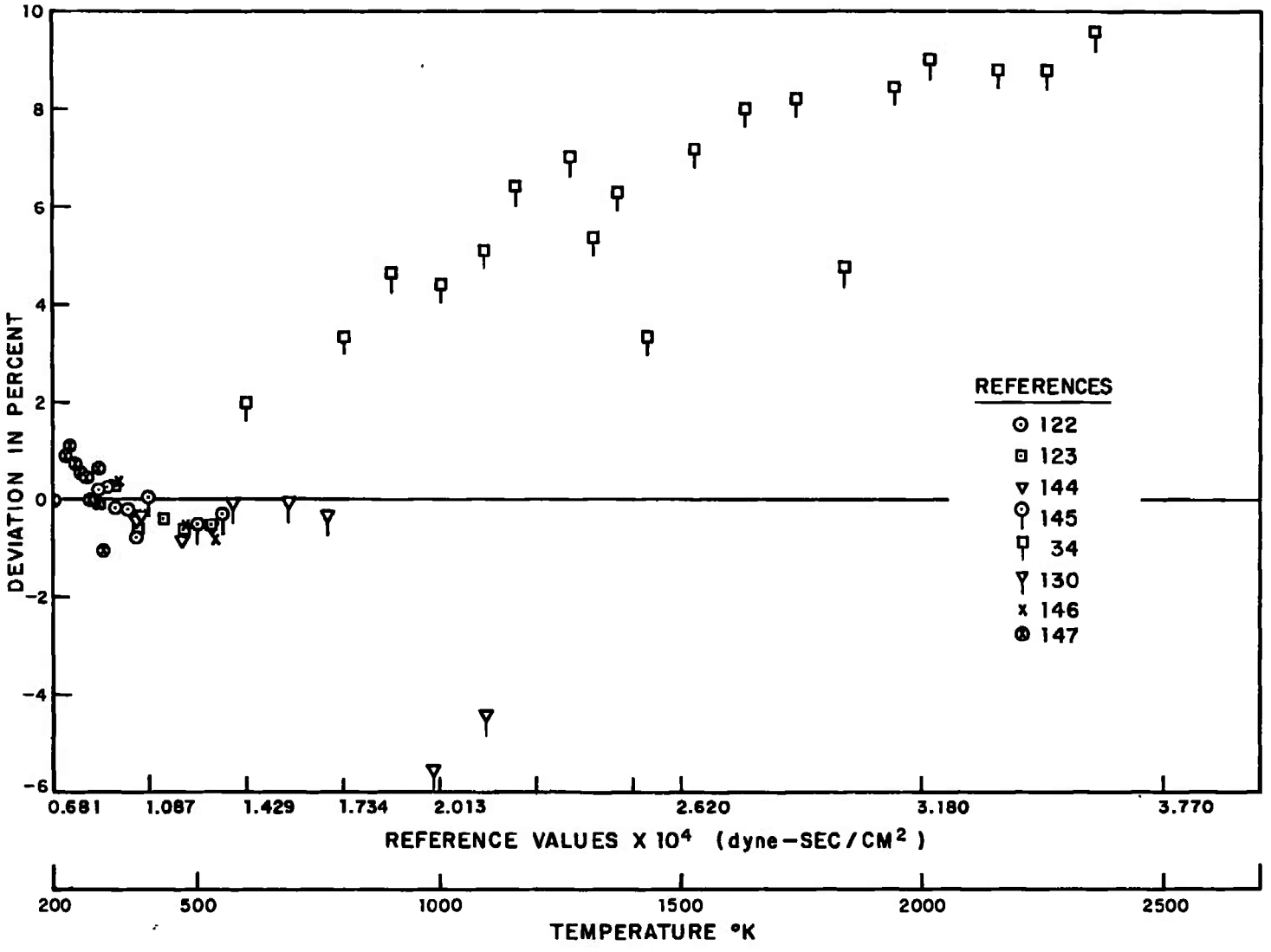

Fig. 11 Viscosity deviation chart for hydrogen

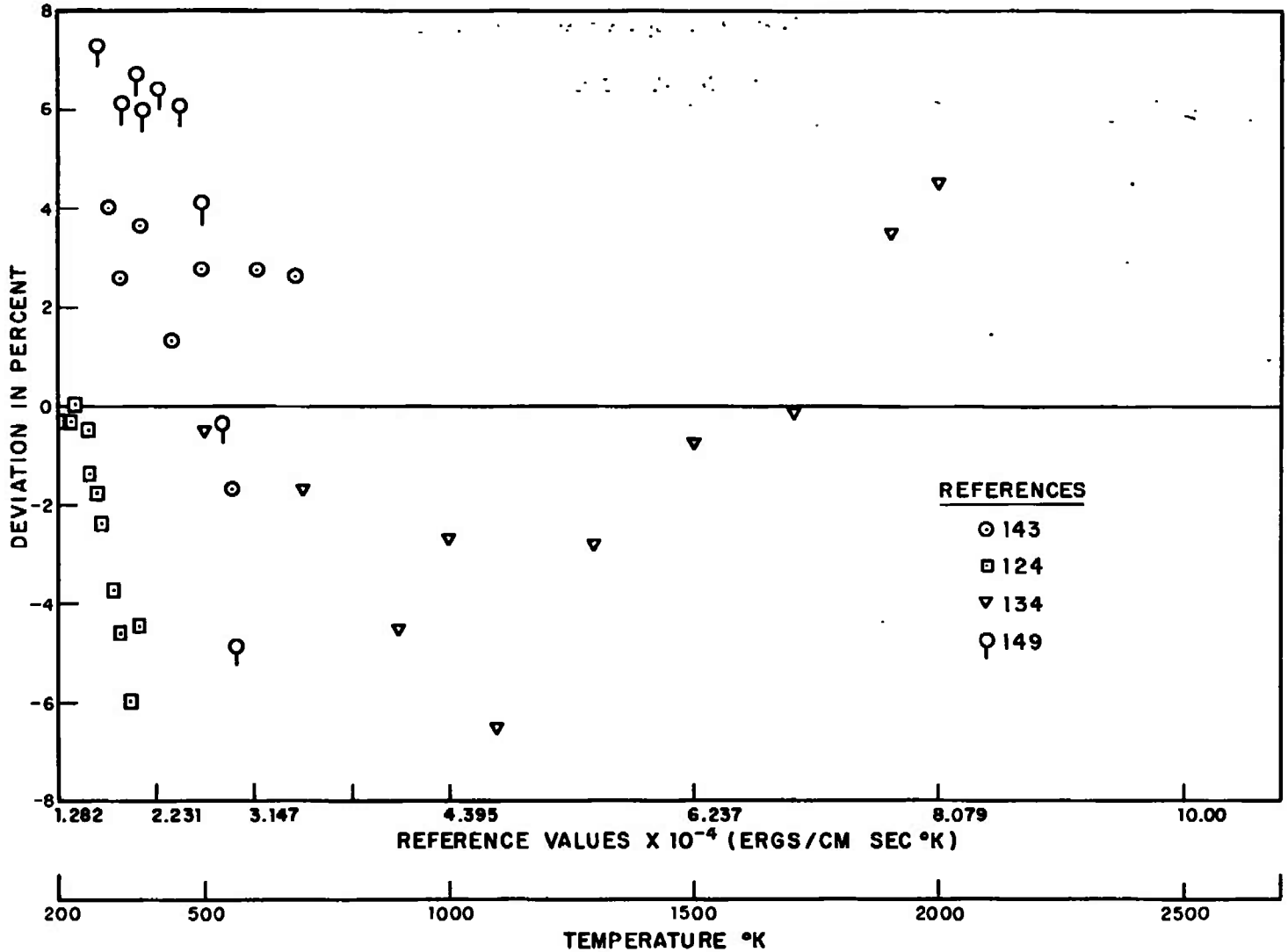

Fig. 12 Thermal conductivity deviation chart for hydrogen

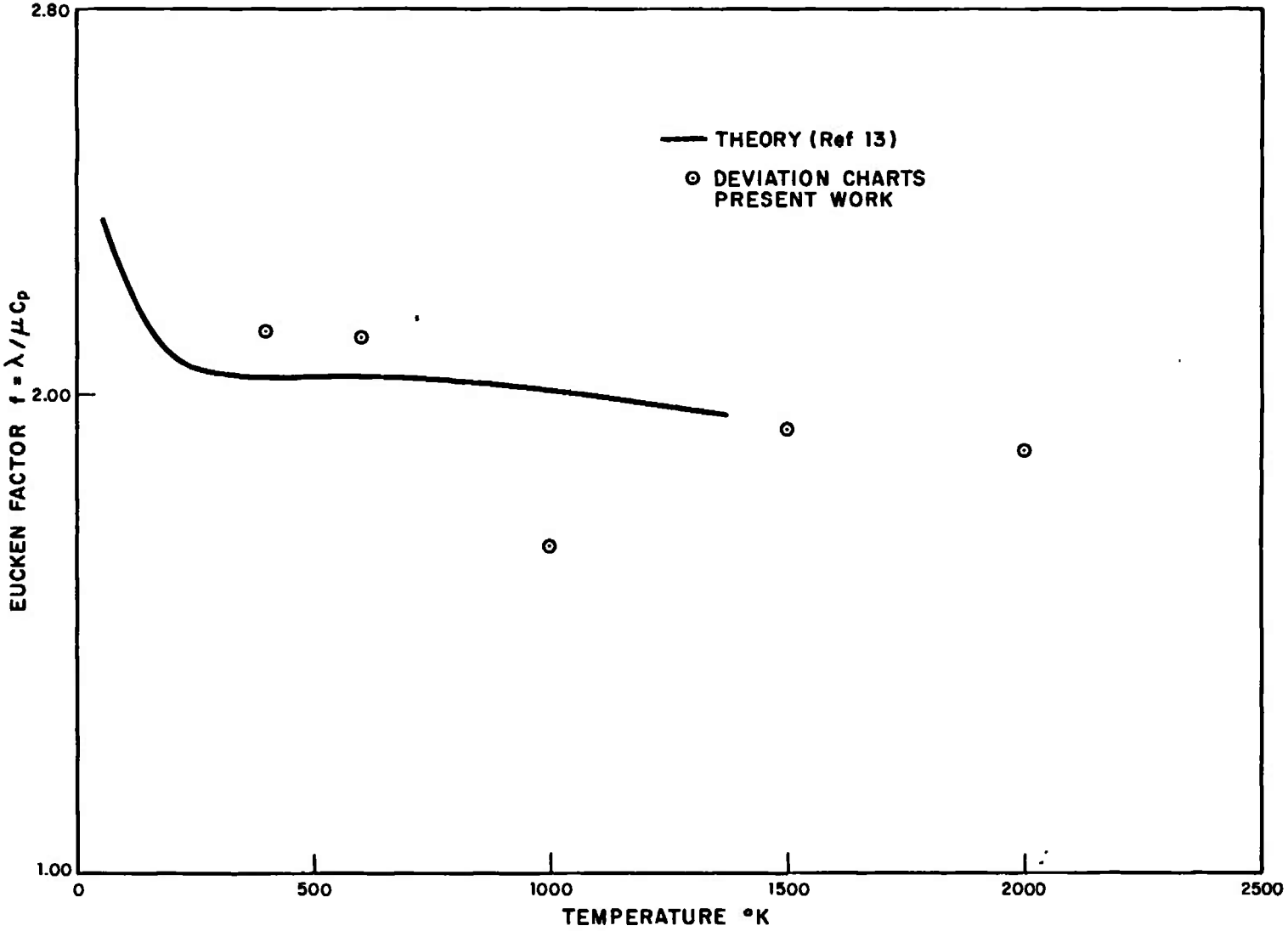

Fig. 13 Eucken factor for hydrogen

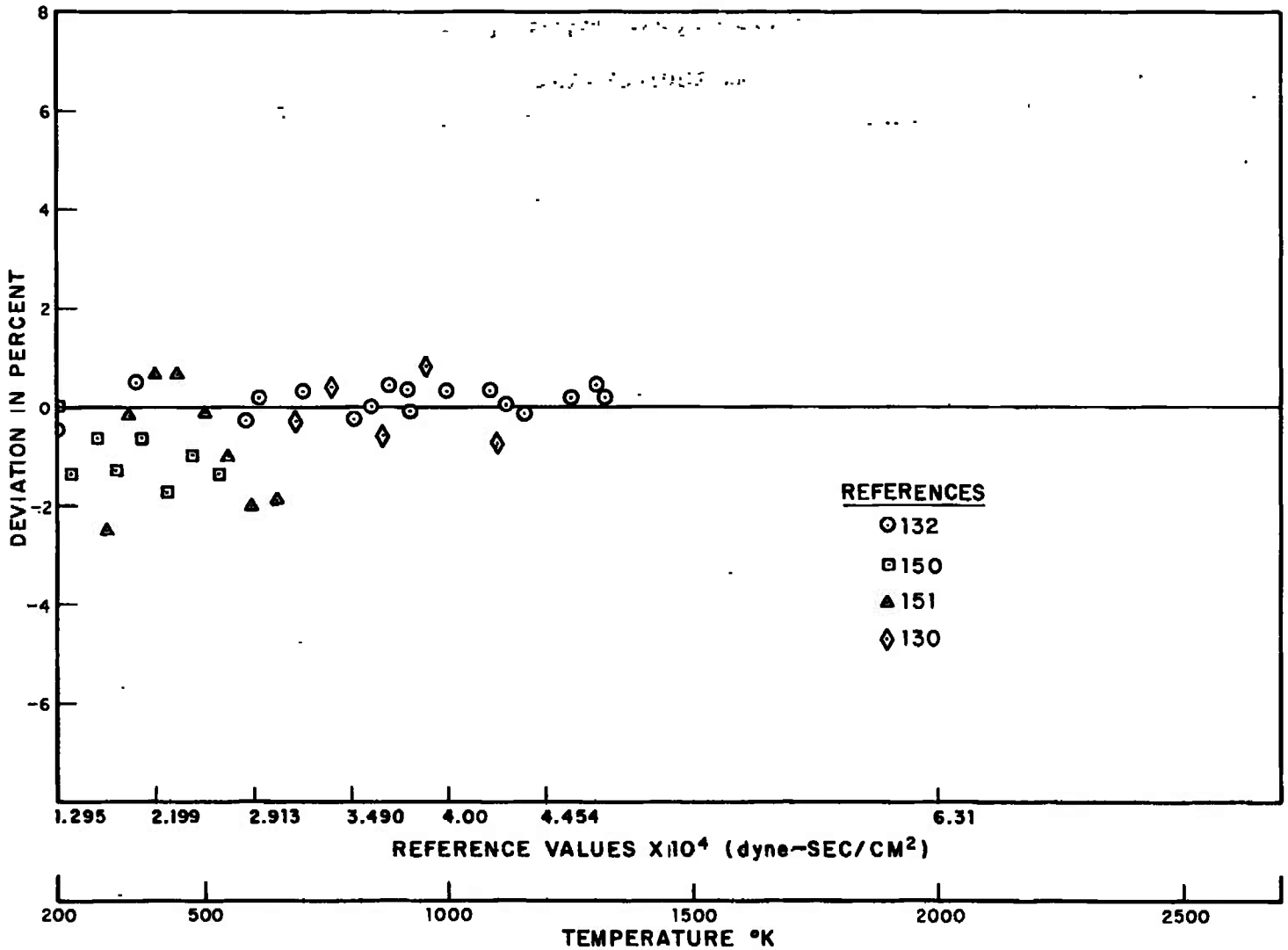

Fig. 14 Viscosity deviation chart for nitrogen

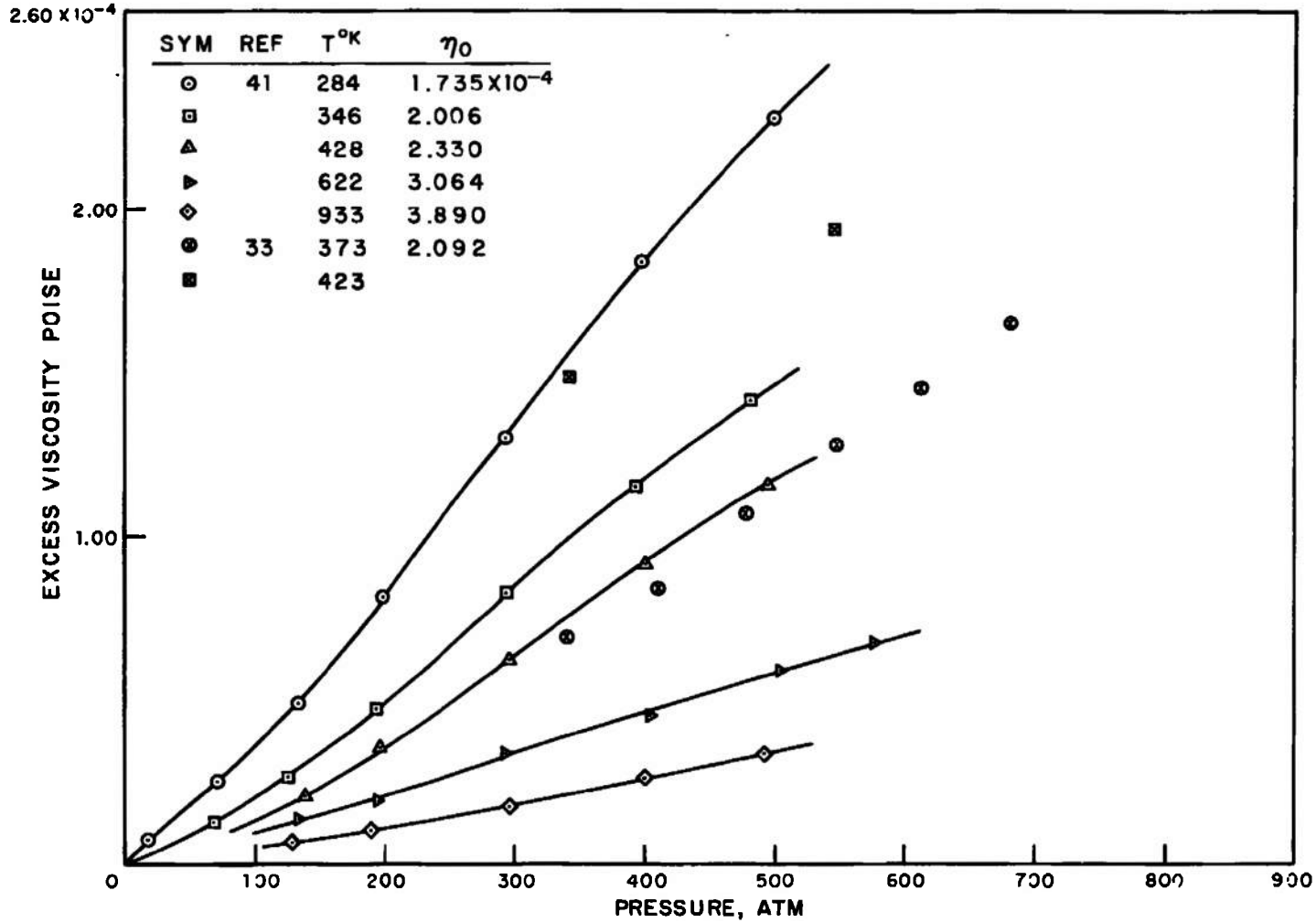

Fig. 15 Excess viscosity for nitrogen

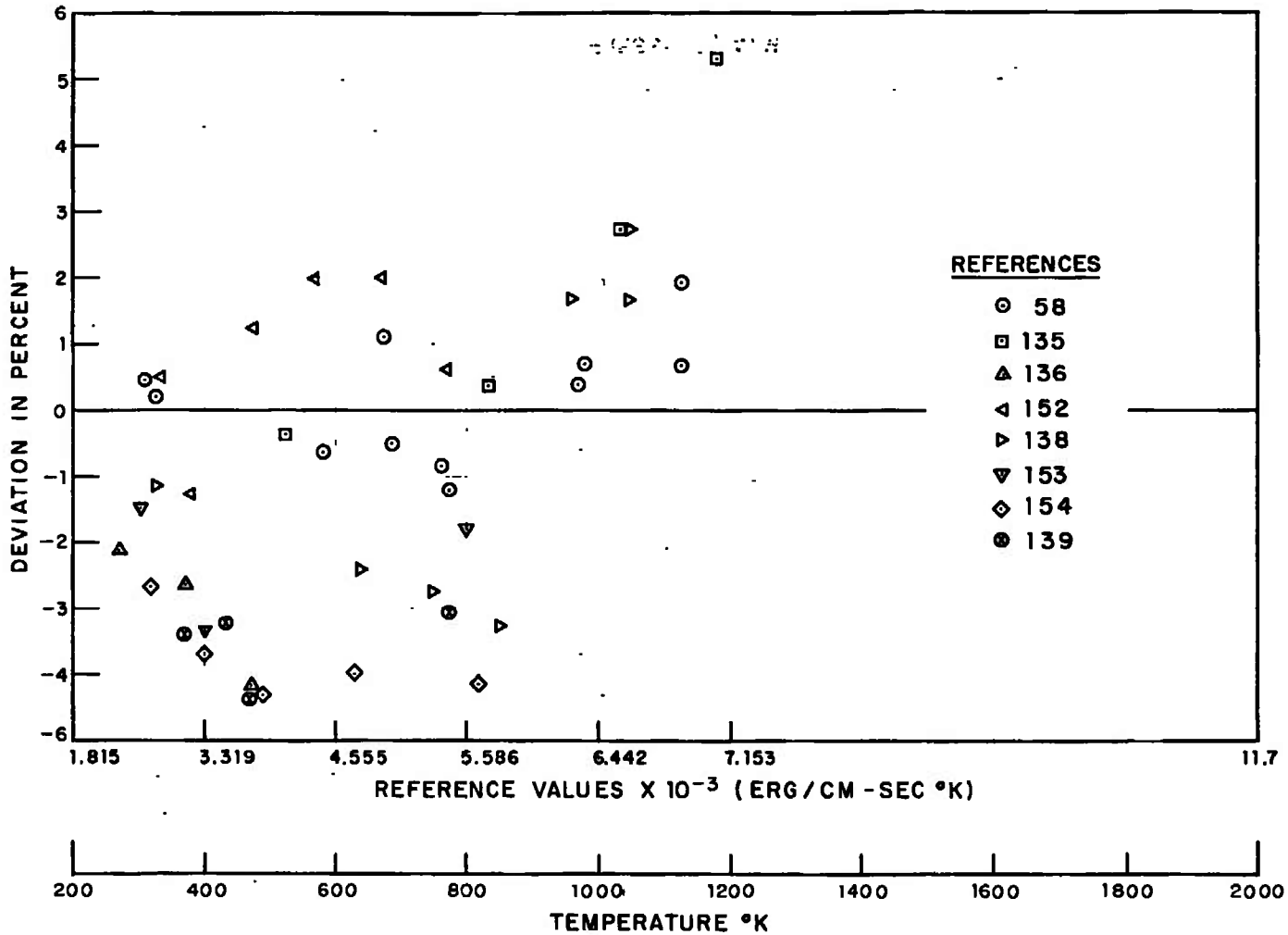

Fig. 16 Thermal conductivity deviation chart for nitrogen

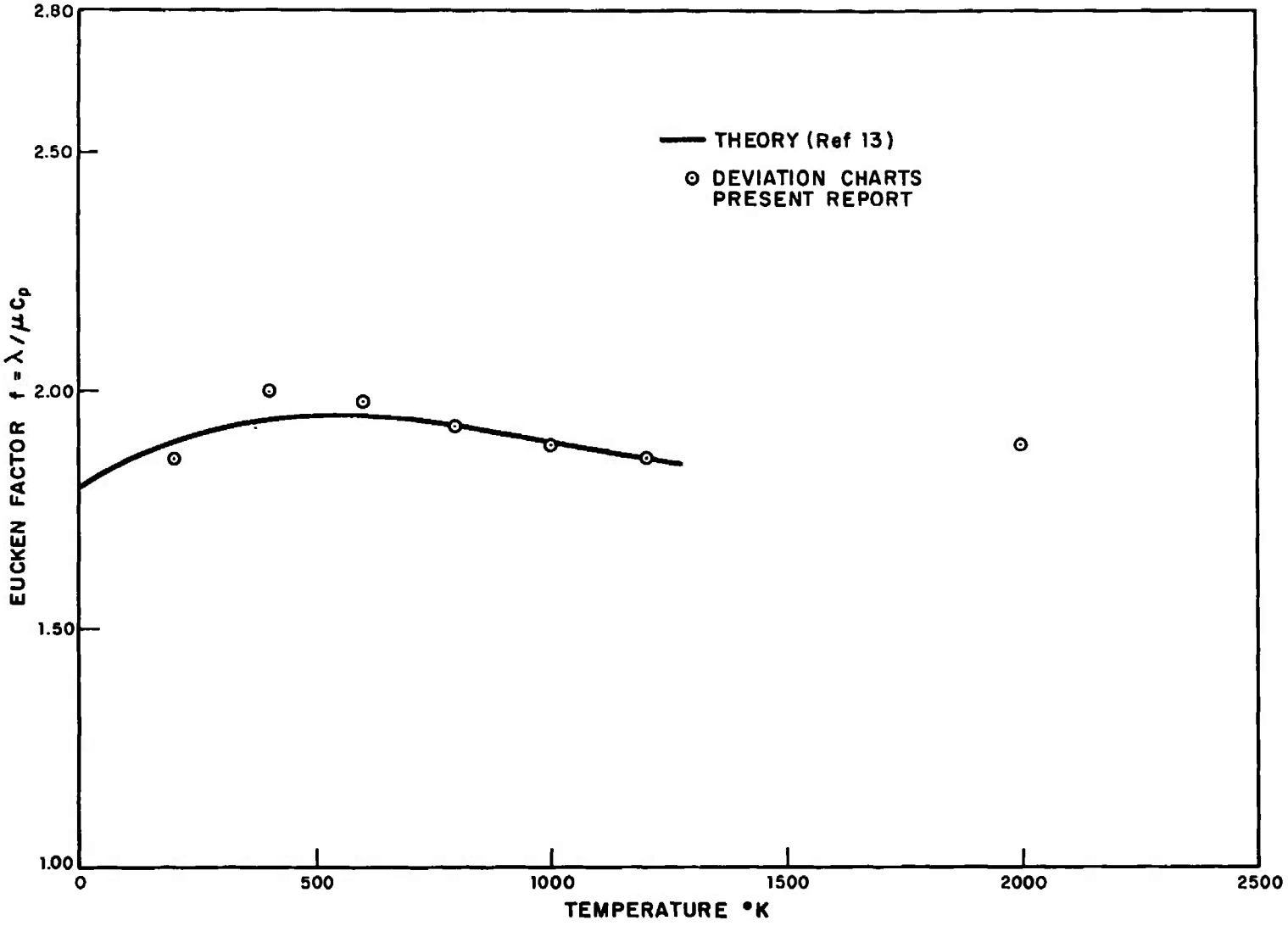

Fig. 17 Eucken factor for nitrogen

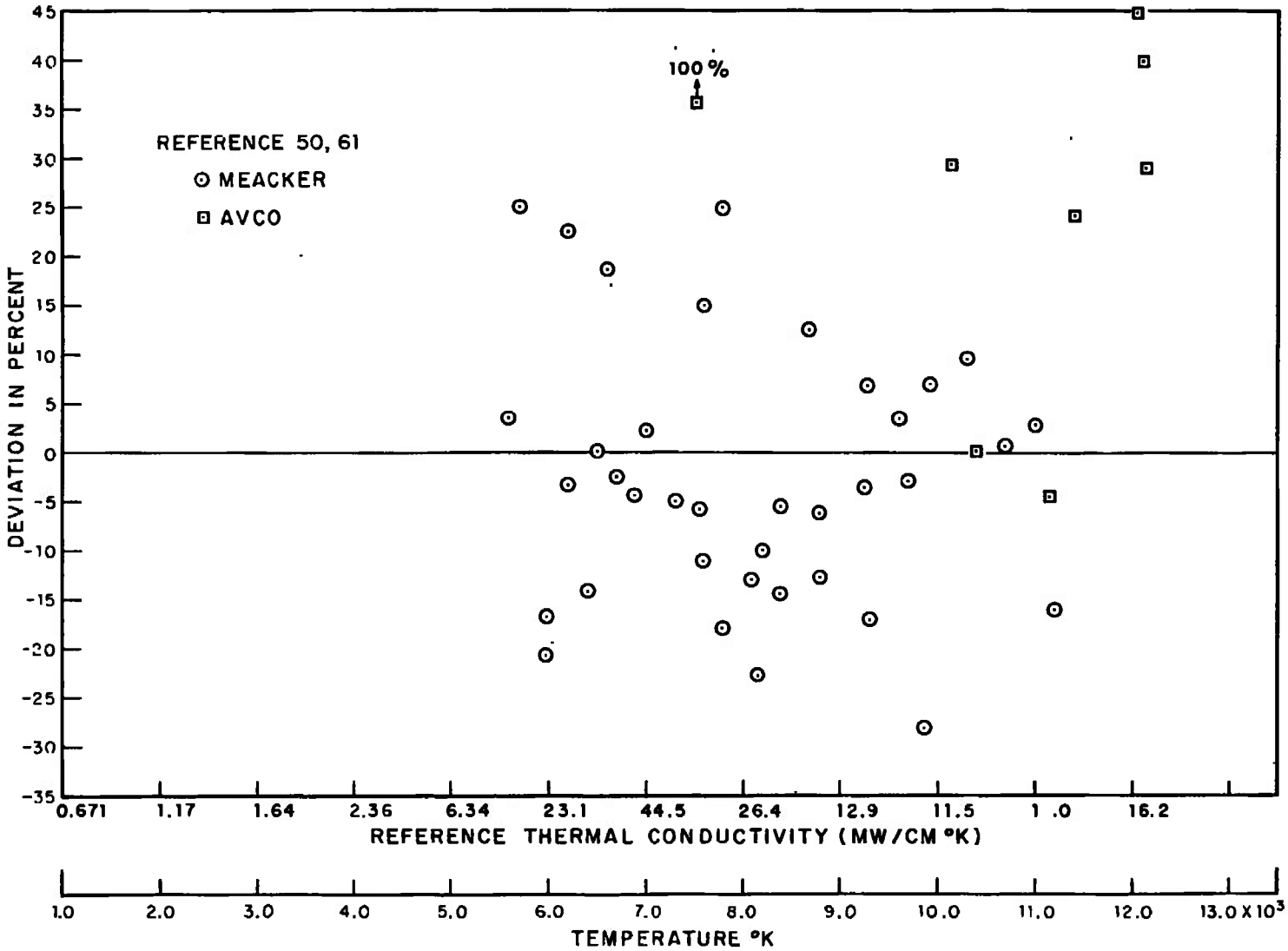

Fig. 18 High temperature thermal conductivity deviation chart for nitrogen

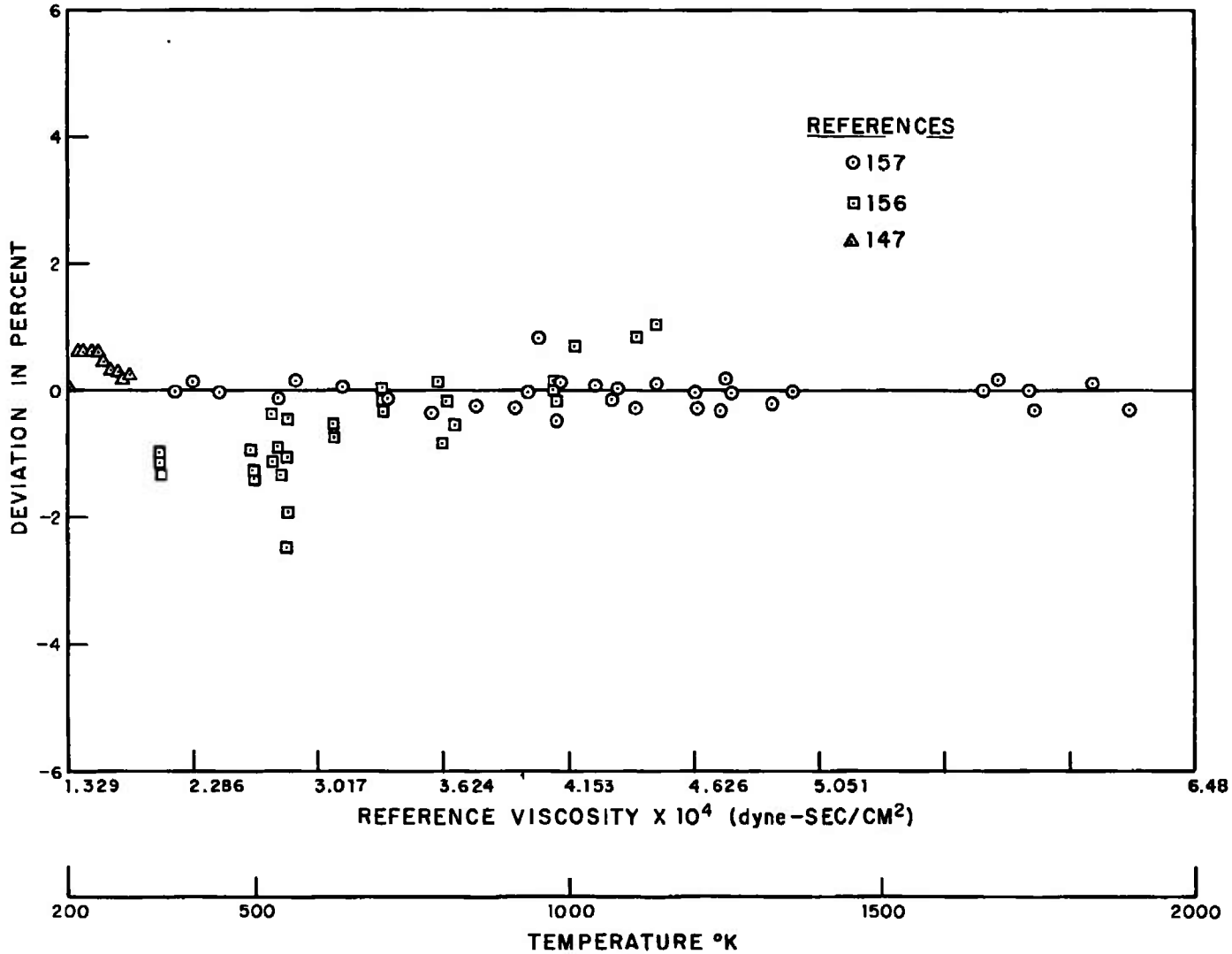

Fig. 19 Viscosity deviation chart for air

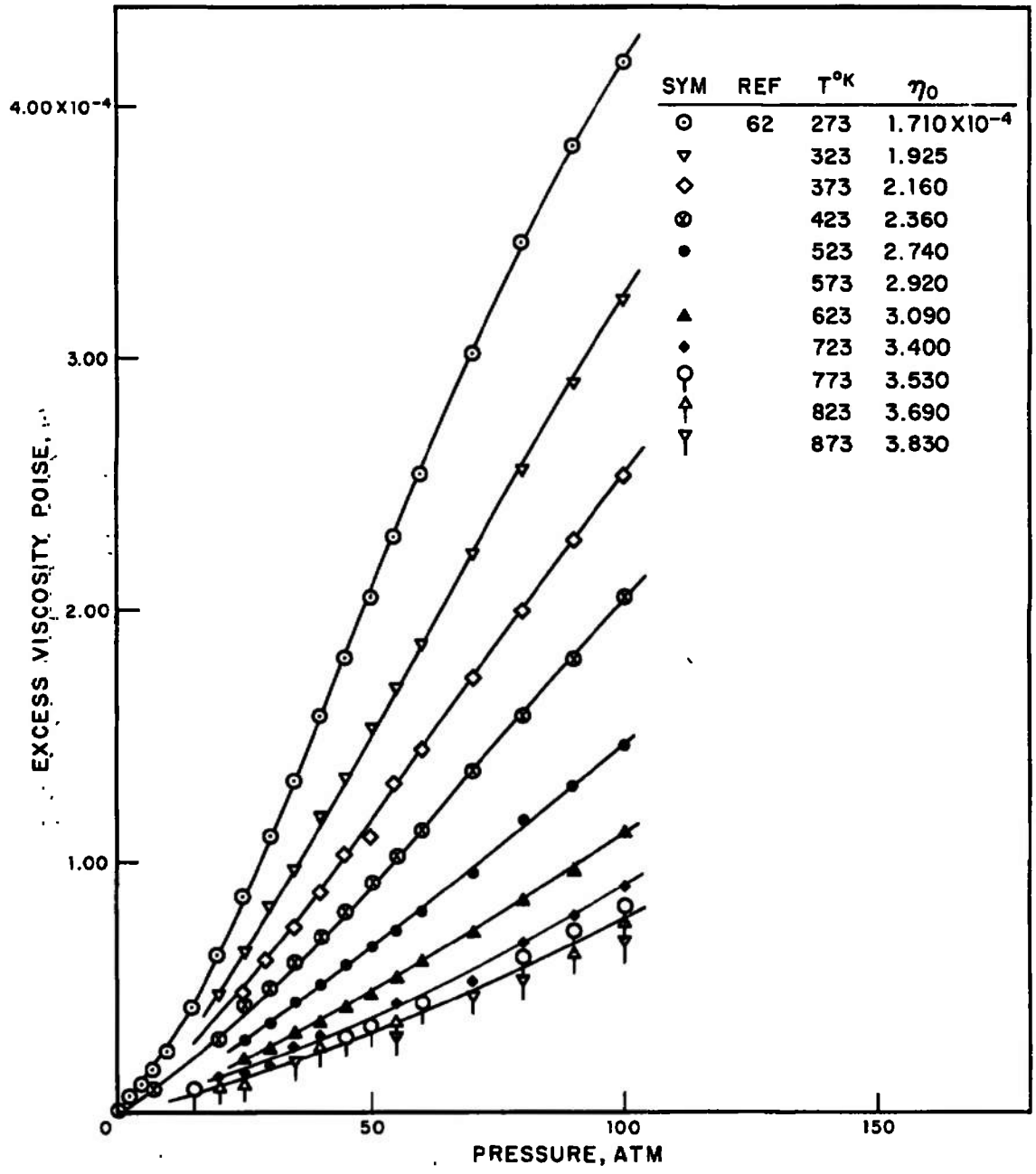

Fig. 20 Excess viscosity for air

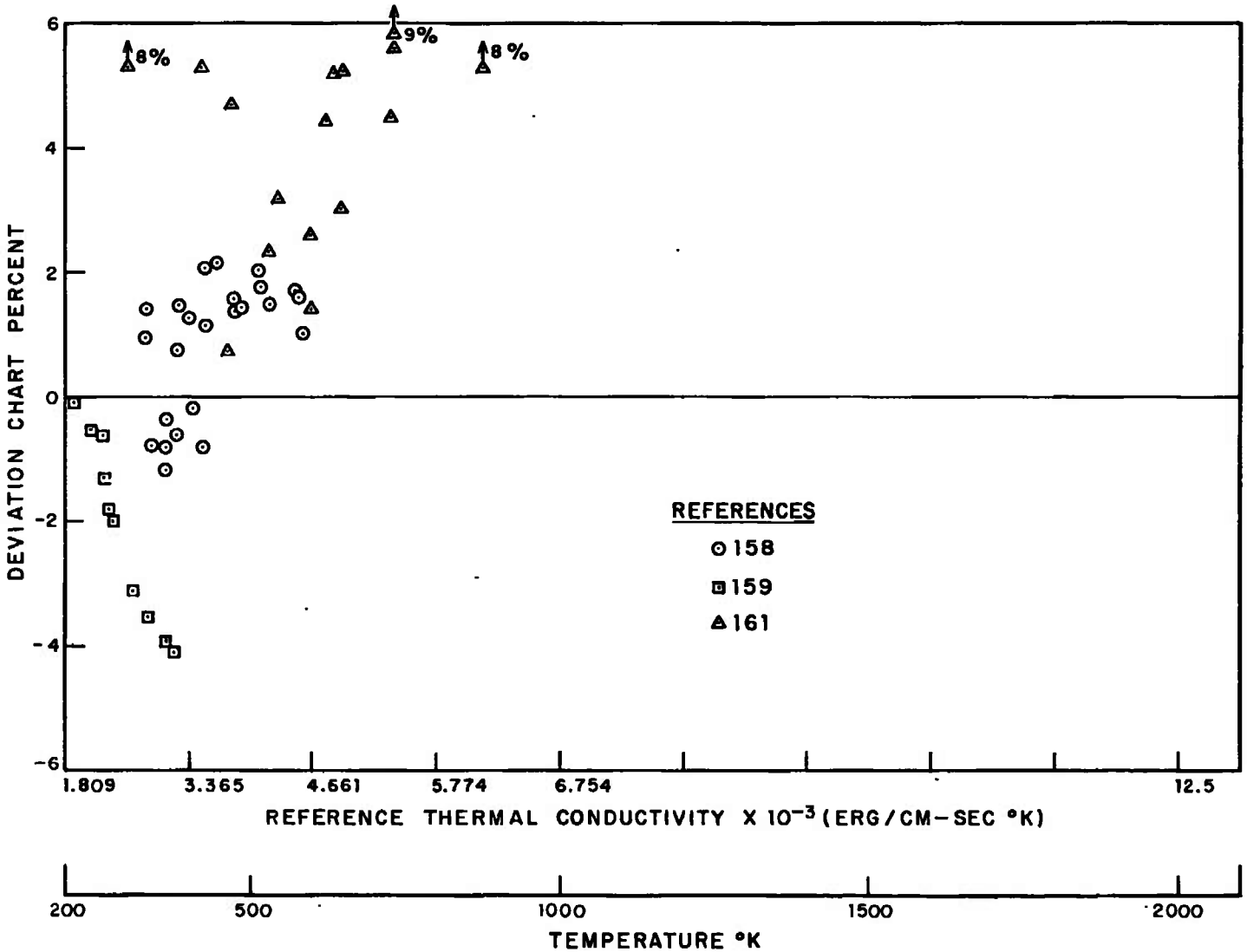

Fig. 21 Thermal conductivity deviation chart for air

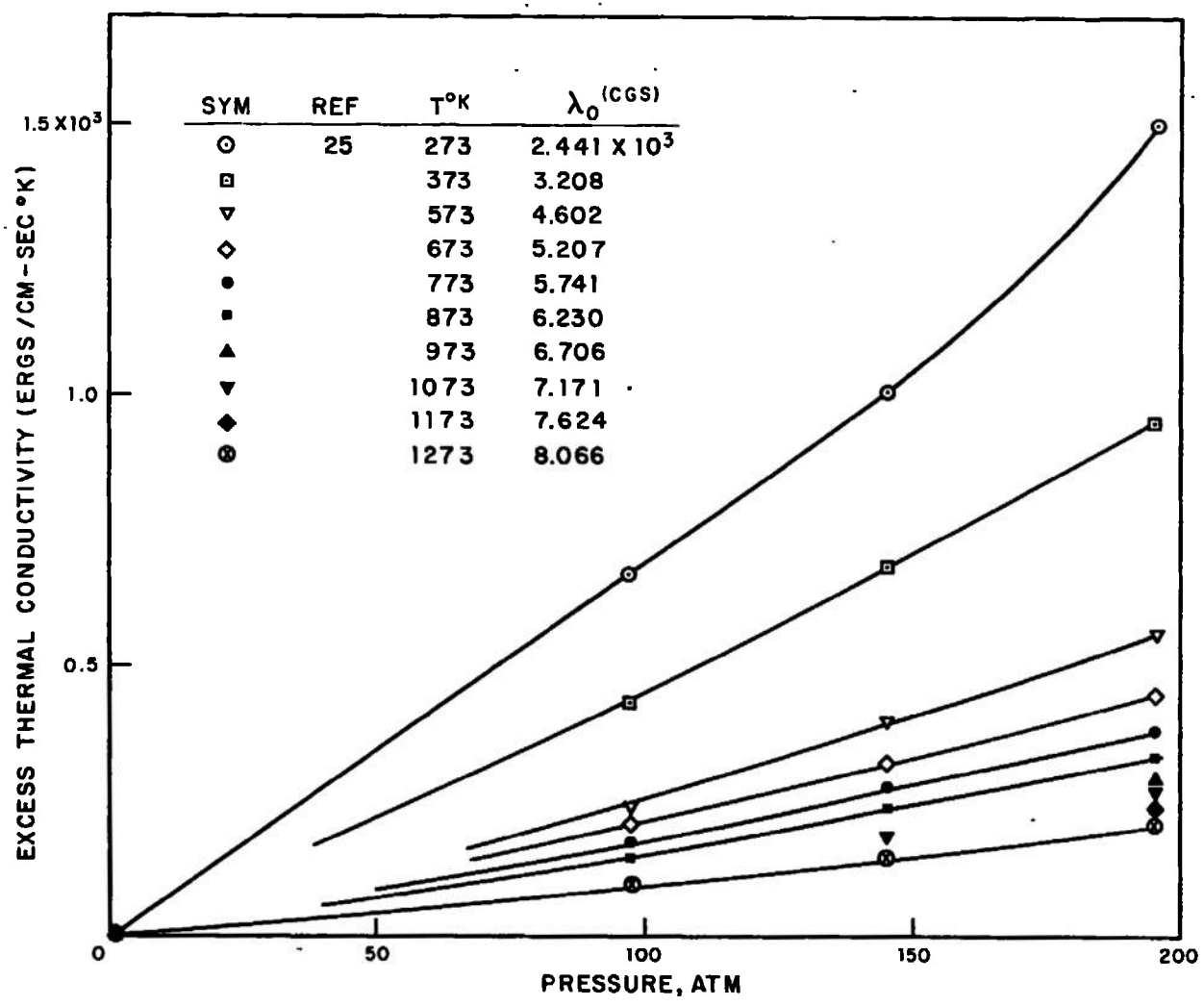

Fig. 22 Excess thermal conductivity for air

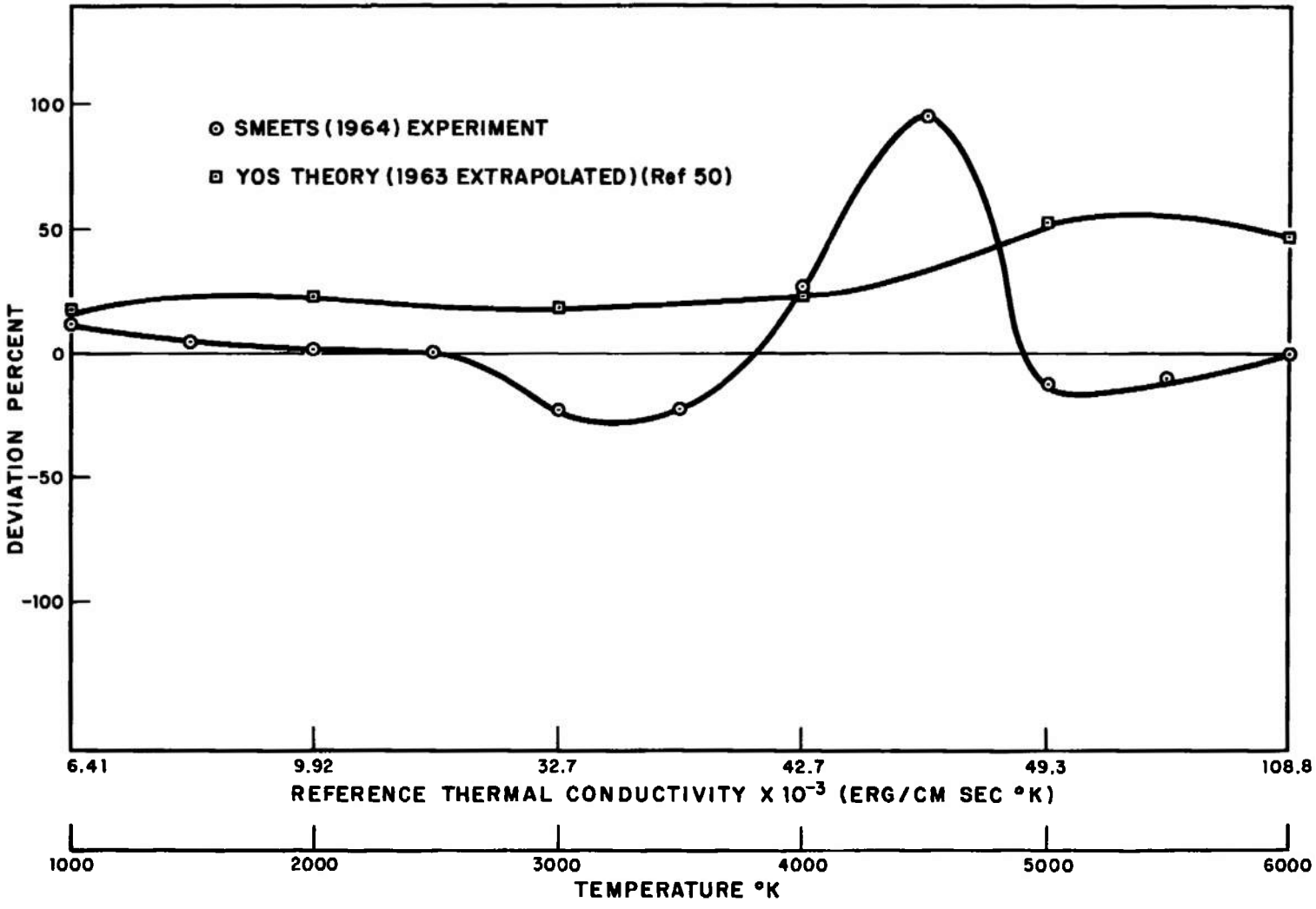

Fig. 23 High temperature thermal conductivity deviation chart for air

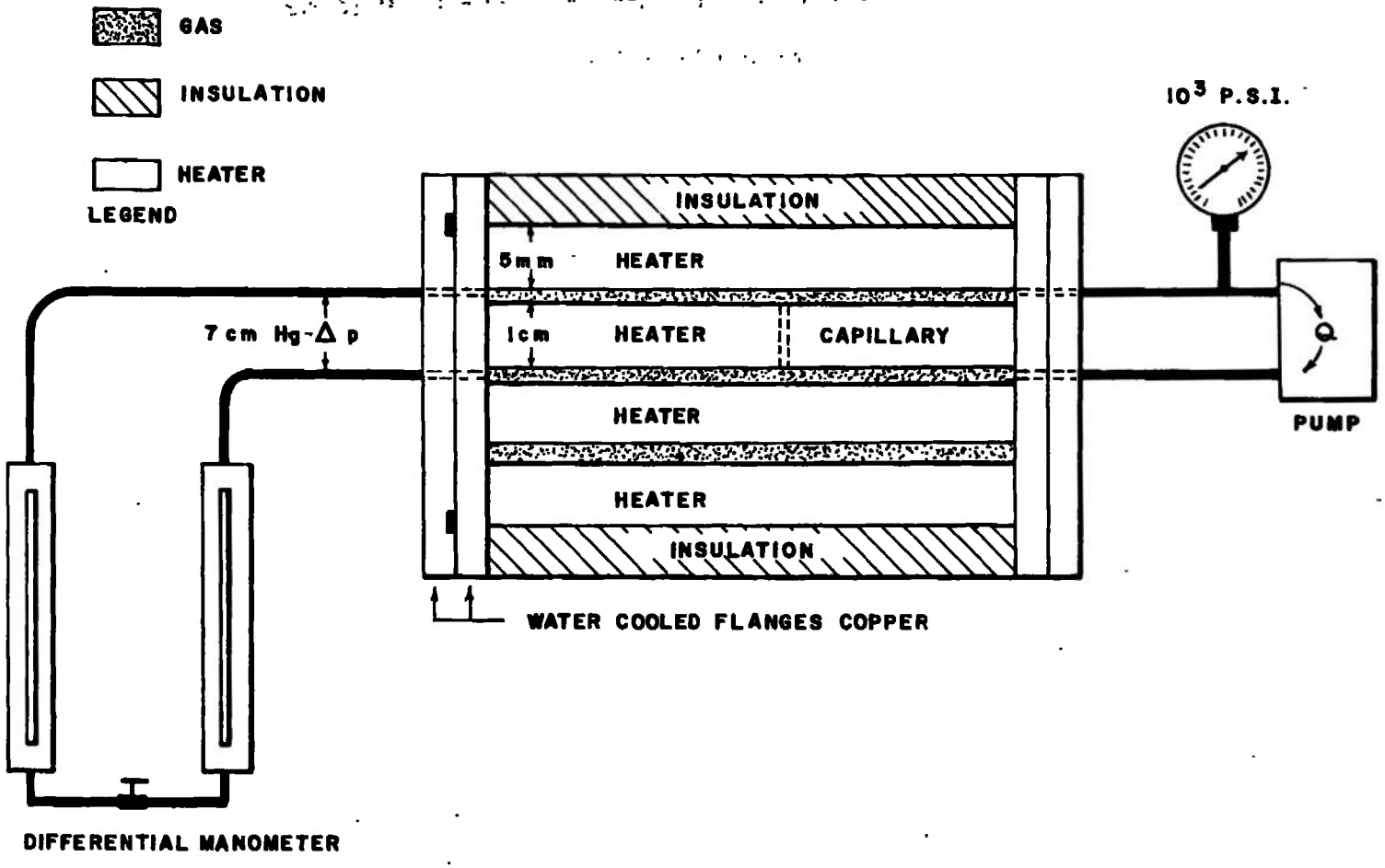

Fig. 24 Cutaway schematic of a high temperature capillary viscometer

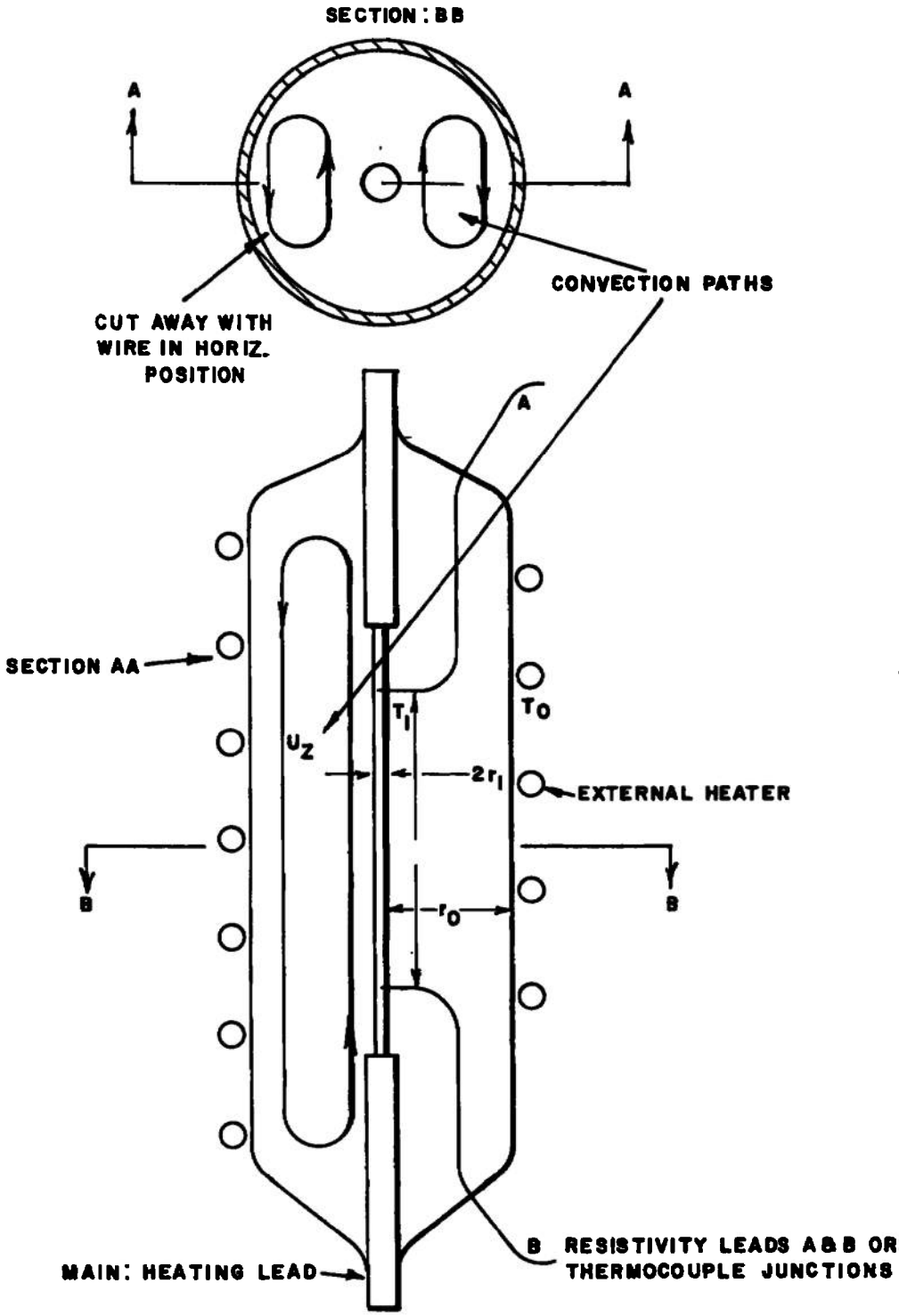

Fig. 25 Thin wire thermal conductivity cell

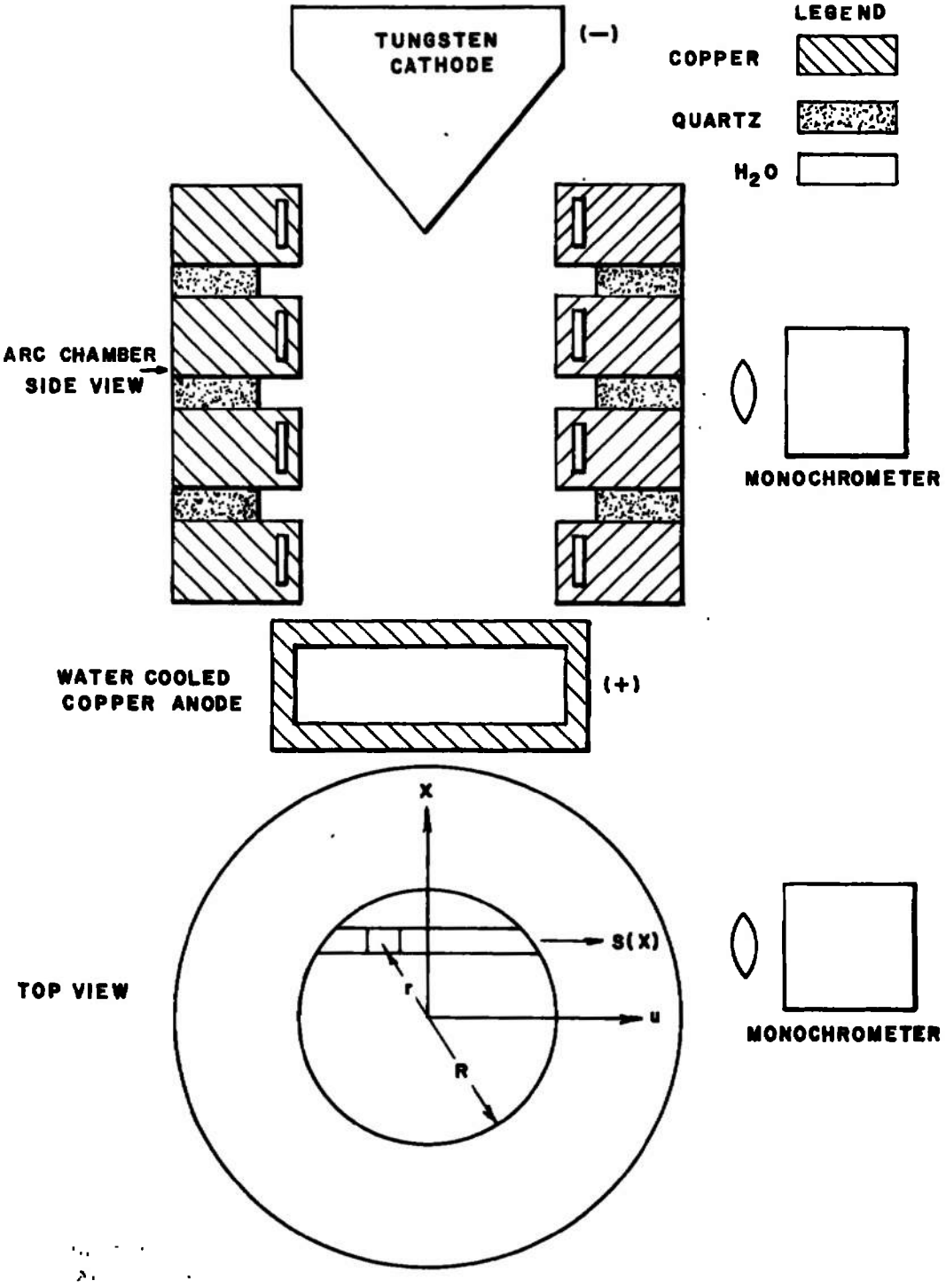

Fig. 26 The constricted arc

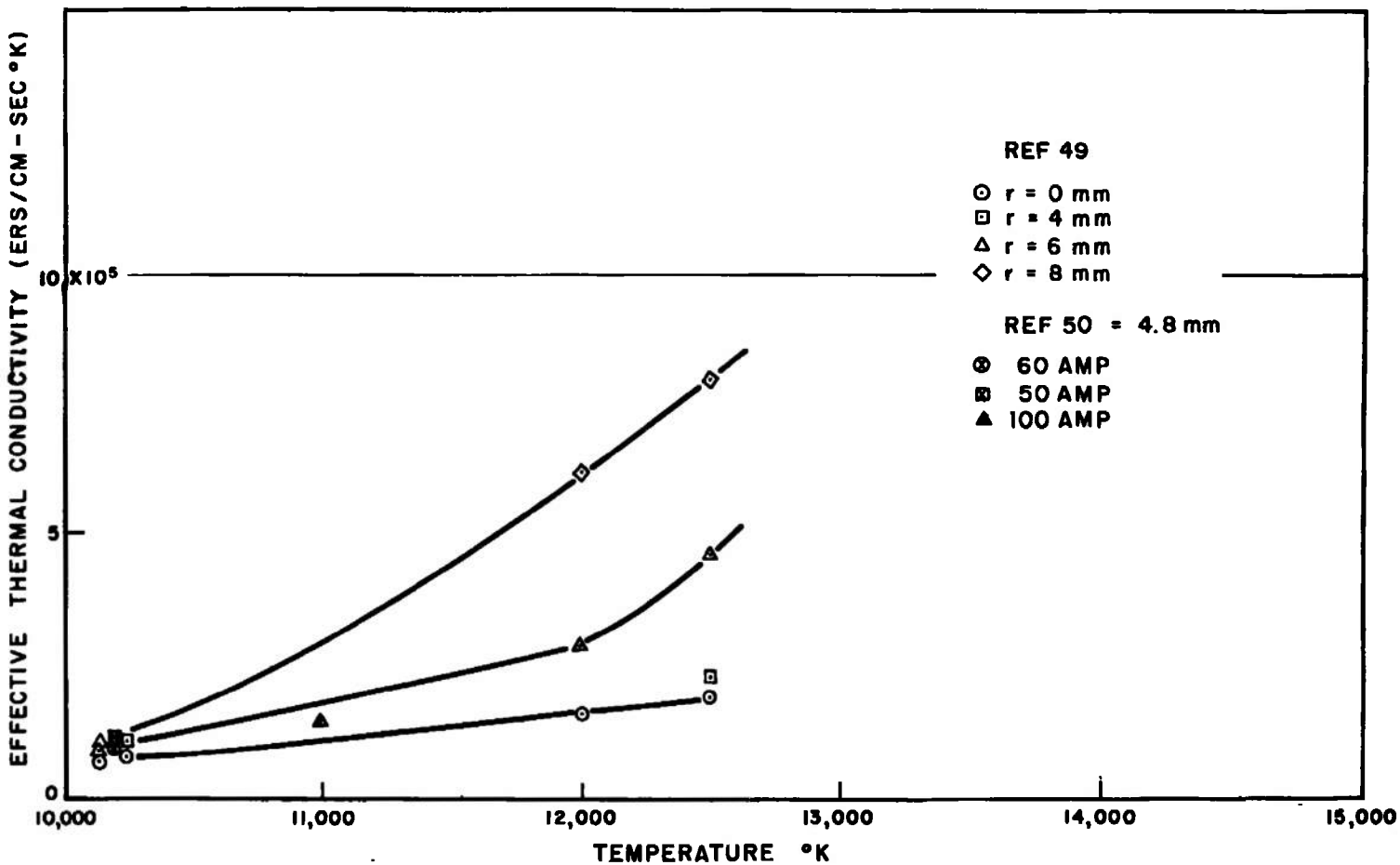

Fig. 27 The effect of arc current and diameter of the effective thermal conductivity

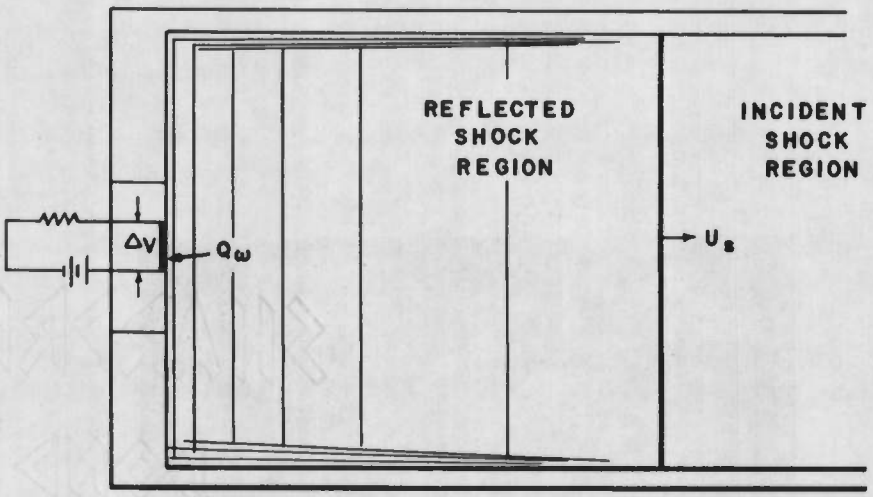

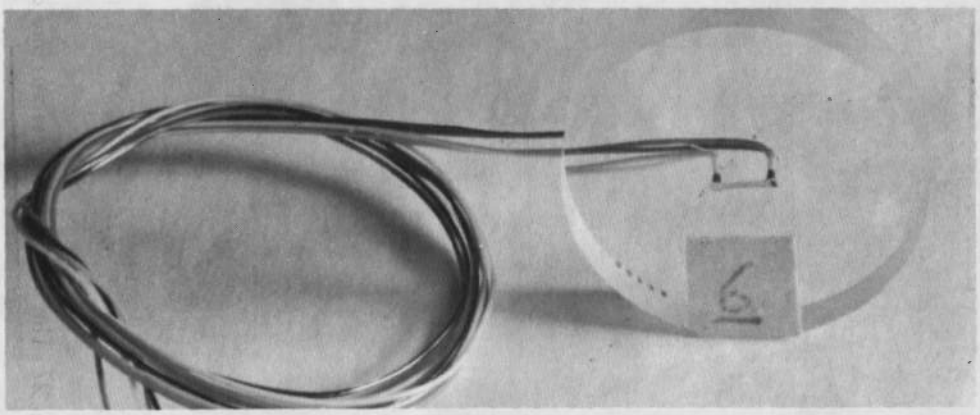

Fig. 28 Heat transfer in the reflected shock region

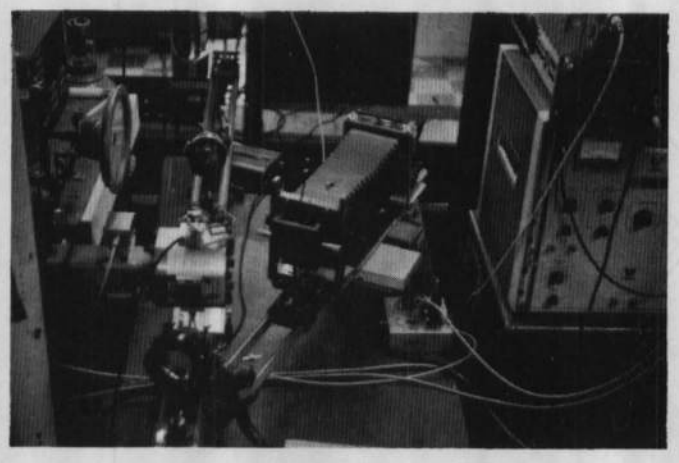

Fig. 29 Experimental apparatus for schlieren measurements

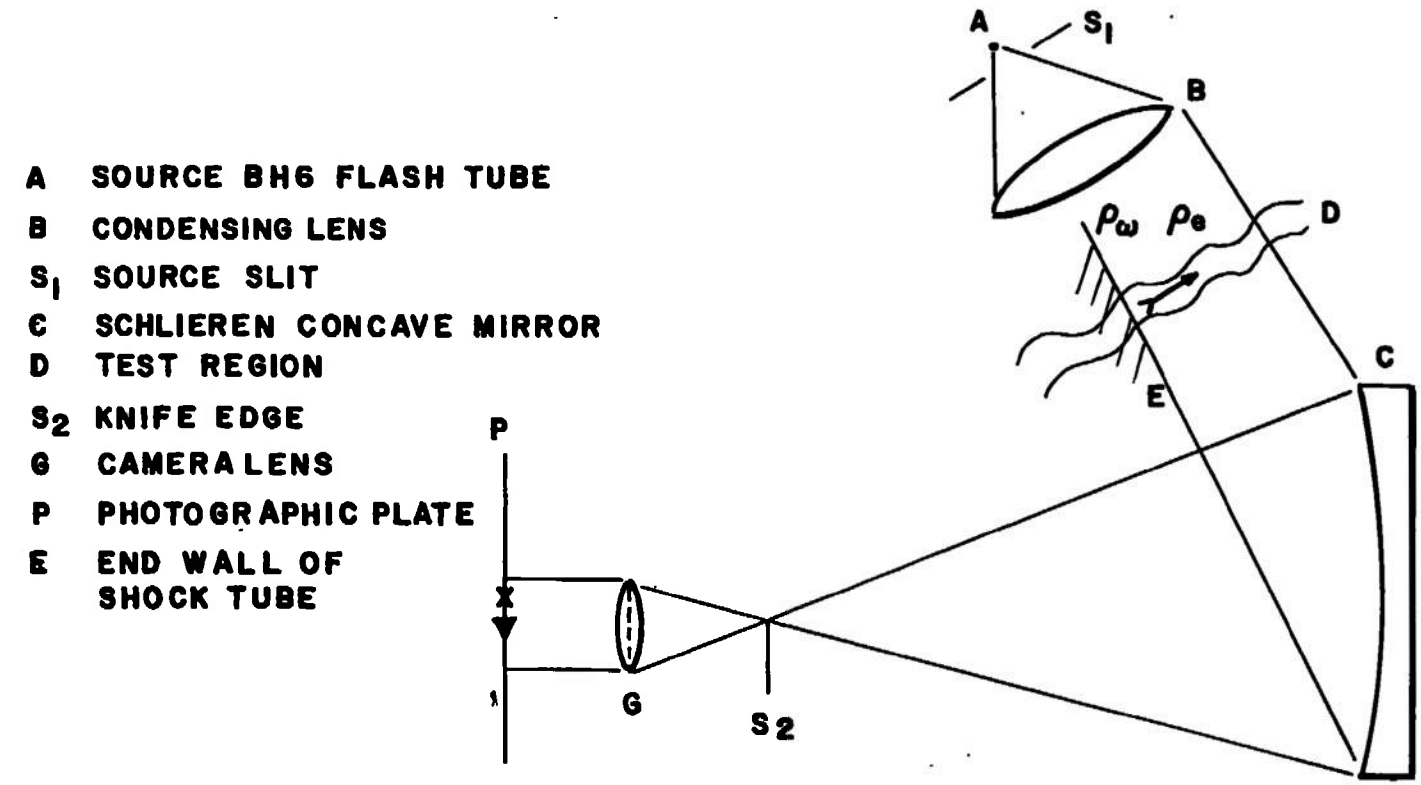

Fig. 30 Schematic of schlieren system

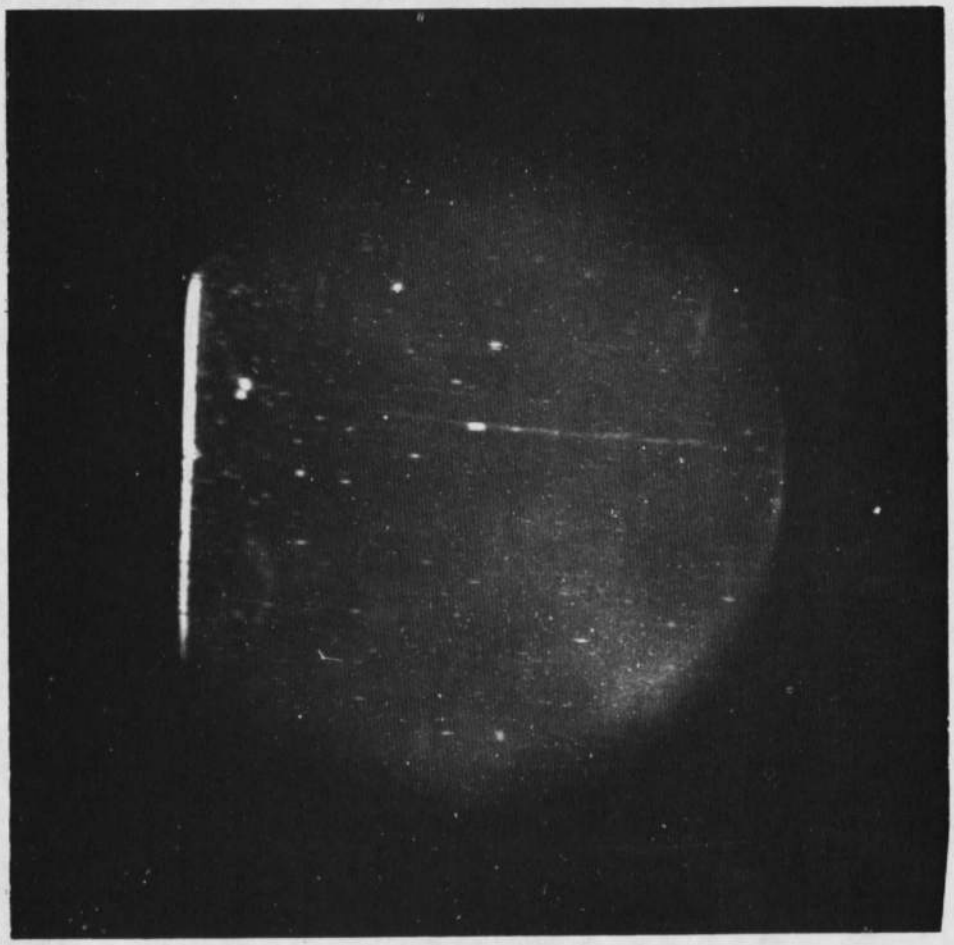

Fig. 31 Schlieren photograph of end wall boundary layer

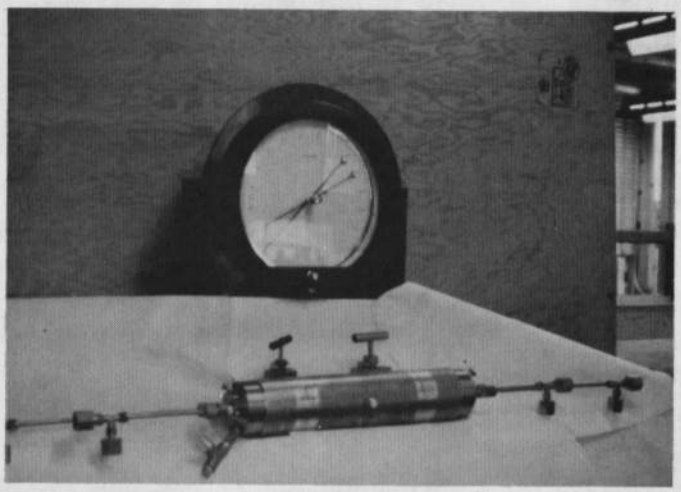

Fig. 32 Test chamber for high pressure sound speed measurements

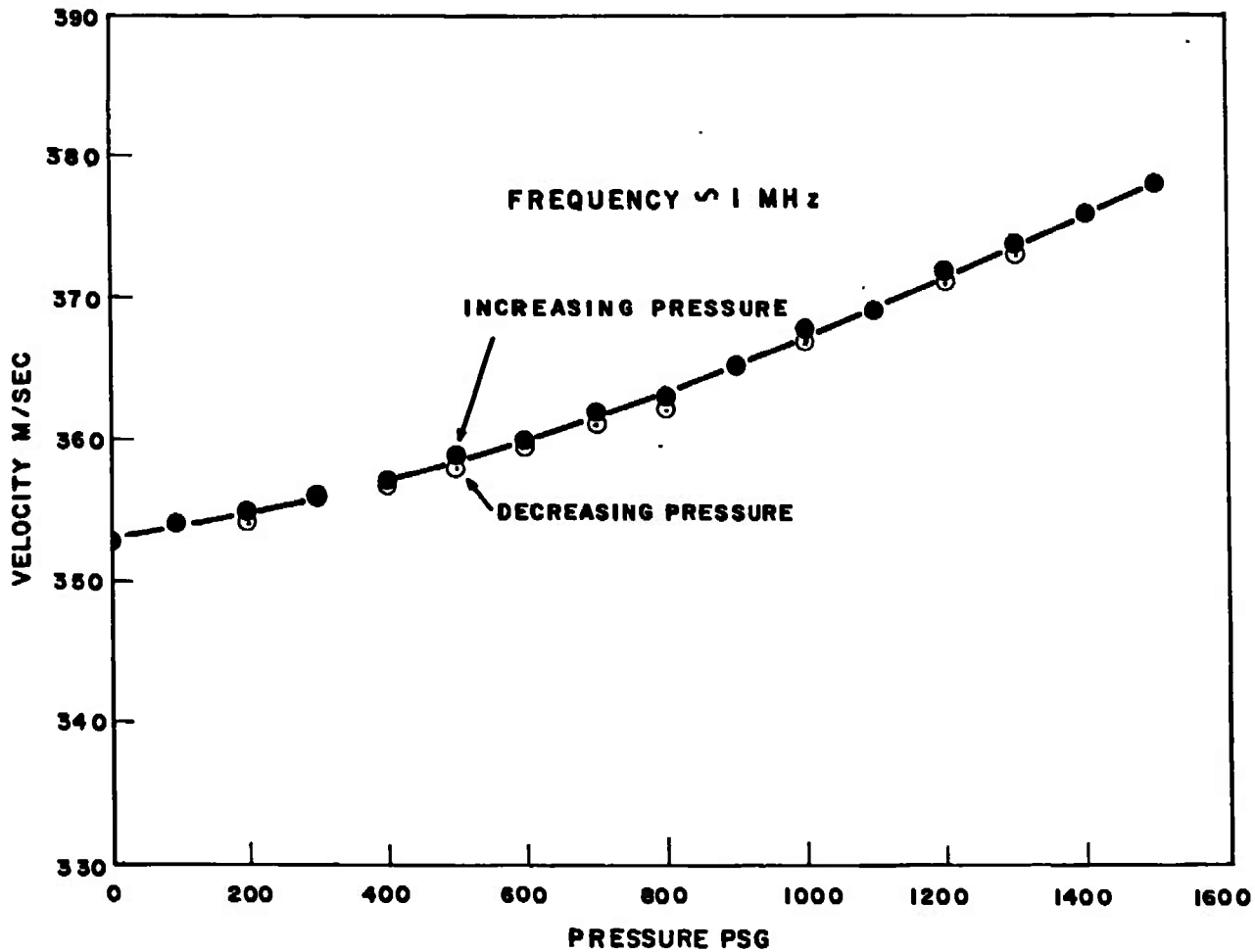

Fig. 33 Velocity of sound in nitrogen gas at room temperature

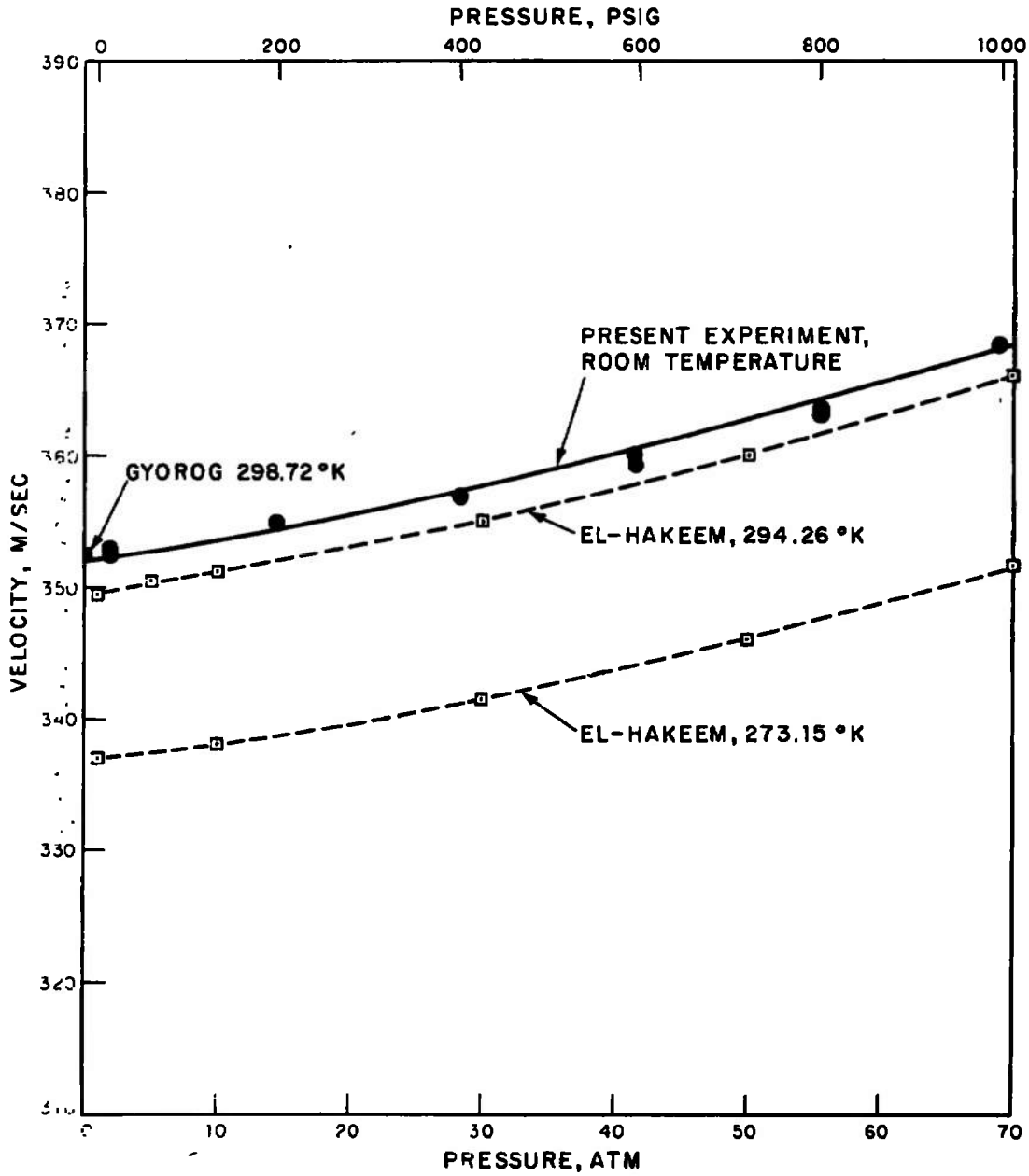

Fig. 34 Velocity of sound in nitrogen gas as a function of pressure

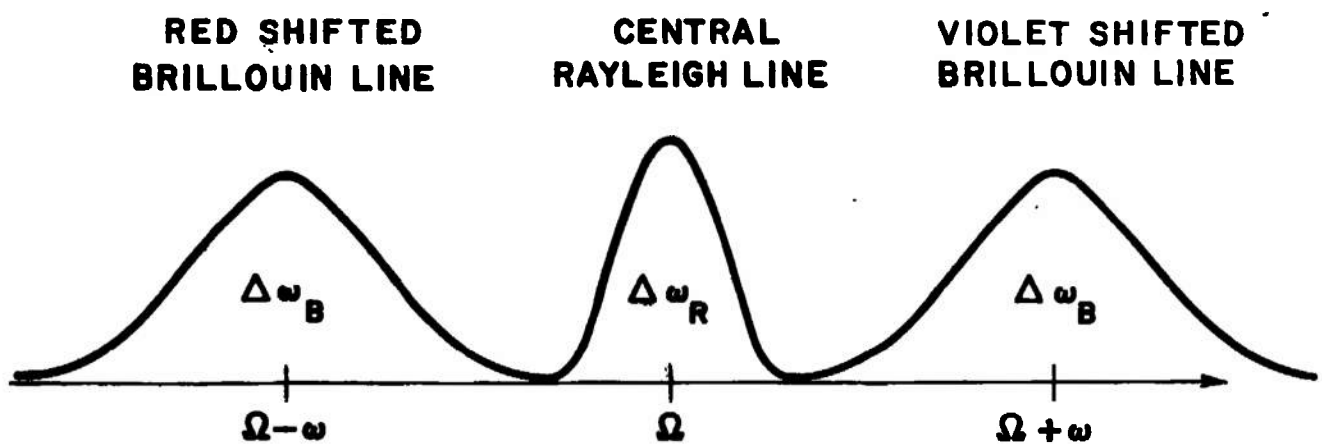

Fig. 35 Scattered intensity spectrum

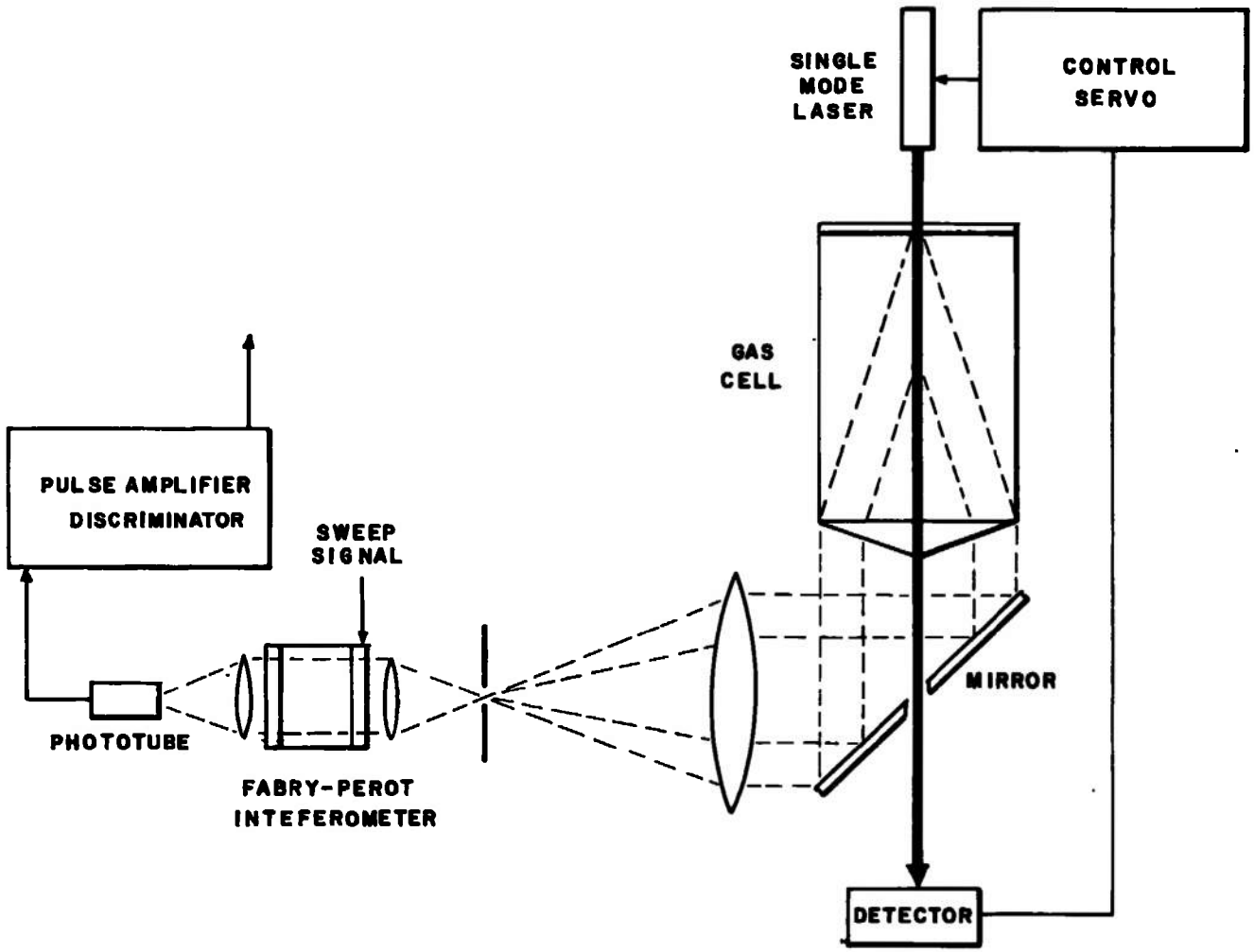

Fig. 36 Model laser gas scattering system

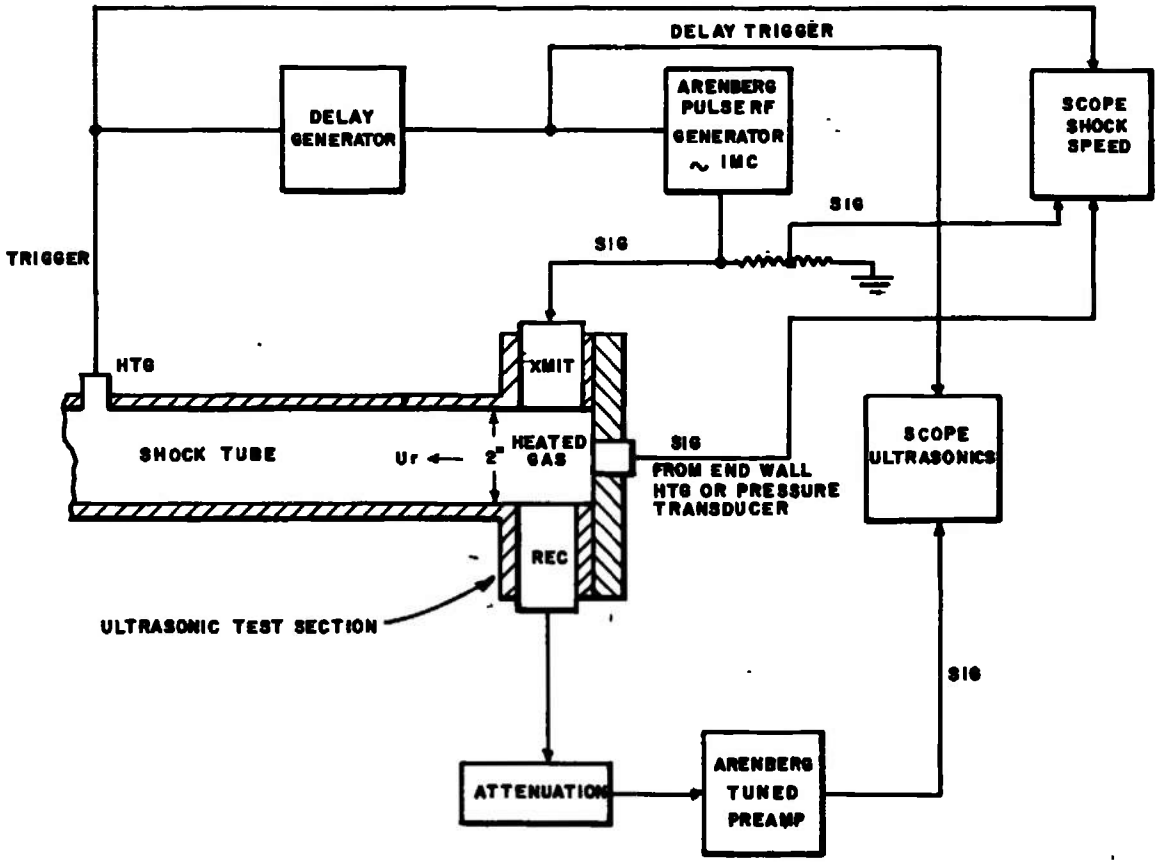

Fig. 37 Diagram of apparatus for ultrasonic measurements in the shock tube

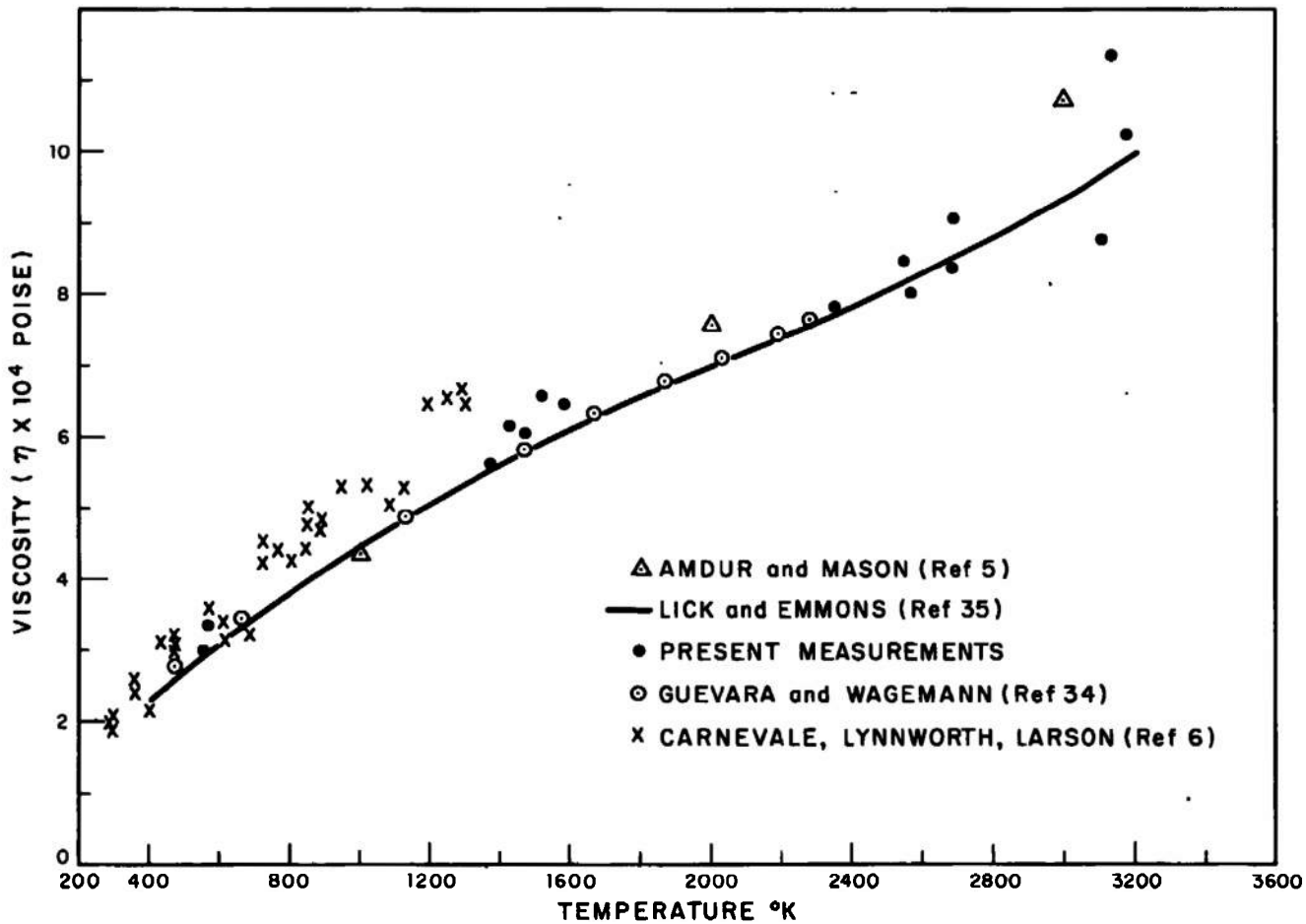

Fig. 38 Experimental viscosities for helium

UNCLASSIFIED

Security Classification

DOCUMENT CONTROL DATA - R & D

(Security classification of title, body of abstract and indexing annotation must be entered when the overall report is classified)

1. ORIGINATING ACTIVITY (Corporate author)	2a. REPORT SECURITY CLASSIFICATION
Panametrics, Inc. Waltham, Massachusetts	UNCLASSIFIED
	2b. GROUP N/A

3. REPORT TITLE

EXPERIMENTAL DETERMINATION OF GAS PROPERTIES AT HIGH TEMPERATURES AND/OR PRESSURES

4. DESCRIPTIVE NOTES (Type of report and inclusive dates)

Interim Report August 1966 to October 1967

5. AUTHOR(S) (First name, middle initial, last name)

E. H. Carnevale, C. Carey, T. Marshall, and S. Uva, Panametrics, Inc.

6. REPORT DATE	7a. TOTAL NO. OF PAGES	7b. NO. OF REFS
June 1968	118	120

8a. CONTRACT OR GRANT NO.	9a. ORIGINATOR'S REPORT NUMBER(S)
AF 40(600)-1191 b. PROJECT NO. 8951 c. Program Element 6240533F d. Task 895102	AEDC-TR-68-105
	9b. OTHER REPORT NO(S) (Any other numbers that may be assigned this report) N/A

10. DISTRIBUTION STATEMENT

This document has been approved for public release and sale; its distribution is unlimited.

11. SUPPLEMENTARY NOTES	12. SPONSORING MILITARY ACTIVITY
Available in DDC.	Arnold Engineering Development Center, Air Force Systems Command, Arnold Air Force Station, Tenn.37389

13. ABSTRACT

The available viscosity and thermal conductivity data in helium, argon, hydrogen, nitrogen, are reviewed. Deviation charts vs temperature are drawn up for each of the gases of interest in the temperature range 200-2500°K. High temperature thermal conductivity measurements in air, argon and nitrogen are also reviewed at temperatures between 2000 and 12,000°K. The methods of measuring thermal conductivity and viscosity are discussed with emphasis on the extension of available techniques to higher temperatures and/or pressures. Major emphasis is placed on constricted arc, heat transfer, schlieren, and ultrasonic techniques. Finally, measurements of helium thermal conductivity in the temperature range ~400-3000°K by the ultrasonic technique in the shock tube are presented.

DD FORM 1 NOV 65 1473

UNCLASSIFIED

Security Classification

14. KEY WORDS	LINK A		LINK B		LINK C	
	ROLE	WT	ROLE	WT	ROLE	WT
gases, properties of						
viscosity						
thermal conductivity						
kinetic theory						
diffusion						
transport properties						

1. Gases -- Properties
1. " -- Viscosity
2. " -- Thermal conductivity
3 " -- Transport properties
4 " -- Diffusion
5 " --